## TABLE OF CONTENTS

Page

## LIST OF FIGURES

## LIST OF ABBREVIATIONS

| | |
|---|---|
| AP | Access Point |
| AWGN | Additive White Gaussians Noise |
| AF | Amplify-and-Forward |
| ARQs | Automatic Repeat Requests |
| BPSK | Binary Phase Shift Keying |
| BER | Bit Error Rate |
| CSI | Channel State Information |
| CCI | Co-Channel Interference |
| CDF | Cumulative Distribution Function |
| DF | Decode-and-Forward |
| DSRC | Dedicated Short Range Communications |
| EC | Ergodic capacity |
| 5G | Fifth-Generation |
| FC | Fog Computing |
| FDR | Full Duplex Relay |
| HDR | Half Duplex Relaying |
| ICSI | imperfect channel state information |
| IGS | Improper Gaussian Signaling |
| ISI | Individual Self-Interference |

| | |
|---|---|
| i.i.d. | Independent and Identically Distributed |
| IoAV | Internet of Autonomous Vehicles. |
| i.n.i.d. | Independent and not Identically Distributed |
| ITSs | Intelligent Transportation Systems |
| IVC | Inter-Vehicular Communications |
| LOS | Line-of-Sight |
| LTE | Long Term Evolution |
| MAC | Medium Access Control |
| MANETs | Mobile Ad-Hoc NETworks |
| MEC | Mobile-Edge Computing |
| M2M | Mobile-to-Mobile |
| MGF | Moment Generating Function |
| MIMO | Multiple Input Multiple-Output |
| MMISI | Max-Min Criteria of Individual Self-Interference |
| MMSI | Max-Min Criteria of Self-Interference |
| mmWave | Millimeter Wave |
| MRC | Maximal Ratio Combiner |
| NLOS | Non-Line of Sight |
| OFDM | Orthogonal Frequency Division Multiplexing |
| PDF | Probability Distribution Function |

| | |
|---|---|
| PGS | Proper Gaussian Signalling |
| RF | Radio Frequency |
| RVs | Random Variables |
| SC | Selection Combining |
| SDF | Selective Decode-and-Forward |
| SDN | Software-Defined Networking |
| SI | Self-Interference |
| SINR | Signal-to-Interference-Plus-Noise Ratio |
| SNR | Signal-to-Noise Ratio |
| 3GPP | Third Generation Partnership Project |
| V2I | Vehicle-to-Infrastructure |
| V2V | Vehicle-to-Vehicle |
| VANETs | Vehicular Ad-Hoc NETworks |
| VDH | Vehicular full duplex dual hop |
| VJD | Vehicular Full Duplex Joint Decoding |
| ZF | Zero Forcing |

## LIST OF SYMBOLS AND UNITS OF MEASUREMENTS

| | |
|---|---|
| $S$ | Source node |
| $R$ | Relay node |
| $D$ | Destination node |
| $\mathbb{E}[\cdot]$ | Expectation function |
| $T_R$ | Transmission range |
| $M$ | Total traffic lanes |
| $w$ | Lane width |
| $M_L$ | Left-hand traffic lanes |
| $M_R$ | Right-hand traffic lanes |
| $\delta$ | The intensity of vehicles in each traffic lane |
| $x_S$ | Transmitted symbol signal at the source |
| $x_R$ | Transmitted symbol signal at the relay |
| $x_I$ | Transmitted symbol signal at the interference |
| $P_S$ | Transmitted signal power at the source |
| $P_I$ | Transmitted power of the interference signal |
| $P_R$ | Transmitted signal power at the relay |
| $h_{SR}$ | The channel coefficient for the source-relay link |
| $h_{RR}$ | The channel coefficient for the relay-relay link |
| $h_{RD}$ | The channel coefficient for the relay-destination link |

| | |
|---|---|
| $h_{ID}$ | The channel coefficient for the interference link |
| $L$ | Cascading degree |
| $n_R$ | White Gaussian noise (AWGN) at relay |
| $n_D$ | White Gaussian noise (AWGN) at destination |
| $N_0$ | Noise variance |
| $y_{D_R}$ | The received signal at the destination |
| $y_{SRR}$ | The received signal at the relay |
| $y_{D_{R_{\text{dir}}}}$ | The received signal at the destination in the presence of $S-D$ link |
| $y_{D_{R_{\text{ind}}}}$ | The received signal at the destination in the absence of $S-D$ link |
| $\kappa$ | The amplification factor |
| $d_{pq}$ | Distance between $p$ and $q$ |
| $\eta$ | Path loss exponent |
| $\gamma_{ij}$ | The instantaneous SNR at $j^{th}$ node from $i^{th}$ node |
| $\bar{\gamma}_{ij}$ | The average SNR at $j^{th}$ node from $i^{th}$ node |
| $f(.)$ | Probability density function |
| $F(.)$ | Cumulative distribution function |
| $\overline{F}(.)$ | Complementary cumulative distribution function |
| $\Gamma(\cdot)$ | Gamma function |
| $\Gamma(\cdot,\cdot)$ | Upper incomplete gamma function |
| $\gamma(\cdot,\cdot)$ | Lower incomplete gamma function |

| | |
|---|---|
| $\gamma_{th}$ | Predefined threshold |
| $\gamma^{SC}$ | Signal-to-interference-plus-noise ratio when selection combining is applied at the destination |
| $\gamma_{asy}$ | Asymptotic signal-to-noise ratio |
| $\gamma_{eq}$ | Equivalent signal-to-interference-plus-noise ratio |
| $R_T$ | Target rate |
| $R_S$ | Fixed rate of the transmitter |
| max | Maximum value |
| min | Minimum value |
| $P(.)$ | Outage probability |
| $P_{e2e}(.)$ | End-to-end outage probability |
| $P_c(.)$ | Probability of blockage |
| $\gamma_{\text{MMSI}}$ | Signal-to-interference-plus-noise ratio in the case of max-min criteria of self-interference scheme |
| $\gamma_{\text{MMISI}}$ | Signal-to-interference-plus-noise ratio in the case of max-min criteria of individual self-interference scheme |
| $G$ | Throughput |
| $\exp(\cdot)$ | Exponential function |
| $Q(\cdot)$ | $Q$ function |
| $\log_2$ | Logarithm with base 2 |
| ln | Natural logarithm |

| | |
|---|---|
| $m_{ij}$ | Shape parameter for the $i$-$j$ link |
| $G_{\Theta,\Omega}^{\beta,\varepsilon}(.\|.)$ | Meijer's G-function |
| $G_{\Delta,[\Theta,\Omega],\Upsilon,[\Phi,\Psi]}^{\beta,\varepsilon,\varepsilon,\zeta,\nu}(.\|.)$ | Extended generalized bivariate Meijer's G-function |
| $P_p(LOS_{OBS})$ | Probability that the $S$ to $D$ link is obstructed |
| $\Lambda_S$ | Source height |
| $\Lambda_D$ | Destination height |
| $\chi$ | Mean height of the obstacle |
| $\sigma_{OBS}$ | Standard deviation of the obstacles' height |
| $\Lambda_{EF}$ | Effective height of the straight line between $S$ and $D$ |
| $d_{OBS}$ | Distance between the source and the obstacle |
| $\Lambda_A$ | Height of the antenna |
| $r_F$ | Radius of the first Fresnel zone ellipsoid |
| $\lfloor . \rfloor$ | Roundup operator |
| $\lambda$ | Wavelength |
| $\mathrm{EC}_{lower}$ | Ergodic capacity lower bound |
| $\mathrm{EC}_{upper}$ | Ergodic capacity upper bound |
| $M(.)$ | Moment generating function |
| $j!$ | Factorial $j$ |
| $\binom{j}{k}$ | Binomial coefficient |
| $\gamma_{up}$ | Upper bound of signal-to-noise ratio |

## INTRODUCTION

Every year, thousands of people die or are seriously injured in traffic accidents. Transport Canada's National Collision Database (NCDB) shows that, in 2017, 1,856 people died, and 152,772 were seriously injured Database, T. C. N. C. (2017). Given its potential to decrease the number of killed and injured, V2V communication systems have received considerable attention from both the research and industrial communities in recent years. V2V systems provide many applications to the passengers including Eshteiwi, K., Kaddoum, G., Fredj, K. B., Soujeri, E. & Gagnon, F. (2019); Qureshi, K. N. & Abdullah, A. H. (2013)

- **Safety**: This is one of the most important V2V applications, which include warning messages at intersections or in the case of an obstacle on the road. This application also provides reports on accidents that may happen. A lane change warning message is sent to inform the other vehicles or drivers of who has the priority to pass to avoid accidents Jurgen, R. (2012).

- **Traffic management**: This application includes monitoring the speed limit, assessing traffic at intersections, and intersection control. Traffic management is useful to accommodate the rapid movement of emergency vehicles such as ambulances and police vehicles Raiyn, J. (2019).

- **Driver assistance systems**: In some cases, drivers need help to park their cars and even to set up their cruise control feature. Roadside units can inform drivers so they can better control their vehicles Ahrems, J. (2015); Sivaraman, S. & Trivedi, M. M. (2013).

- **Direction and route optimization**: This feature helps drivers to reach their destination in the shortest time and over the quickest route. Vehicles can share information about the best route in case of an accident, road obstacle or other special condition Abuashour, A. & Kadoch, M. (2017).

- **General information services**: As a result of the rapid development of V2V wireless communications, internet access has become an urgent need, not only to report accidents or congestions, but also to upload and download files, send email and surf the web Singh, P. K., Nandi, S. K. & Nandi, S. (2019).

As a part of the 5G of wireless communications, a vast army of autonomous/semi-autonomous vehicles will take the road and engage with future intelligent transportation systems services. In 5G technology, fifty billion devices will have connectivity capabilities. Among these, ten million vehicles equipped with on-board communication systems and with a variety of autonomous capabilities will be progressively rolled out Tassi, A., Egan, M., Piechocki, R. J. & Nix, A. (2017). As a result of the rapid development of V2V wireless communications, internet access has become an urgent need, not only to report accidents or congestions, but also to upload and download files, send email and surf the web Singh *et al.* (2019). Based on the aforementioned applications, an enhancement of the currently achievable capacity and data rates are extremely important, and are therefore, being explored as part of the fifth-generation (5G) standardization effort by the third Generation Partnership Project (3GPP). One of the key areas to explore under 5G is vehicular cooperative wireless communications Campolo, C., Molinaro, A., Berthet, A. O. & Vinel, A. (2017), wherein the objectives are to reduce the aftermath of multi-path fading and signal degradation within the vehicular wireless communications space. Correspondingly, cooperative relaying systems based on V2V communications, also known as inter-vehicular communications (IVC), have been proposed to increase the diversity and generally improve the performance of wireless communication systems.

V2V cooperative relaying systems increase the diversity and generally improve the performance of wireless communication systems. In addition, the cooperation mechanism between vehicles and infrastructures can extend the coverage area, thereby offering improved road safety and better network connectivity Silva, C. M., Masini, B. M., Ferrari, G. & Thibault,

I. (2017). Vehicular networks operate in the 5.9 GHz with a bandwidth of 75 MHz for dedicated short range communication (DSRC) techniques to support public and commercial applications of V2V and vehicle-to-infrastructure (V2I) communications Commission, F. C. et al. (2001). To reduce the end-to-end delay and to concurrently double the spectral efficiency when self-interference is eliminated Kim, D., Lee, H. & Hong, D. (2015), FDR was proposed and implemented. This is because with full duplex, also known as in-band full duplex, the relays avoid any spectral efficiency loss by transmitting and receiving over the same band simultaneously. However, in FDR, the performance could be severely degraded because of the SI at the relay node due to the simultaneous transmission and reception over the same channel, which cannot be perfectly eliminated Duarte, M. & Sabharwal, A. (Nov. 2010); Jain, M., Choi, J. I., Kim, T., Bharadia, D., Seth, S., Srinivasan, K., Levis, P., Katti, S. & Sinha, P. (2011). Meanwhile, in half duplex relaying, also known as out-of-band full duplex, the relays encounter a spectral efficiency loss as they transmit and receive in different time slots or over different frequency bands. As a result, in practical FDR protocol designs, the impact of self-interference should be taken into account for a more accurate system analysis.

In vehicular communications, given the relatively small height of the antennas set on the vehicles, other vehicles such as vans, lorries, and buses present between a pair of communicating vehicles can obstruct the signal Boban, M., Vinhoza, T. T., Ferreira, M., Barros, J. & Tonguz, O. K. (2011). From the communication link blockage perspective, vehicles as obstacles have a significant impact on signal propagation; therefore, in order to properly model V2V communication, it is imperative to account for vehicles as obstacles. Furthermore, the effect of vehicles as obstacles cannot be neglected, even in the case of relatively sparse vehicular networks and averaging the additional attenuation due to vehicles, would fail to adequately describe the complex and significant impact of vehicles on the received signal power Boban, M., Vinhoza, T. T., Ferreira, M., Barros, J. & Tonguz, O. K. (2010). Furthermore, neglecting vehicles as obstacles in VANET modeling has profound effects on the performance evaluation of vehicular com-

munications Akhtar, N., Ergen, S. C. & Ozkasap, O. (2014); Boban *et al.* (2010); Boban, M., Dupleich, D., Iqbal, N., Luo, J., Schneider, C., Müller, R., Yu, Z., Steer, D., Jamsa, T., Li, J. et al. (2019).

**Problem Statement**

VANETs have unique characteristics that distinguish them from Mobile Ad-Hoc NETworks(MANETs), including link failure, a highly dynamic network. The main drawback of VANETs is the network instability, which reduces network efficiency. VANETs have been attracting significant attention from the research community due to their high demands in terms of quality of service, reliability, and throughput. In this context, it was shown that cooperation between the vehicles can increase the reliability of the network by increasing the strength of the communication links Laneman, J. N., Tse, D. N. & Wornell, G. W. (Dec. 2004) and extending the coverage and connectivity of V2V networks Silva *et al.* (2017). Moreover, cooperating vehicles can also help compensate for human errors, leading to a decrease in the number of accidents. Advanced vehicular applications also include intelligent transportation systems (ITSs) which are anticipated to offer passengers several applications such as vehicle parking, accident response, and traffic congestion avoidance Qureshi & Abdullah (2013). Therefore, it is evident that for such applications, ultra-low latency transmission and high data rates are of paramount importance. To this end, full duplex relaying (FDR), which is capable of potentially reducing the end-to-end delay and to concurrently double the spectral efficiency when the self-interference is eliminated, was introduced as a promising solution to such critical applications Kim *et al.* (2015). In the context of traditional half-duplex relaying (HDR) networks, the impact of co-channel interference (CCI) due to frequency reuse on the system performance has been extensively studied in the literature Ikki, S. S. & Aissa, S. (2012b); Lee, K.-C., Li, C.-P., Wang, T.-Y. & Li, H.-J. (2014); Trigui, I., Affes, S. & Stephenne, A. (2013a); Trigui, I., Affes, S. & Stéphenne, A. (2013b); Zhu, G., Zhong, C., Suraweera, H. A., Zhang, Z., Yuen, C. & Yin, R. (2014b). However, it is noted that FDR networks, which are characterized by more frequency reuse, are more

susceptible to CCI than their conventional HDR counterparts Almradi, A., Xiao, P. & Hamdi, K. A. (2018). As a result, in practical FDR protocol designs, the impact of self-interference should be taken into account for a more accurate system analysis. Moreover, the vast majority of the related works in the literature do not account for the effect of obstacles between the source-destination (S-D) link which was shown to significantly impact the LOS component and the received signal power in both sparse and dense vehicular networks Boban *et al.* (2011). Therefore, to fill this gap, this work considers a cooperative V2V scenario using FD AF relaying under the impact of both SI at the relay and CCI at the destination. However, in V2V communications, given the relatively small height of the antennas set on the vehicles, other vehicles such as vans, lorries, and buses present between a pair of communicating vehicles can obstruct the signal Boban *et al.* (2011). To this end, the study of full duplex relaying in vehicular communications impaired by self and co-channel interferences, and blockage by other vehicles are necessary for a pragmatic evaluation of the performance limit of practical V2V communications.

**Research Objectives**

The fundamental goal of our research is to propose and analyse different V2V wireless communication systems at the physical layer level. To do so, we will provide exact and lower/upper bounds expressions for average signal-to-noise ratios (SNR), signal-to-interference-plus-noise ratio (SINR), outage probability, probability of blockage, ergodic capacity, throughput and then compare the analytical with simulation results. In this thesis, we will focus on the investigation of full duplex variable gain amplify-and-forward (AF) relaying in V2V cooperative wireless communication over independent but not necessarily identically distributed (i.n.i.d) $L$-Nakagami-$m$ fading channels. The objectives that we aim to accomplish through this research are divided into four phases of this work.

**In the first phase**, we consider the fact that due to the vehicles mobility in vehicular communications, channels are much more challenging than those in cellular communication and can be modeled by a multiplicative channel model, named as the cascaded fading channel model, produced by multiplying the channel gains of independent scattering groups around mobile units. Consequently, we explore and analyze the performance of variable gain AF full duplex relaying of V2V wireless cooperative communication over a more general fading channel such as generalized cascade $L$-Nakagami-$m$ fading channels which can be used to describe many fading distributions environments.

**In the second phase**, we investigate and analyze the performance of a realistic full duplex vehicular cooperative wireless communication model, where the effect of blockage on V2V communications is taken into account. The influence of key system parameters such as the CCI at the destination, target rate, mean height of the obstacles, the source's height, and the distance between the source and the obstacles on the system's performance are investigated.

**In the third phase**, we design and analyze the performance of full duplex variable gain AF relaying in vehicular communication taking into account both SI and CCI at the relay and destination nodes, respectively. To this end, exact, lower, and upper bounds expressions of the ergodic capacity are derived. These expressions yield an efficient way for the assessment of the ergodic capacity of the considered dual-hop FDR systems with SI and CCI.

**In the last phase**, we evaluate the performance of two different relay selection schemes in dense multi-lane highway vehicular cooperative communications over mmWave networks, where the impact of SI at the relay node and blockage probability in the central lane are considered. We propose a probabilistic model capturing the occurrences of LOS and NLOS propagation, which depends on movement of the vehicles between the central and adjacent lane, and provide analytical expressions for the outage probability and throughput.

**Contributions and Outline**

In Chapter 1, we detail the theoretical background and related works on cooperative communications, relaying and combining techniques, transmission modes, and millimeter wave. Moreover, the contribution of our thesis are summarized as follow:

In Chapter 2, we analyze FD AF relaying V2V networks over i.n.i.d generalized $L$-Nakagami-$m$ fading channels with SI at the relay node. We derive novel expressions for the probability density function (PDF) and cumulative distribution function (CDF) of the SINR at the relay. In addition, a lower bound expression for the end-to-end outage probability is derived. Our results show that channel cascading significantly impacts the end-to-end outage probability of FD relaying V2V systems, where the cascading of the source-relay link is shown to be more significant than the relay-destination link.

In Chapter 3, we evaluate the performance of AF-based FDR vehicular communications over i.n.i.d Nakagami-$m$ fading channels. In this scenario, CCI, SI, and blockage from other vehicles on the road are considered. To analyze the performance, we first derive novel exact, asymptotic outage probabilities, and symbol error rate lower bound of the proposed system. These analytical expressions are expressed in terms of the blockage probability and then used to evaluate the throughput of the proposed system. From the obtained results, the significant impact of the considered interference and blockage on the system performance is demonstrated. In addition, the results confirm that the outage probability, throughput, and symbol error rate are degraded by increasing the average height of the obstacles.

In Chapter 4, we investigate the ergodic capacity of vehicular communications with both SI at the relay and CCI at the destination, respectively. The analysis assumes the AF relying technique over i.n.i.d Nakagami-$m$ fading channels. In this context, a novel exact as well as lower bound expression for the ergodic capacity are derived. Moreover, the upper bound expression is also derived based on the asymptotic outage probability. Our results show the

perfect match between the analytical and theoretical curves and the tightness of the lower and upper bounds. Interestingly, the presented results show that FDR with SI and CCI still offers higher ergodic capacity than interference-free half duplex relaying, especially at medium to high SNRs.

In Chapter 5, two best FDR schemes are investigated and analyzed for a dual-hop V2V communication system over mmWave network in a dense multi-lane highway. In the first scheme, called SI vehicle relaying selection, the FDR models the source-relay and the relay-relay links by using one channel state information (CSI) coefficient. Meanwhile, in the second scheme, named ISI vehicle relaying selection, the CSI of the source-relay and the relay-relay links are estimated separately. Moreover, the relay-destination link is modeled by one CSI coefficient in both aforementioned schemes. In this Chapter, we propose a probabilistic model capturing the occurrences of line-of-sight (LOS) and non-line-of-sight (NLOS) propagations, which depends on the movement of the vehicles between the central and adjacent lanes. Moreover, the blockage between the source and destination links is considered in our analysis. In this context, the Nakagami-*m* fading channel model is considered due to its excellent representation of the V2V communication environment. The LOS/NLOS probabilities combined together with the probability of blockage are used to analyze the system performance. The lower bound expressions of the end-to-end outage probabilities are derived and then used to express the throughput of the proposed system.

**Author's Publications**

The outcomes of the author's Ph.D. research are either published or submitted to the IEEE journals and conferences, which are listed below.

**Eshteiwi, K.** , Selim, B., and Kaddoum, G. "Full Duplex Relaying of V2V over Cascaded Nakgamai-*m* Fading Channels ", *IEEE International Symposium on Networks, Computers and Communications (ISNCC'20)*, March, 2020, accepted for publication.

**Eshteiwi, K.**, Kaddoum, G., Selim, B., and Gagnon, F., "Impact of Co-Channel Interference and Vehicles as Obstacles on Full-Duplex V2V Cooperative Wireless Network", *IEEE Trans. Veh. Technol.*, May, 2020, accepted for publication.

**Eshteiwi, K.**, Alam, M. S., and Kaddoum, G.,"Exact and Asymptotic Ergodic Capacity of Full Duplex Relaying with Co-Channel Interference in Vehicular Communications", MDPI sensors Journal, December, 2019.

**Eshteiwi, K.**, Kaddoum, G., Ben Fredj, K. , Soujeri, E. and Gagnon, F., "Performance Analysis of Full-Duplex Vehicle Relay-Based Selection in Dense Multi-lane Highways", *IEEE Access*, Vol. 7, pp. 61581–61595, March 2019.

**Eshteiwi, K.**, Ben Fredj, K. , Kaddoum, G. and Gagnon, F. , "Performance analysis of peer-to-peer V2V wireless communications in the presence of interference", *IEEE PIMRC*, Oct. 2017.

**Eshteiwi, K.**, Kaddoum, G., and Gagnon, F. "Impact of Imperfect Channel Estimation Error and Jamming on the Performance of Decode-and-Forward Relaying", *IEEE ICUWB*, Oct. 2015.

Kaddoum, G., Soujeri, E. , Arcila, C. , and **Eshteiwi, K.**, "I-DCSK: An Improved Noncoherent Communication System Architecture", *IEEE Trans. on Circuits Syst.*, Sep. 2015.

# CHAPTER 1

# LITERATURE REVIEW

## 1.1 Cooperative Communications

In the next-generation of wireless communication networks, high data rate transmission and low bit error probability are essential requirements. On the other hand, due to the time-varying nature of the wireless channel and the often limited resources for transmission, a transmitted signal faces various detrimental effects, such as interference, Doppler spread, propagation path loss, shadowing, delay spread, and multipath fading, making it difficult to achieve high data rates. However, it is possible to increase the transmission data rates by increasing the transmission bandwidth or using higher transmission power. However, from a practical point of view, increasing the transmission bandwidth or the transmit power is not always feasible due to high system deployment costs. Furthermore, increasing the transmit power results in an increased interference to other transmissions and also decreases the battery life time of the transmitters. In general, the error probability observed in fading channels is much higher than that observed in a non-fading environment, namely Additive White Gaussians Noise (AWGN) channels.

In wireless communications, occurrences of deep fades in the propagation channel make reliable communications difficult or impossible. In general, diversity techniques can enhance reliability by transmitting the same information through different independent paths, thereby increasing the probability of successful transmission Yılman, E. (2006). Diversity can be achieved over the time, frequency, or space domains. With the rapid development of multimedia services, the next generations of wireless communications demand higher data rates and highly reliable transmission link guaranteeing an appropriate quality of service.

Utilizing the concept of cooperative communications has recently been proposed to overcome this drawback and it has gained considerable interest from the research community. The key idea behind cooperative communications is to use an antenna of the third intermediate terminal, a so-called relay node, which supports the direct communication as represented in Fig. 1.1. Af-

ter receiving the source's message, the relay processes and forwards it to the destination. The benefits of MIMO systems can thus be attained in a distributed fashion. Furthermore, cooperative communications can efficiently combat the severity of fading and shadowing effects through the cooperation of relay terminals. It has been shown that using the relay can extend the coverage of wireless networks Jaiswal, V. (2010). In parallel relays transmission, presented in Fig. 1.2, a number of relays help forward the transmitted data to the destination node. The authors in Surobhi, N. A. (2009), Kim, Y. & Liu, H. (2008) presented several relay configurations, such as serial and hybrid configurations. Cooperative communication dates back to the ground breaking work of Van der Meulen Van Der Meulen, E. C. (1971) in the 1970's, with his introduction of a relay channel model, consisting of one source, one destination and one relay; whose major objective was to facilitate data transfer from the source to the destination. Later, Cover and El Gamal Cover, T. M. & Gamal, A. E. (1979) intensively investigated the relay channel model, and proposed a number of fundamental relaying techniques such as DF.

Cooperative relaying known to be an efficient method to eliminate fading and to provide spatial diversity in wireless networks. DF and AF remain the most popular cooperative wireless protocols. Cooperative wireless relay networks have many applications in machine-to-machine (M2M), energy harvesting (EH), cognitive radio (CR), and V2V communication systems. In this thesis, we focus on V2V cooperative wireless relay networks because the inter-connected and autonomous vehicles of the future will need to exchange information at a high data rate and low latency in different vehicular wireless applications such as driver assistance, inter-vehicle communication, traffic management, road safety and video streaming.

## 1.2 Relaying Protocols

Relaying protocols users can be classified into two basic cooperative schemes:

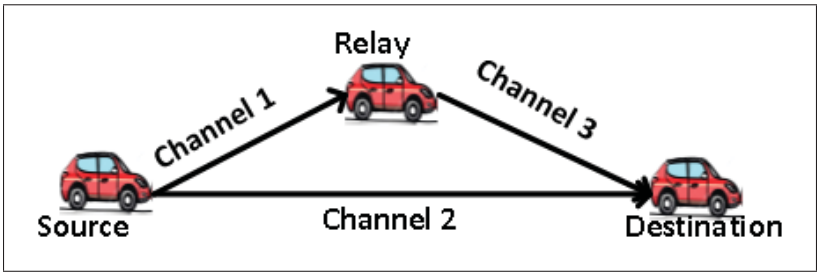


Figure 1.1 Vehicular cooperative communication system using one relay node

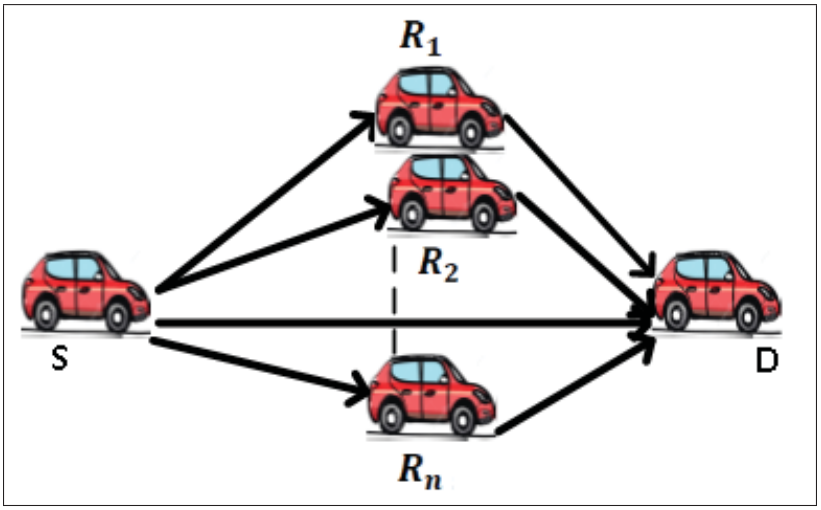


Figure 1.2 Vehicular cooperative communication system using multiple relays

### 1.2.1 Amplify-and-Forward Relaying

In the AF technique, as the name suggests, the relay simply transmits an amplified version of the received signal to the destination node. When a relay station has minimal computing power the AF technique could be ideal. However, the main drawback of this technique is that when the noise in the received signal is also amplified at the relay node, the destination receives two independently- faded versions of the signal Mahmood, A. (2010), shown in Fig. 1.3, the AF relaying scheme benefits from a simple implementation and low computational load for the relay nodes, with caveat that it amplifies the noise in the transmitted signal leading to some

performance deterioration Kim & Liu (2008). The instantaneous mutual information between source and destination can be written as Liu, K. R., Sadek, A. K., Su, W. & Kwasinski, A. (2009)

$$I_{AF} = 0.5\log_2(1+\gamma_{SD}+\gamma_{eq}) \tag{1.1}$$

and

$$\gamma_{eq} = \frac{\gamma_{SR}\gamma_{RD}}{\gamma_{SR}+\gamma_{RD}+1} \tag{1.2}$$

where $\gamma_{SD}$ is the SNR of S-D link, $\gamma_{SR}$ is the SNR of the S-R link, and $\gamma_{RD}$ is the SNR of the R-D link.

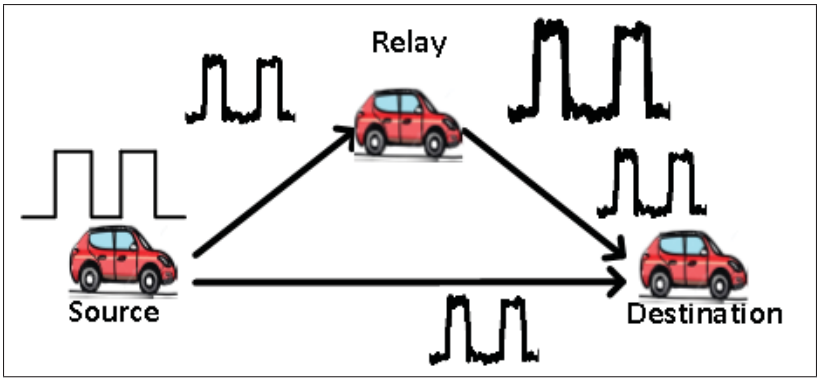


Figure 1.3 Amplify and forward relaying protocol

### 1.2.2 Decode-and-Forward Relaying

In the DF technique, shown in Fig. 1.4, the relay detects the received data from the source, decodes, re-encodes and then forwards it to the desired destination. An error-correcting code at the relay station can also be implemented. If the relay node has enough computing power, this step could help the relay node correct the received bit errors Mahmood (2010). The principal advantage of the DF relaying scheme is that the noise is not amplified and transmitted to the destination. The drawbacks of the DF relaying scheme are the error propagation at the relay node due to the possibility of erroneous decoding of the coded signals, and the high computational load on the relay terminals Kim & Liu (2008). The instantaneous mutual information

between the source and destination can be written as Liu *et al.* (2009)

$$I_{DF} = 0.5 \min[\log_2(1+\gamma_{SR}), \log_2(1+\gamma_{SD}+\gamma_{RD})] \tag{1.3}$$

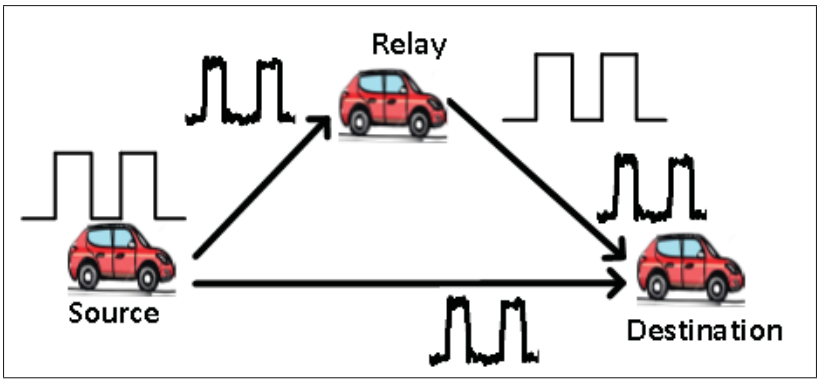


Figure 1.4 Decode and forward relaying protocol

## 1.3 Combining techniques

Combining the signals from different antennas at the receiver can be used to improve the total quality of the signal that is to be detected. Diversity combining that takes place in the radio frequency (RF) signals is called pre-detection combining, while diversity combining that takes place in the baseband is called post-detection combining. In this thesis, we are going to explore the pre-detection combining. There are several ways to exploit signals from multiple diversity branches:

### 1.3.1 Selective Combining

The best signal copy is selected to proceed (demodulated and decoded), while all other copies are discarded. Selection Combiner (SC) chooses the branch with the highest signal-to-noise ratio (SNR) (or equivalently, with the strongest signal assuming equal noise power among the branches). To obtain a significant diversity gain, independent fading in the channels should be achieved. Additionally, since the output of the SC is equal to the signal on only one of the

branches, the coherent sum of the individual branch signals is not required. Therefore, the SC scheme can be used in conjunction with differentially coherent and non-coherent modulation techniques since it does not require knowledge of the signal phases on each branch. Hence, SC presents the 'lower bound' of the diversity that can be achieved in a system. Though SC requires some sort of channel knowledge, it results in bandwidth savings. As mentioned in Ikki, S. S. & Ahmed, M. H. (2008), the SC technique has two important advantages over regular cooperative diversity networks i) it reduces the inefficient amount of used channel resources to the best relay node and ii) it maintains the full diversity order. Moreover, SC is implemented in vehicular communication to decrease the number of costly RF chains at the receiver side, where only a single RF chain needs to be employed at both the transmitter and the receiver nodes Alghorani, Y. & Seyfi, M. (2017). In SC, the destination selects the branch with the highest SNR and the available output is the signal transmitted from that selected branch Surobhi (2009), Molisch, A. F. (2012) and Jaiswal (2010).

### 1.3.2 Maximal Ratio Combining

Here, all the copies of the signal are combined (before or after the demodulation), and the combined signal is decoded. Maximal ratio combining (MRC) compensates for the phases, and weights the signals from the different antenna branches according to their SNR then sum them. Sometimes one of the branches has a much lower SNR than the other branches and this will reduce the overall SNR to a lower value at the output. In order to maximize the SNR at the output, each branch is adjusted with a weight before all the signals are combined coherently. In order to maximize the SNR at the output, a branch with a higher SNR will be given a higher weight. Here, the individual signals must be co-phased before being summed, which generally requires an individual receiver and phasing circuit for each antenna element. MRC produces an output SNR equal to the sum of the individual SNRs. Thus, it has the advantage of producing an output with an acceptable SNR even when none of the individual signals are themselves acceptable Rappaport, T. S. et al. (1996).

## 1.4 Transmission Modes

The transmission thorough the relay node can be classified into two basic modes as follow:

### 1.4.1 Half Duplex Mode

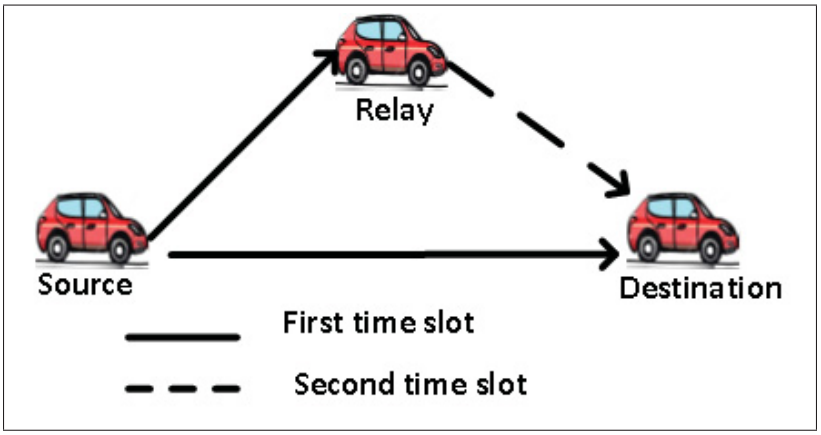


Figure 1.5 Half duplex V2V cooperative wireless communication

Traditional dual-hop relaying networks and base stations operate in the HD mode, where two orthogonal channels (i.e., in a time division duplex or frequency division duplex manner) are essential to initiate communications as shown in Fig. 1.5. In the first time slot, the source node transmits to the relay and destination nodes, just the relay node transmits to the destination node in the second time slot Laneman *et al.* (Dec. 2004); Laneman, J. (2006). In this context, the relays are subject to a spectral efficiency loss as they transmit and receive in different time slots or over different frequency bands.

### 1.4.2 Full Duplex Mode

Full duplex, also known as in-band full duplex relaying, techniques have recently become an interesting research area due to their ability to increase the spectral efficiency and reducing the end-to-end delay compared to half-duplex relaying Kim *et al.* (2015). This is because the relays avoid any spectral efficiency loss by transmitting and receiving over the same band si-

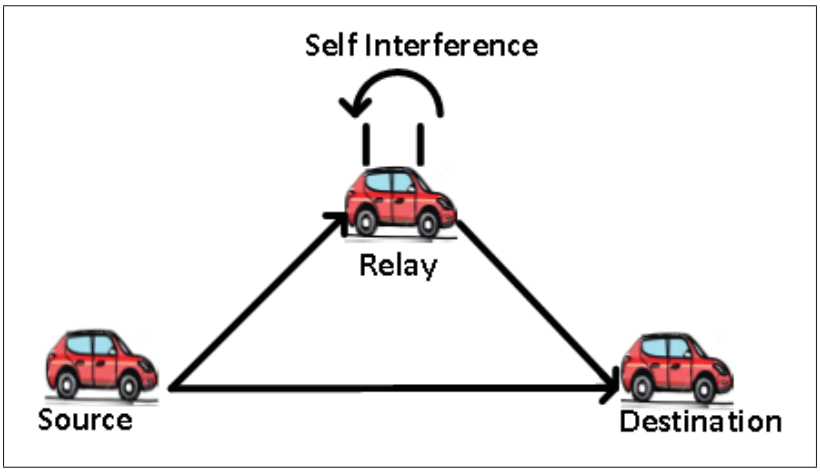


Figure 1.6 Full duplex V2V cooperative wireless communication

multaneously. However, the performance of FDR systems is affected by SI at the relay nodes, as shown in Fig. 1.6, which arises due to the simultaneous transmission and reception and cannot be perfectly eliminated, where the received signal is significantly weaker than the transmitted signal due to heavy path loss and fading Duarte & Sabharwal (Nov. 2010); Jain *et al.* (2011).

## 1.5 Millimeter Wave

The growth and expansion of intelligent transportation technologies for the next generation vehicular communications have brought with them a few key challenges. Focusing on inter-vehicle congestions during heavy traffic or accidents, an ultra-low latency transmission is vital to send ultra-fast warning messages within an extremely short time frame Yang, X., Liu, L., Vaidya, N. H. & Zhao, F. (2004). This is because the inter-connected and autonomous vehicles of the future will need to exchange information at a high data rate and low latency. In this context, emerging technologies have recently used mmWave frequency bands $(30-300)$ GHz to provide an alternative solution in order to offer both high data rates, of up to 7 Gbps in the frequency band (57-64 GHz) as shown in Fig. 1.7. The frequency bands were allocated by the U.S. Federal Communication Commission (FCC) Commission *et al.* (2001) for industrial,

scientific, and medical (ISM) applications, and low latency of less than 10 msec Ghosh, A., Thomas, T. A., Cudak, M. C., Ratasuk, R., Moorut, P., Vook, F. W., Rappaport, T. S., MacCartney, G. R., Sun, S. & Nie, S. (2014). Correspondingly, as a part of the fifth generation (5G) of wireless communications, millions of autonomous and semi-autonomous vehicles will be connected to engage with future ITS services. In this context, operating in the mmWave range of the radio frequency spectrum has been proposed as a viable solution for overcoming the rate and latency limitations of existing V2V communications Tassi *et al.* (2017).

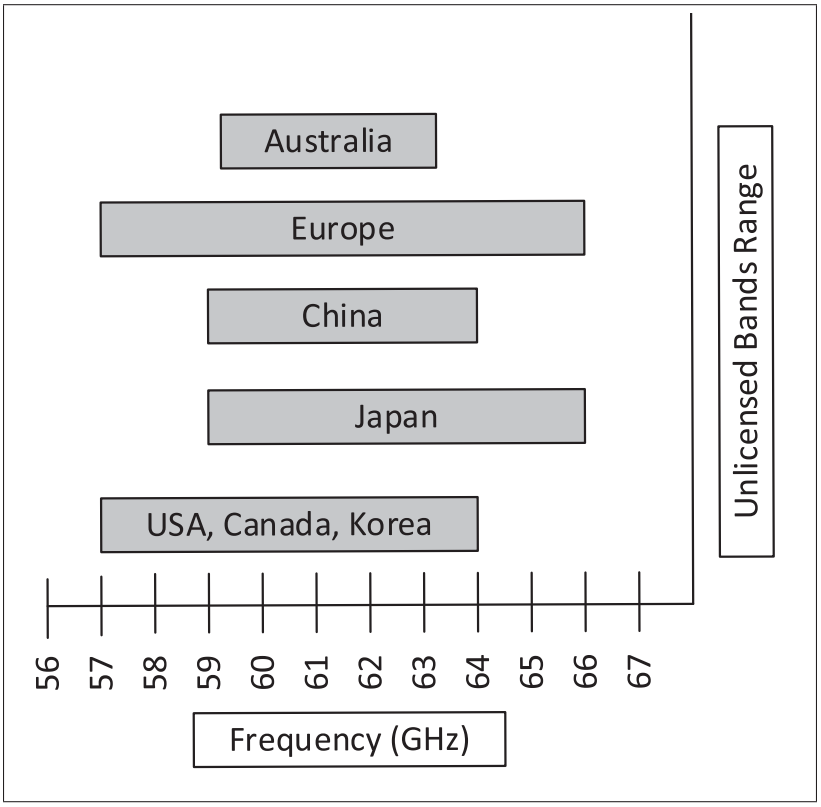


Figure 1.7 Unlicensed frequency bands allocations

## 1.6 V2V Communications

In the context of vehicular communications, several V2V half-duplex relaying (HDR) techniques have been studied and investigated in the literature. The communication between the source-destination (*S-D*) nodes could be established by a road access point (AP) Ilhan, H., Al-

tunbas, I. & Uysal, M. (2008), a mobile vehicle Li, Z., Zhao, Y., Chen, H. & Hu, H. (2010) or multiple mobile vehicles in Akin, A. I., Ilhan, H. & Özdemir, Ö. (2015). The authors in Ilhan, H., Uysal, M. & Altunbas, I. (2009) studied two different cooperative relaying schemes. In the first scheme, the V2V communication is assisted by an AP, while in the second one, V2V is assisted by relaying vehicles where only the bit error rate (BER) is analysed over double Nakagami-$m$ fading channels.

Moreover, the authors in Nguyen, S. Q. & Kong, H. Y. (2016) present a V2V dual-hop cooperative network with decode-and-forward (DF) relaying, where the communication between the two vehicles is assisted by the vehicles within one cluster and by APs acting as relays in adjacent clusters. In Ilhan, H. (2015), the authors present V2V DF relaying cooperative wireless communication over Cascaded Nakagami-$m$ channels. The performance of multi-hop V2V cooperative wireless communications over cascaded Rayleigh fading channels was considered in Alghorani, Y., Kaddoum, G., Muhaidat, S., Pierre, S. & Al-Dhahir, N. (2016), and a V2V multiple-input and multiple-output (MIMO) channel model was investigated in Alghorani & Seyfi (2017). Additionally, a two-way HDR V2V wireless communication scheme over double-Rayleigh fading channels was proposed in Shakeri, R., Khakzad, H., Taherpour, A. & Gazor, S. (2014), and over mixed Nakagami$-m$ and double Nakgamai$-m$ channels in Hu, Y., Li, H., Zhang, C. & Li, J. (2014b). The performance of V2V communication in a single dense lane topology was examined in Pitsiladis, G. T., Papanikolaou, D., Panagopoulos, A. D. & Antoniou, C. (2015), while Farooq, M. J., ElSawy, H. & Alouini, M.-S. (2016) proposed a multi-lane topology with different packet forwarding schemes. Within the scope of peer-to-peer V2V communications, the impacts of co-channel interference and imperfect channel estimation are studied over Rice distribution in Bithas, P. S., Efthymoglou, G. P. & Kanatas, A. G. (Kuala Lumpur, Malaysia 2016). In Eshteiwi, K., Ben Fredj, K., Kaddoum, G. & Gagnon, F. (Sep. 2017), an exact expression is derived for the PDF of peer-to-peer V2V communications taking into account the impact of interference and then used to obtain the BER.

In both V2V and V2I communications, the relays can be vehicles or fixed units (or a combination of the two). A dual-hop V2V cooperation assisted by a single roadside fixed relay was

studied in Ilhan *et al.* (2008) and the BER was analysed, while in Tirkan, Z., Shirkhani, M., Taherpour, A. & Uysal, M. (2012), V2V communications assisted by a vehicle relay was considered and an optimum power allocation was applied to minimize the BER. A relay selection in V2V communications with DF relaying was represented in Seyfi, M., Muhaidat, S., Liang, J. & Uysal, M. (2011) over cascaded Rayleigh fading channels. The outage probability was derived for the proposed system when perfect channel estimation is available at the destination node.

In Hu *et al.* (2014b), a roadside-based two-way partial relay selection scheme was proposed with AF relaying. The asymptotic outage probability and closed form symbol error rate were obtained over non-identical channels such as Nakagami$-m$ and double Nakagami$-m$. Moreover, a relay cooperation scheme was analyzed in Ilhan *et al.* (2009) where vehicles or fixed roadside units act as intermediate terminals to forward the received information to the destination in V2V wireless communications. In this context, AF relaying was used over double Nakagami-*m* fading channels. The performance of one-way multi-hop V2V communication was investigated in Alghorani, Y., Kaddoum, G., Muhaidat, S., Pierre, S. & Al-Dhahir, N. (2015b) over cascaded Rayleigh distributed channels and a closed form of the outage probability was obtained. In addition, the authors in Boban *et al.* (2011) proposed an experimental vehicular communication system where other vehicles act as obstacles to model a V2V channel. Different distances between transmitter (Tx) and receiver (Rx) were assumed and both line of sight (LOS) and non-line of sight (NLOS) cases considered to analyze the strength of the received signal.

The authors in Tadayon, N. & Kaddoum, G. (2018) presented a packet-level modeling of cooperative communications using different cooperative protocols such as AF, DF and opportunistic-relaying, and evaluated their performance in terms of delay, throughput, and buffer length. Meanwhile, the authors in Le, T.-D. & Kaddoum, G. (2020) proposed a distributed access algorithm to maximize the vehicle utility by using the optimal access control of vehicles in V2I systems. The authors in Kaur, K., Garg, S., Kaddoum, G., Kumar, N. & Gagnon, F. (2019) presented an efficient approach to minimize the energy and load balancing by deploying multiple

software-defined networking (SDN) technology for internet of autonomous vehicles (IoAV). Moreover, the authors in Garg, S., Kaur, K., Kaddoum, G., Ahmed, S. H. & Jayakody, D. N. K. (2019b) designed a SDN for two sets of security modules such as authentication module and intrusion detection module, to provide end-to-end security and privacy in 5G enabled vehicular networks.

Overall, FDR-based vehicular communication is still in its infancy and very few works have been published, especially from the physical layer and performance analysis perspectives. Therefore, the current literature is limited to the V2V HD scenario, except for the case of Mafra, S. B., Fernandez, E. M. & Souza, R. D. (2016), where the authors presented simulation results of a V2V full duplex relay selection wireless cooperative communication using joint decoding as proposed in Khafagy, M., Ismail, A., Alouini, M. S. & Aissa, S. (2013). In Bazzi, A., Masini, B. M. & Zanella, A. (2015), the authors investigated the long term evolution (LTE) technique for V2V beaconing services by exploiting full duplex direct communications, while analyzing the joint resource assignment and power allocation problems for full duplex vehicular communication from a medium access control (MAC) layer perspective in Yang, T., Zhang, R., Cheng, X. & Yang, L. (2016).

## 1.7 V2V Fading Channels

Vehicular networks, with their numerous multimedia and safety applications, promise to revolutionize our modern lives. However, high data rate applications still face substantial challenges since vehicular wireless transmissions are severely degraded by fading. In fact, it was shown that fading effects in V2V channels follow a cascaded channel model such as the $L$-Nakagami-$m$ fading model Karagiannidis, G. K., Sagias, N. C. & Mathiopoulos, P. T. (2007). Consequently, fading effects in V2V communications are much more challenging than in cellular communications, due to the multiplication of the channel gains of independent scattering groups around mobile units Molisch, A. F., Tufvesson, F., Karedal, J. & Mecklenbrauker, C. F. (2009). Thus, cooperative relaying was introduced as a promising solution that can potentially increase the capacity and radio coverage area with minimal increment in the capital expendi-

ture. In this context, two-way HD dual-hop mobile-to-mobile communications over cascaded Nakagami-*m* channels using AF relaying were studied in Zhang, C., Ge, J., Li, J. & Hu, Y. (2013), while vehicular communications over cascaded Nakagami-*m* using fixed gain AF relaying and employing physical layer network coding were analysed in Ata, S. Ö. & Altunbaş, İ. (2016). The performance of multi-hop V2V wireless cooperative communications over cascaded Rayleigh fading channels was considered in Alghorani *et al.* (2016), and a MIMO-based V2V cascaded Rayleigh fading channel model was investigated in Alghorani & Seyfi (2017). In addition, due to the motion of both transmitter and receiver in M2M communications which leads scattering of the signal, a double-bouncing procedure was modeled as a product of fading amplitudes Andersen, J. B. (2002) and was investigated by numerous works such as double-Nakagami Karagiannidis *et al.* (2007), double generalized Gamma distribution Bithas, P. S., Kanatas, A. G., da Costa, D. B., Upadhyay, P. K. & Dias, U. S. (2017), double-Rayleigh Salo, J., El-Sallabi, H. M. & Vainikainen, P. (2006), and double Weibull Sagias, N. C. & Tombras, G. S. (2007). Additionally, a two-way HDR V2V wireless communication scheme over double-Rayleigh fading channels was proposed in Shakeri *et al.* (2014), and over mixed Nakagami$-m$ and double Nakgamai$-m$ channels in Hu *et al.* (2014b). Although instructive, these works do not consider full duplex AF relaying over the realistic case of generalized cascaded Nakagami-*m* channels.

On the other hand, the Nakagami-*m* fading channel model was widely used to model cooperative vehicular communications and short-range communications Eshteiwi *et al.* (2019); Eshteiwi, K., Kaddoum, G. & Alam, M. (2020); Eshteiwi *et al.* (Sep. 2017); He, R., Molisch, A. F., Tufvesson, F., Zhong, Z., Ai, B. & Zhang, T. (2014); Mafra *et al.* (2016); Tassi *et al.* (2017). Furthermore, the Nakagami$-m$ distribution is a more general model which can be used to describe many fading distributions such as Rician, Rayleigh or fading environments that are more severe than Rayleigh fading Cheng, L., Henty, B. E., Stancil, D. D., Bai, F. & Mudalige, P. (2007).

# CHAPTER 2

# FULL DUPLEX RELAYING OF V2V OVER CASCADED NAKGAMAI-*M* FADING CHANNELS

Khaled Eshteiwi [1], Sleim Bassant[1], and Georges Kaddoum [1]

[1] Département de Génie Electrique, École de technologie supérieure,
1100 Notre-Dame Ouest, Montréal, Québec, H3C 1K3, Canada
Accepted in IEEE International Symposium on Networks, Computers and Communications (ISNCC'20), March, 2020.

## 2.1 Abstract

In this paper, we consider full duplex amplify and forward (AF) relay networks in vehicle-to-vehicle (V2V) applications. In this context, taking into account the self-interference (SI) at the relay and assuming independent and not necessarily identically distributed (i.n.i.d) generalized *L*-Nakagami-*m* fading channels, we derive novel expressions for the probability density function (PDF) and cumulative distribution function (CDF) of the signal-to-interference-plus-noise ratio at the relay. Capitalizing on this, a lower bound to the end-to-end outage probability is derived. Monte-Carlo simulation results are presented to corroborate the derived analytical results. Our results show that the channel cascading significantly impacts the end-to-end outage probability of FD relaying V2V systems, where the cascading of the source-relay link is shown to be more significant than the relay-destination link.

## 2.2 Introduction

Vehicular networks, with their numerous multimedia and safety applications, promise to revolutionize our modern lives. However, high data rate applications still face substantial challenges since vehicular wireless transmissions are severely degraded by fading. In fact, it was shown that fading effects in vehicle-to-vehicle (V2V) channels follow a cascaded channel model such as the *L*-Nakagami-*m* fading model, which has been shown to accurately characterize the statistical properties of V2V fading channels Karagiannidis *et al.* (2007). Consequently, fading

effects in V2V communications are much more challenging than in cellular communication, due to the multiplication of the channel gains of independent scattering groups around mobile units Molisch *et al.* (2009). Thus, cooperative relaying was introduced as a promising solution which can potentially increase the capacity as well as radio coverage area with minimal increment in the capital expenditure.

In this context, two-way half duplex dual-hop mobile-to-mobile (M2M) communications over cascade Nakagami-*m* and using amplify-and-forward (AF) relaying was studied in Zhang *et al.* (2013), and for vehicular communication over cascade Nakagami-*m* using fixed gain AF relaying and employing physical layer network coding was analysed in Ata & Altunbaş (2016). The performance of multi-hop V2V wireless cooperative communications over cascade Rayleigh fading channels was considered in Alghorani *et al.* (2016), and a V2V multiple-input and multiple-output (MIMO) cascaded Rayleigh fading channel model was investigated in Alghorani & Seyfi (2017).

Additionally, a two-way half duplex relaying (HDR) V2V wireless communication scheme over double-Rayleigh fading channels was proposed in Shakeri *et al.* (2014), and over mixed Nakagami$-m$ and double Nakgamai$-m$ channels in Hu *et al.* (2014b). Although instructive, these works do not consider full duplex AF relaying over the realistic case of generalized cascaded Nakagami-*m* channels.

In this paper, we analyse the performance of full duplex AF relaying V2V wireless communications over cascaded Nakagami-*m* channels with self-interference (SI) at the relay. To do so, we derive novel expressions for the signal-to-interference-plus-noise ratio (SINR) probability density function (PDF) and cumulative distribution function (CDF) for the considered full duplex relaying scenario and proceed to deriving a novel expression for the lower bound of the end-to-end outage probability of the system. This study is of paramount importance in order to set the practical limits of full duplex AF V2V communication systems, providing much needed pragmatic information to the system designer to improve the system performance. It is shown that the channel cascading significantly degrades the outage probability performance of the

system which highlight the importance of deriving analytical expressions considering realistic fading conditions in V2V such as the $L$-Nakagami-$m$ fading channel.

## 2.3 System Model

We consider a full duplex V2V communication scenario, depicted in Fig. 3.1, where a source $S$ communicates with a destination $D$ via an amplify-and-forward (AF) relay $R$, where there is no direct link between $S$ and $D$. Here, $S$, $R$, and $D$ are assumed to be in motion, where the $S$-$R$, $R$-$R$ and $R$-$D$ channels follow the cascaded Nakagami-$m$ fading model. In this context, the relay node is assumed to be equipped with a pair of antennas, one serving the purpose of transmitting while the other is receiving. Thus, the received signal at $R$ is corrupted by self-interference due to the simultaneous transmission/reception which characterizes the full duplex transmission mode. In this context, the received signal at $R$ is given as

$$y_{SRR} = \sqrt{P_S} h_{SR} x_S + \sqrt{P_R} h_{RR} x_R + n_R, \tag{2.1}$$

where $x_S$ and $x_R$ are the transmitted BPSK signals and $P_S$ and $P_R$ the transmit powers at $S$ and $R$, respectively. Also, $h_{SR}$ and $h_{RR}$ are the channel coefficients for the $S$-$R$ and the self-interference $R$-$R$ links, respectively. These are modeled as mutually i.n.i.d $L$-Nakagami$-m$ random variables. The term $n_R$ corresponds to the additive white Gaussian noise (AWGN) at $R$ with variance $N_o$. The relay amplifies the signal received from $S$ and transmits it to $D$; therefore, at the destination side, the received signal from $R$ is obtained as

$$y_D = \sqrt{P_R} h_{RD} \kappa y_{SRR} + n_D, \tag{2.2}$$

where $h_{RD}$ is the channel coefficient of the $R$-$D$ link, $n_D$ is the AWGN at $D$ with variance $N_o$, and $\kappa$ is the amplification factor at $R$ which satisfies $\kappa \leq \sqrt{P_R/(P_S |h_{SR}|^2 + P_R |h_{RR}|^2 + N_o}$. In this study, we employ the normalized distance model Laneman *et al.* (Dec. 2004) to take

into account the impact of pathloss which implies that $\mathbb{E}(|h_{ij}|^2) = (d_{SD}/d_{ij})^{\eta}$, where $d_{ij}$ is the relative distance from $i$ to $j$, $ij \in \{SR, RR, RD\}$, and $\eta$ is the pathloss exponent.

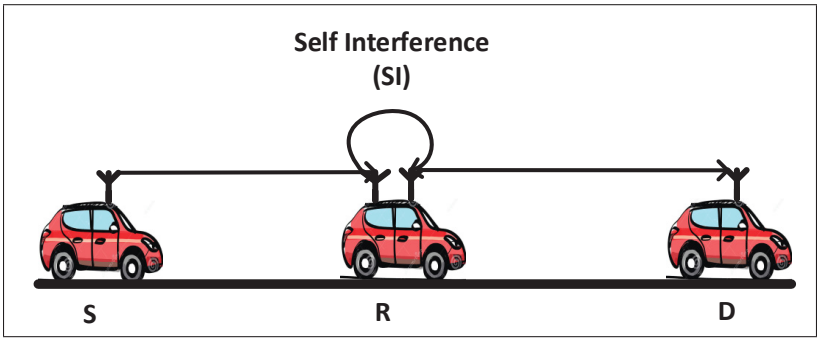


Figure 2.1 Diagram of the considered V2V full duplex relay network

## 2.4 Performance Analysis

In this section, we present an analysis of the outage performance of the considered system. First, we derive both PDF and CDF expressions for the SINR of the *S-R* link including the self-interference Eshteiwi *et al.* (Sep. 2017). Once the CDF is obtained, the corresponding outage probability expression is derived.

### 2.4.1 PDF of the *S-R* link including self interference

Here, we derive the SINR PDF of the *S-R* link including self-interference. According to Eq. (2.1), the received SINR at the relay node, $\gamma_{SRR}$ is formulated as

$$\gamma_{SRR} = \frac{\gamma_{SR}}{\gamma_{RR}+1}, \tag{2.3}$$

where $\gamma_{SR} = P_S |h_{SR}|^2 / N_o$ and $\gamma_{RR} = P_R |h_{RR}|^2 / N_o$ are the instantaneous SNR of *S-R* and *R-R* (loop interference) links respectively. The channel coefficients in the proposed system are modelled as $L$-Nakagami$-m$ distribution. Since the channels are independent and not identi-

cally distributed (i.n.i.d), the PDF of $\gamma_{SR}$ and $\gamma_{RR}$ can be respectively evaluated as Karagiannidis *et al.* (2007)

$$f_{\gamma_{SR}}(x) = \frac{G_{0,L_{SR}}^{L_{SR},0}\left(\underset{m_1,m_2,....m_{L_{SR}}}{-}\middle|\frac{x}{\bar{\gamma}_{SR}}\prod_{i=1}^{L_{SR}} m_i\right)}{x\prod_{i=1}^{L_{SR}}\Gamma(m_i)}, \tag{2.4}$$

and

$$f_{\gamma_{RR}}(x) = \frac{G_{0,L_{RR}}^{L_{RR},0}\left(\underset{m_1,m_2,....m_{L_{RR}}}{-}\middle|\frac{x}{\bar{\gamma}_{RR}}\prod_{j=1}^{L_{RR}} m_j\right)}{x\prod_{j=1}^{L_{RR}}\Gamma(m_j)}, \tag{2.5}$$

where $m_i$ is the shape parameter, $\bar{\gamma}_{ij} = \frac{P_i}{N_o}\prod_{ij=0}^{L_{ij}}\Omega_{ij}$, $\Omega_{ij} = \mathbb{E}(|h_{ij}|^2)$, $L_{ij}$ is cascading degree, and $G_{0,L_{ij}}^{L_{ij},0}(\cdot|\cdot)$ is Meijer's G-function (Jeffrey, A. & Zwillinger, D., 2007, Eq. (9.301)). Here, the PDF of the ratio of two i.n.i.d $L$-Nakagami$-m$ random variables (RVs) in Eq.(2.3) can be written as Eshteiwi *et al.* (Sep. 2017)

$$f_{\gamma_{SRR}}(x) = \int_0^\infty (y+1) f_{\gamma_{SR}}(x(y+1)) f_{\gamma_{RR}}(y)\, dy. \tag{2.6}$$

Substituting Eq. (2.4) and Eq. (2.5) into Eq. (2.6) and setting $\beta = \frac{x}{\bar{\gamma}_{SR}}\prod_{i=1}^{L_{SR}} m_i$, $\zeta = \frac{1}{\bar{\gamma}_{RR}}\prod_{j=1}^{L_{RR}} m_j$, and $\tau = \beta y$ and after some mathematical manipulations, we get

$$f_{\gamma_{SRR}}(x) = \frac{1}{x\left(\prod_{i=1}^{L_{SR}} m_i \prod_{j=1}^{L_{RR}} m_j\right)} I_1, \tag{2.7}$$

where

$$I_1 = \int_0^\infty \tau^{-1} G_{0,L_{SR}}^{L_{SR},0}\left(\underset{m_1,m_2,....m_{L_{SR}}}{-}\middle|\tau+\beta\right) G_{0,L_{RR}}^{L_{RR},0}\left(\underset{m_1,m_2,....m_{L_{RR}}}{-}\middle|\frac{\tau\zeta}{\beta}\right) d\tau. \tag{2.8}$$

$I_1$ can be solved using (Prudnikov, A., Brychkov, Y. & Marichev, O., 1990, Eq. (2.24.1.3)), and consequently, we obtain the PDF of $f_{\gamma_{SRR}}(x)$ as shown in Eq. (2.9).

$$f_{\gamma_{SRR}}(x) = \frac{1}{x\prod_{i=1}^{L_{SR}} m_i \prod_{j=1}^{L_{RR}} m_j} \sum_{k=0}^{\infty} \frac{(-1)^k}{k!} \left( \frac{x}{\bar{\gamma}_{SR} \prod_{i=1}^{L_{SR}} m_i} \right)^k \times G_{L_{SR}+1, L_{RR}+1}^{L_{RR}, L_{SR}+1} \left( \begin{matrix} 1, k-m_1+1, \ldots, k-m_{L_{SR}}+1 \\ m1, \ldots . m_{L_{RR}}, k+1 \end{matrix} \middle| \frac{\bar{\gamma}_{SR} \prod_{j=1}^{L_{RR}} m_j}{x\bar{\gamma}_{RR} \prod_{i=1}^{L_{SR}} m_i} \right). \tag{2.9}$$

### 2.4.2 CDF of the *S*-*R* link including self interference

Here, we derive the CDF expression for the *S*-*R* link including self-interference, the CDF can be written as

$$F_{\gamma_{SRR}}(x) = \int_0^{\infty} F_{\gamma_{SR}}(x(y+1)) f_{\gamma_{RR}}(y)\, dy, \tag{2.10}$$

where the CDF of $\gamma_{SR}$ is given by

$$F_{\gamma_{SR}}(x) = \frac{G_{1, L_{SR}+1}^{L_{SR}, 1} \left( \begin{matrix} 1 \\ m_1, m_2, \ldots . m_{L_{SR}}, 0 \end{matrix} \middle| \frac{x}{\bar{\gamma}_{SR}} \prod_{i=1}^{L_{SR}} m_i \right)}{\prod_{i=1}^{L_{SR}} \Gamma(m_i)}. \tag{2.11}$$

Substituting Eq. (2.5) and Eq. (2.11) into Eq. (2.10), and following mathematical simplifications, we get

$$F_{\gamma_{SRR}}(x) = \left( \prod_{i=1}^{L_{SR}} m_i \prod_{j=1}^{L_{RR}} m_j \right)^{-1} I_2, \tag{2.12}$$

where

$$I_2 = \int_0^{\infty} \tau^{-1} G_{1, L_{SR}+1}^{L_{SR}, 1} \left( \begin{matrix} 1 \\ m_1, m_2, \ldots . m_{L_{SR}}, 0 \end{matrix} \middle| \tau + \beta \right) G_{0, L_{RR}}^{L_{RR}, 0} \left( \begin{matrix} - \\ m_1, m_2, \ldots . m_{L_{RR}} \end{matrix} \middle| \frac{\tau\zeta}{\beta} \right) d\tau. \tag{2.13}$$

$I_2$ can be solved using (Prudnikov *et al.*, 1990, Eq. (2.24.1.3)) and thus, we get CDF of $F_{\gamma_{SRR}}(x)$ as shown in Eq. (2.14).

$$F_{\gamma_{SRR}}(x) = \frac{1}{\prod_{i=1}^{L_{SR}} m_i \prod_{j=1}^{L_{RR}} m_j} \sum_{k=0}^{\infty} \frac{(-1)^k}{k!} \left( \frac{x}{\bar{\gamma}_{SR}} \prod_{i=1}^{L_{SR}} m_i \right)^k \times G_{L_{SR}+2, L_{RR}+2}^{L_{RR}+1, L_{SR}+1} \left( \begin{matrix} 1, k-m_1+1, \ldots, k-m_{L_{SR}}+1, k+1 \\ m_1, \ldots . m_{L_{RR}}, k, k+1 \end{matrix} \middle| \frac{\bar{\gamma}_{SR} \prod_{j=1}^{L_{RR}} m_j}{x \bar{\gamma}_{RR} \prod_{i=1}^{L_{SR}} m_i} \right). \tag{2.14}$$

### 2.4.3 Outage probability

We define the outage probability as the probability that the equivalent SINR of the received signal at the destination is smaller than a predefined threshold $\gamma_{th} = 2^{R_T} - 1$, where $R_T$ is the target rate in bits/sec/Hz. According to Eq. (2.2), the equivalent instantaneous SINR of the received signal at $D$, $\gamma_{eq}$, can be written as

$$\gamma_{eq} = \frac{\gamma_{SRR}\gamma_{RD}}{\gamma_{SRR} + \gamma_{RD} + 1}, \tag{2.15}$$

where $\gamma_{RD} = P_R |h_{RD}|^2 / N_o$. The exact outage probability derivation is very complicated and untractable, therefore we will consider a lower bound to SINR in this article. The equivalent SINR can be upper bounded by Ikki, S. & Ahmed, M. H. (2007)

$$\gamma_{eq} \leq \gamma_{up} = \min(\gamma_{SRR}, \gamma_{RD}). \tag{2.16}$$

Therefore, the outage probability can be written as

$$P_{\gamma_{up}}(\gamma_{th}) = P(\gamma_{up} \leq \gamma_{th}). \tag{2.17}$$

Inserting Eq. (2.16) into Eq. (2.17), the outage probability of the equivalent SINR is lower-bounded by

$$\begin{aligned} P_{\gamma_{up}}(\gamma_{th}) &= \Pr(\min(\gamma_{SRR}, \gamma_{RD}) \leq \gamma_{th}) \\ &= 1 - (1 - F_{\gamma_{SRR}}(\gamma_{th}))(1 - F_{\gamma_{RD}}(\gamma_{th})), \end{aligned} \tag{2.18}$$

where $F_{\gamma_{SRR}}(\gamma_{th})$ is previously defined in (2.14) and $F_{\gamma_{RD}}(\gamma_{th})$ can be written as Karagiannidis *et al.* (2007)

$$F_{\gamma_{RD}}(\gamma_{th}) = \frac{G_{1,L_{RD}+1}^{L_{RD},1}\left(\left.{}_{m_1,m_2,\ldots,m_{L_{RD}},0}^{1}\right| \frac{\gamma_{th}}{\bar{\gamma}_{RD}} \prod_{i=1}^{L_{RD}} m_i\right)}{\prod_{i=1}^{L_{RD}} \Gamma(m_i)}. \tag{2.19}$$

Substituting Eq. (2.14) and Eq. (2.19) into Eq. (2.18), we obtain the outage probability lower bound as shown in Eq. (2.20).

$$\begin{aligned} P_{\gamma_{up}}(\gamma_{th}) = {} & \frac{1}{\prod_{i=1}^{L_{SR}} m_i \prod_{j=1}^{L_{RR}} m_j} \sum_{k=0}^{\infty} \frac{(-1)^k}{k!} \left(\frac{\gamma_{th}}{\bar{\gamma}_{SR}} \prod_{i=1}^{L_{SR}} m_i\right)^k G_{L_{SR}+2,L_{RR}+2}^{L_{RR}+1,L_{SR}+1}\left(\left.{}_{m_1,\ldots m_{L_{RR}},k,k+1}^{1,k-m_1+1,\ldots,k-m_{L_{SR}}+1,k+1}\right| \frac{\bar{\gamma}_{SR} \prod_{j=1}^{L_{RR}} m_j}{\gamma_{th} \bar{\gamma}_{RR} \prod_{i=1}^{L_{SR}} m_i}\right) \\ & + \frac{G_{1,L_{RD}+1}^{L_{RD},1}\left(\left.{}_{m_1,m_2,\ldots m_{L_{RD}},0}^{1}\right| \frac{\gamma_{th}}{\bar{\gamma}_{RD}} \prod_{i=1}^{L_{RD}} m_i\right)}{\prod_{i=1}^{L_{RD}} \Gamma(m_i)} - \frac{1}{\prod_{i=1}^{L_{SR}} m_i \prod_{j=1}^{L_{RR}} m_j} \sum_{k=0}^{\infty} \frac{(-1)^k}{k!} \left(\frac{\gamma_{th}}{\bar{\gamma}_{SR}} \prod_{i=1}^{L_{SR}} m_i\right)^k \\ & \times G_{L_{SR}+2,L_{RR}+2}^{L_{RR}+1,L_{SR}+1}\left(\left.{}_{m_1,\ldots m_{L_{RR}},k,k+1}^{1,k-m_1+1,\ldots,k-m_{L_{SR}}+1,k+1}\right| \frac{\bar{\gamma}_{SR} \prod_{j=1}^{L_{RR}} m_j}{\gamma_{th} \bar{\gamma}_{RR} \prod_{i=1}^{L_{SR}} m_i}\right) \frac{G_{1,L_{RD}+1}^{L_{RD},1}\left(\left.{}_{m_1,\ldots m_{L_{RD}},0}^{1}\right| \frac{\gamma_{th}}{\bar{\gamma}_{RD}} \prod_{i=1}^{L_{RD}} m_i\right)}{\prod_{i=1}^{L_{RD}} \Gamma(m_i)}. \end{aligned} \tag{2.20}$$

## 2.5 Simulation Results

In this section, we present the numerical results of the analytical outage probability of V2V wireless networks where BPSK modulation is considered. We consider a full duplex relaying (FDR) network where the source communicates with the destination via an AF including SI at the relay node. Moreover, the channels are assumed to follow i.n.i.d generalized $L$-Nakagami-$m$ fading channels and a path loss exponent of $\eta = 3.18$. In addition, the system simulation setup includes the average SI of $\overline{\gamma}_{RR} = 5$ dB, shape parameter $m_{ij} = 2$, and we have $d_{SR} + d_{RD} = 1$, where $d_{SR} = 0.5$. Without loss of generality, all AWGN terms are assumed to be zero-mean complex Gaussian random variables with equal variances $N_o$ and $R_T = 1$ bit/sec/Hz. In all forthcoming results, Monte-Carlo simulation using $10^6$ samples are presented to corroborate the derived analytical results where, unless otherwise stated, the derived analytical expressions are represented by solid lines with markers whereas the dashed lines depict the corresponding simulation results.

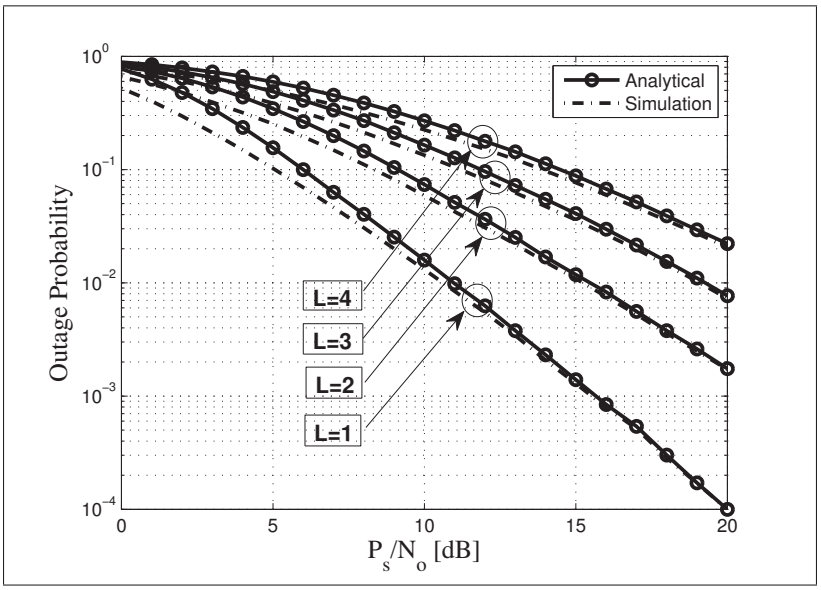


Figure 2.2 Outage probability vs. $P_S/N_o$ for different values of $L$ with $\overline{\gamma}_{RR} = 5$ dB, $m_{ij} = 2$, $d_{SR} = 0.5$, $d_{RD} = 0.5$, and $\eta = 3.18$

Fig. 2.2 depicts the outage probability of the considered dual-hop FDR V2V cooperative communication system versus $P_S/N_o$ for different asymmetric values of $L$, the derived lower bound is tightly characterizes the actual performance of the system, especially at medium and high $P_S/N_o$ values. In addition, from the obtained results it is observed that the outage performance is significantly affected by the cascading effect where, increasing $L$ leads to a degradation in the system performance. For instance, in order to obtain an outage probability of $10^{-2}$, the SNR should be increased of approximately 5 dB and 4 dB when the channel goes from Nakagami-$m$ to double Nakagami-$m$ and from double Nakagami-$m$ to $L$-Nakagami-$m$ with $L = 3$, respectively.

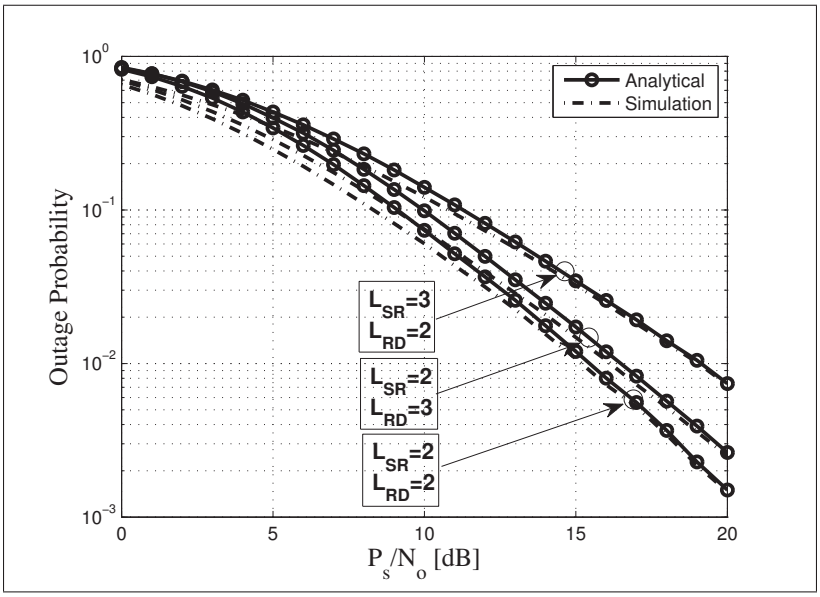


Figure 2.3 Outage probability vs. $P_S/N_o$ for different values of $L_{SR}$ and $L_{RD}$ with $\overline{\gamma}_{RR} = 5$ dB, $m_{ij} = 2$, $d_{SR} = 0.5$, $d_{RD} = 0.5$, and $\eta = 3.18$

Fig. 2.3 shows the outage probability of the considered system for different $L_{SR}$ and $L_{RD}$. Interestingly, it is observed that the effect of cascading on the end-to-end outage probability are more pronounced for the source-relay link are more pronounced than the relay-destination link. For instance, it is observed that for a target outage probability of $10^{-2}$, there is a $P_S/N_o$

loss of nearly 4dB when $L_{SR}$ is increased from 2 to 3. This is due to the considered AF relaying protocol.

## 2.6 Conclusions

In this paper, we analyzed the performance of full duplex V2V wireless communications using AF relaying over i.n.i.d generalized $L$-Nakagami-$m$ fading channels. Self-interference at the relay was taken into account where novel PDF and CDF expressions for the SINR at the relay were derived. Moreover, a lower bound expression to the end-to-end outage probability was derived. Our results show the significant impact cascaded channels on the end-to-end outage probability of the system. This highlights the importance of accurately characterizing the channel in the analysis of the considered cooperative V2V communication scenario in order to evaluate the practical limits of such systems.

# CHAPTER 3

# IMPACT OF CO-CHANNEL INTERFERENCE AND VEHICLES AS OBSTACLES ON FULL-DUPLEX V2V COOPERATIVE WIRELESS NETWORK

Khaled Eshteiwi [1], Georges Kaddoum[1], Sleim Bassant[1], and François Gagnon [1]

[1] Département de Génie Electrique, École de technologie supérieure,
1100 Notre-Dame Ouest, Montréal, Québec, H3C 1K3, Canada
Article accepted in IEEE Transactions on Vehicular Technology, May, 2020.

## 3.1 Abstract

Vehicular communications, with their promise to provide drivers and passengers with a wide range of applications, are attracting significant attention from both research and industry. In this paper, we study the performance of full duplex amplify and forward (AF) relaying-based vehicle-to-vehicle (V2V) cooperative wireless communications over Nakagami-*m* fading channels. In such systems, in practical scenarios, the communication link inevitably suffers from co-channel interference, residual self-interference, and blockage from other vehicles on the road. In this context, we consider independent and not necessarily identically distributed (i.n.i.d) Nakagami-*m* fading channels and derive novel exact and asymptotic outage probabilities of the exact equivalent and approximated signal-to-interference-plus-noise ratio (SINR), respectively. Building on this, the end-to-end exact and asymptotic outage probabilities are expressed in terms of the blockage probability and then used to evaluate the throughput of the proposed system. In addition, a lower bound to the symbol error rate of the considered system is also derived. Monte-Carlo simulation results are provided to demonstrate the accuracy of the proposed analytical expressions. The results demonstrate the significant impact of the considered interference and blockage on the system performance. Precisely, it is shown that the system performance is degraded when the average height of the obstacles is increased. This highlights the importance of taking into account these phenomena in the performance evaluation in order to assess the practical limit of V2V cooperative wireless communications.

## 3.2 Introduction

Vehicular Ad-Hoc NETworks (VANETs), with their numerous applications and limitless potential, including intelligent transportation systems (ITSs), are anticipated to enable several applications such as vehicle parking, accident response, self driving and traffic congestion avoidance Qureshi & Abdullah (2013). VANETS are drawing increasing interest from researchers in response to the demands of the technology with regard to reliability, quality of service, and throughput. In these applications, high data rates coupled with ultra-low latency transmission are crucial in order to optimize cooperation among vehicles through strong communication links Laneman *et al.* (Dec. 2004) as well as to expand the connectivity and coverage of vehicle-to-vehicle (V2V) networks Silva *et al.* (2017). It is noteworthy that cooperating vehicles can help compensate for human errors, leading to a decrease in the number of accidents.

One solution with enormous potential for supporting these critical applications is full duplex relaying (FDR). This approach simultaneously decreases end-to-end delays while doubling spectral efciency Kim *et al.* (2015). For instance, in Kwon, T., Lim, S., Choi, S. & Hong, D. (Sep. 2010) the outage probability performance of both full duplex (FD) and half duplex (HD) relaying was investigated for decode-and-forward (DF) relaying over Rayleigh fading channels. It was shown that FD provides a superior performance than HD in terms of outage probability. In the related work Sharma, P. K. & Garg, P. (Feb. 2013), the researchers investigated FD and HD relay outage behaviour by applying the DF technique. They concluded that FD works better than HD under this strategy, mainly due to the transmission requirement of fewer time slots. In a similar study, *et al.* Krikidis, I., Suraweera, H. A., Smith, P. J. & Yuen, C. (2012) explored FD relaying using a variety of relay selection schemes, such as optimal/sub-optimal best relay selection across Rayleigh fading channels. They also looked into hybrid relay techniques that dynamically switch from HD to FD modes in accordance with channel state information (CSI). Other investigations tested performance levels of FD DF as well as amplify-and-forward (AF) relay selection across Nakagami-*m* fading channels. The focus of these analyses was on the outage probability Wang, Y., Xu, Y., Li, N., Xie, W., Xu, K. & Xia, X. (2016) and ergodic capacity Shi, Z., Ma, S., Hou, F. & Tam, K.-W. (2015). In Nguyen, B. C. & Tran, X. N.

(2019) and Nguyen, B. C., Hoang, T. M. et al. (2019), double Rayleigh fading conditions were assumed for analyses of FD AF and FD DF relay-based V2V communication systems, respectively. In Airod, F. E., Chafnaji, H. & Tamtaoui, A. (2017), the researchers derived the closed form outage probability of FD AF relaying in the presence of a direct link between the source and destination, while the researchers in Li, S., Yang, K., Zhou, M., Wu, J., Song, L., Li, Y. & Li, H. (2017c) studied relay location optimization and power allocation for FD AF relay systems in order to reduce residual self-interference (RSI) and minimize rates of system symbol error.

However, in practice, self-interference (SI) is an issue in FDR when utilizing the same channel for simultaneous data reception and transmission Duarte & Sabharwal (Nov. 2010); Jain *et al.* (2011). Due in part to this problem, unidirectional and bidirectional wireless cooperative relaying schemes were studied under a number of different communication scenarios. Assuming Rayleigh fading conditions, the authors in Alves, H., Fraidenraich, G., Souza, R. D., Bennis, M. & Latva-aho, M. (2012) presented a comparison between FD and HD selective and incremental DF relaying techniques under both self-interference and source-destination interference at the relay and destination, respectively. Similarly, considering these interferences, in Alves, H., da Costa, D. B., Souza, R. D. & Latva-aho, M. (June 2013), the performance of block Markov FDR was investigated, where tight closed-form approximate expressions for the outage probability and throughput over Nakagami-*m* fading channels were derived. Moreover, a bidirectional FD mode was investigated for a single relay and multiple-relays in Kothapalli, N., Sharma, P. & Kumar, V. (2016) and Cui, H., Ma, M. & Song, L. (2014), respectively. In Khafagy, M. G., Ismail, A., Alouini, M.-S. & Aïssa, S. (2015b), an incremental selective protocol was proposed for FD relying over Nakagami-*m* fading channels, when the source-destination link is seen as interference at the destination node. It was shown that the selective cooperation protocol outperforms conventional non-selective protocols in terms of outage probability. On the other hand, in large part due to the strength of the SI channels at relays, FD relay techniques often experience hardware malfunction, leading to degradation in system performance Taghizadeh, O., Rothe, M., Cirik, A. C. & Mathar, R. (2015); Taghizadeh, O., Zhang,

J. & Haardt, M. (2016); Taghizadeh, O., Cirik, A. C. & Mathar, R. (2017). For instance, researchers in Taghizadeh *et al.* (2017) examined transmitter and receiver hardware impairments for MIMO-based AF-based FDR. They suggested using optimization strategies to offset any deterioration in performance, while in Taghizadeh *et al.* (2015), the authors explored how inaccuracies affect analog hardware components, along with the impact of SI in performance FD AF relays and limits to interference estimation within digital domains.

Furthermore, how co-channel interference (CCI) from frequency reuse is receiving increasing attention in the recent literature, especially in regard to conventional half duplex relaying (HDR) networks Ikki, S. S. & Aissa, S. (2012a); Li, M., Lin, M., Zhu, W.-P., Huang, Y., Wong, K.-K. & Yu, Q. (2017a); Trigui, I., Affes, S. & Stéphenne, A. (2015); Zhu, G., Zhong, C., Suraweera, H. A., Zhang, Z. & Yuen, C. (2014a). Specifically, the authors in Trigui *et al.* (2015) analyzed the ergodic capacity of HD AF relaying with CCI at the relay node. In Ikki & Aissa (2012a), the authors presented two-way AF relaying in the presence of CCI over independent but not necessarily identically distributed (i.n.i.d) Rayleigh fading channels where the error probability and outage probability were derived. In Zhu *et al.* (2014a), the authors considered multiple antennas at AF relay node under the effect of CCI, where different relay processing schemes are proposed to combat the CCI. The authors in Li *et al.* (2017a) investigated HD AF multiple-input multiple-output (MIMO) networks considering multiple CCI at the relay node over Rayleigh fading channels.

It is worth noting that FD relay networks, which have greater frequency reuse, can be more prone to CCI than traditional HD Almradi *et al.* (2018). For this reason, it is useful to gauge the effects of CCI on FD relay network performance. To that end, related work saw researchers in Almradi *et al.* (2018) studying zero forcing (ZF) beamforming in MIMO AF-based FDR and HDR, and CCI across Rayleigh fading channels. Moreover, researchers in Alves, H., Souza, R. D., da Costa, D. B. & Latva-aho, M. (2015); Sharma, G., Sharma, P. K. & Garg, P. (2014), looked closely at CCI outage probability performance for FD DF relay networks, while in Almradi, A. & Hamdi, K. A. (2017a), the researchers studied the effects of CCI at relay nodes in one-way MIMO FDR across Rayleigh fading channels.

However, as a part of the fifth generation (5G) of wireless communications,a vast army of autonomous/semi-autonomous vehicles will take to the road and engage with future ITS services. To deal with the vehicular influx, the millimeter-wave (mmWave) range of the radio frequency spectrum is considered the current best option to mitigate rate or latency limitations in today's V2V communications. Meanwhile, in V2V communications, given the relatively small height of the antennas set on the vehicles, other vehicles such as vans, lorries, and buses present between a pair of communicating vehicles can obstruct the signal Boban *et al.* (2011).The authors in Boban *et al.* (2011) showed that, in both sparse and dense vehicular networks, obstructing vehicles significantly impact the line-of-sight (LOS) component and the received signal power and have consequently concluded that this phenomenon should be taken into account in the analysis of V2V communications. In addition, considering a large highway section using real world road topology and real traffic database, the authors in Akhtar, N., Ergen, S. C. & Ozkasap, O. (2015) showed the impact of obstacles on the received power of the LOS component of the signal. In this vein, communication blockages over dedicated short range communications (DSRC) or mmWave networks have been recently investigated in vehicular communications. The impact of vehicles as obstacles on the signal propagation path of the 5.9 GHz band has been experimentally studied in Boban *et al.* (2011); Meireles, R., Boban, M., Steenkiste, P., Tonguz, O. & Barros, J. (2010), where blockage of the LOS between the transmitter and the receiver can occur. Moreover, V2V channel measurements in urban and highway roads for different frequency bands such as the DSRC and mmWave bands in the presence of vehicle blockage were experimentally analyzed in Boban *et al.* (2019). Similarly, V2V relaying performance analysis and measurement have been considered when a large vehicle, such as a bus, obstructs the LOS between the source and destination in He, R., Molisch, A. F., Tufvesson, F., Wang, R., Zhang, T., Li, Z., Zhong, Z. & Ai, B. (2016); Yang, M., Ai, B., He, R., Chen, L., Li, X., Huang, Z., Li, J. & Huang, C. (2018). Moreover, Tassi *et al.* (2017) modelled the blockage by large vehicles in highway mmWave vehicle-to-infrastructure (V2I) communications over Nakagami-*m* channels. Finally, V2V communications in mmWave with AF-based FDR, where the presence/absence of LOS propagation between the source and des-

tination is taken into account in the analysis of the outage probability lower bound, has been recently investigated in Eshteiwi *et al.* (2019).

While informative, none of these studies provide a holistic analysis. To the best of our current knowledge, no study has yet analyzed FD dual-hope AF relay systems across Nakagami-m fading and interference-impaired channels. Moreover, the vast majority of the related works in the literature do not account for the effect of obstacles between the source-relay (S-R) and the relay-destination (R-D). This is a significant gap, considering how substantially the LOS component acts on received signal power for different kinds of vehicular networks Boban *et al.* (2011).

To bridge this research gap, this work seeks to extend the aforementioned works by considering a cooperative V2V scenario using FD AF relaying under the impact of both SI at the relay and CCI at the destination. In addition, since in practical V2V systems, large vehicles such as vans and lorries can be present between the S-R and R-D nodes and may consequently block the communication links, two vehicle obstacles, i.e., one in each communication link, are considered. In this context, this paper derives novel exact and lower bound analytical expressions for the outage probability, the throughput, and the average symbol error rate of FD AF relaying V2V communication systems, taking into account the SI, CCI, and vehicle blockage, over i.n.i.d Nakagami-*m* fading channels. The proposed work will use the blockage model presented in Akhtar *et al.* (2015); Boban *et al.* (2011) where the blockage affects the LOS component between the source and destination by degrading the power of the transmitted signal. The vehicles around the target then act like obstacles blocking the communicating pair and impeding the LOS component between transmitter and receiver. Precisely, the main contributions of this paper can be summarized as follows:

- We derive closed form expressions for the exact outage probability of the equivalent end-to-end signal-to-interference-plus-noise ratio (SINR) of FD AF relaying over Nakagami-*m* fading channels under the effects of SI at the relay, CCI at the destination, and vehicle blockage in the communication links.

- We derive a lower bound expression to the symbol error rate of FD AF relaying over Nakagami-*m* fading channels under the effect of SI, CCI, and blockage.
- To provide insights into the performance of V2V communications in the asymptotic regime, we derive the asymptotic outage probability of the aforementioned system.
- Based on the exact and asymptotic outage probabilities, we derive the throughput of the proposed system.
- We analyze the influence of vehicles as obstacles on the outage performance and show the impact of blockage on the communication links.

The remainder of this paper is organized as follows: Section 3.3 presents the system model. The exact and asymptotic outage probabilities, the throughput, and the average symbol error rate lower bound of the proposed V2V system are derived in Section 3.4 while Section 3.5 presents the corresponding simulation results. Finally, closing remarks are discussed in Section 3.6.

## 3.3 System model

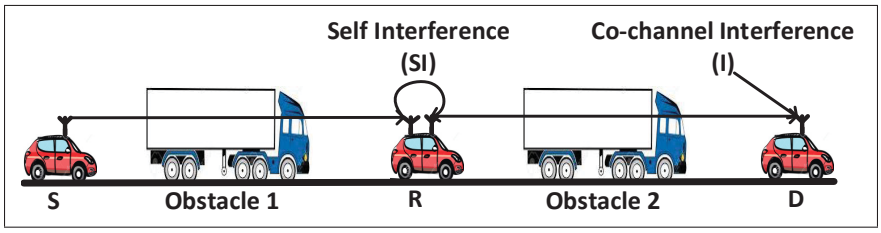


Figure 3.1 Diagram of the considered V2V full duplex relay network

We consider a full duplex V2V communication scenario, depicted in Fig. 3.1, where in the absence of a direct link, the source S communicates with the destination D via a FD AF relay R, where there is no direct link between S and D. It should be noted that in the AF technique, the relay simply transmits an amplified version of the received signal to the destination node. This simple approach is particularly suitable with low complexity devices. The AF

technique also introduces a minimal latency and therefore is most suitable for the low latency requirements of vehicular communications Kim & Liu (2008). We consider the Nakagami-*m* fading channel which was shown to accurately characterize vehicular communications and short-range communications scenarios, and therefore has been widely used in the literature Eshteiwi *et al.* (2019); He *et al.* (2014); Mafra *et al.* (2016); Tassi *et al.* (2017). Moreover, this fading model spans a wide range of fading distributions that can capture several scenarios Cheng *et al.* (2007). In fact the Nakagami$-m$ fading distribution provides an alternate approximation to the widely used Rician distribution and has been employed to simplify the analysis in numerous works, e.g. Nguyen, X.-X. & Do, D.-T. (2019); Toka, M. & Kucur, O. (2018); Xu, Z. & Nguyen, N.-P. (2018). Motivated by these attributes, in this work, we opted for the Nakagami-*m* fading channel to model the fading effects.

In this context, the relay node is assumed to be equipped with a pair of antennas, one serving the purpose of transmitting while the other is receiving. Thus, the received signal at R is corrupted by self-interference due to the simultaneous transmission/reception which characterizes the FD transmission mode. In addition, we consider that D experiences CCI resulting from the spectrum re-usage of adjacent user I. Finally, we also account for the presence of obstacles such as cars, trucks, and lorries on the road, which might block the transmitted signal over the communication links.

In this context, the received signal at R is given as

$$y_{\mathrm{SRR}} = \sqrt{P_{\mathrm{S}}} h_{\mathrm{SR}} x_{\mathrm{S}} + \sqrt{P_{\mathrm{R}}} h_{\mathrm{RR}} x_{\mathrm{R}} + n_{\mathrm{R}}, \tag{3.1}$$

where $x_{\mathrm{S}}$ and $x_{\mathrm{R}}$ are the transmitted binary phase-shift keying (BPSK) signals with unit power and $P_{\mathrm{S}}$ and $P_{\mathrm{R}}$ are the transmit powers at S and R, respectively while the term $n_{\mathrm{R}}$ corresponds to the additive white Gaussian noise (AWGN) at R with zero mean and variance $N_o$. Moreover, $h_{\mathrm{SR}}$ and $h_{\mathrm{RR}}$ are the channel coefficients of the S-R and the RSI channel, respectively. All the channels are assumed to be quasi-static and remain constant during one time slot, but change independently from one slot to another according to a Nakagami-m distribution, which

is typically the case in V2V communication traffic scenarios This assumption applies to networks with a low mobility and corresponds to slow fading channels da Costa, D. B. & Aissa, S. (2009); Jalil, A. M., Meghdadi, V. & Cances, J.-P. (2010); Krikidis, I., Thompson, J., McLaughlin, S. & Goertz, N. (2008). Here, perfect CSI is considered available at the destination node Alghorani & Seyfi (2017); Alghorani, Y., Kaddoum, G., Muhaidat, S. & Pierre, S. (2015a); Tassi *et al.* (2017). This assumption is justified since a feedback channel could be used to send pilot signals to acquire knowledge about the channel properties before the transmission Caire, G., Jindal, N., Kobayashi, M. & Ravindran, N. (2010). It is assumed that R executes an imperfect loop interference cancellation algorithm and that the RSI, is modeled as a Nakagami-$m$ random variable. Here, the SI represents the RSI after the application of an imperfect interference cancellation technique at the relay. Since isolation and cancellation techniques for FDR, see Duarte & Sabharwal (Nov. 2010); Duarte, M., Dick, C. & Sabharwal, A. (2012); Jain *et al.* (2011); Riihonen, T., Werner, S. & Wichman, R. (2009b,1,1) and the references therein, cannot perfectly prevent relay transmissions from leaking towards the receiver and causing undesirable interference. As a result, a level of RSI is inevitable. For notational convenience, in this article, $h_{\mathrm{RR}}$ denotes the RSI channel after undergoing an inadequate self-interference cancellation, which is unknown.

All the aforementioned channels are modelled as mutually i.n.i.d Nakagami$-m$ random variables. In addition, we employ the normalized distances model Ikki, S. S. & Ahmed, M. H. (Spring 2009); Laneman *et al.* (Dec. 2004); Lateef, H., McLernon, D. C. & Ghogho, M. (June 2010) to model the impact of pathloss which implies that $\mathbb{E}(\left|h_{\mathrm{ij}}\right|^2) = (d_{\mathrm{SD}}/d_{\mathrm{ij}})^{\eta}$, where ij $\in \{\mathrm{SR}, \mathrm{RR}, \mathrm{RD}, \mathrm{ID}\}$. Here, $\eta$ is the pathloss exponent, $d_{\mathrm{ij}}$ is the distance between vehicle i and j and $\mathbb{E}(.)$ is the expectation operator. At the destination side, the received signal from R is obtained as

$$y_{\mathrm{D}} = \sqrt{P_{\mathrm{R}}} h_{\mathrm{RD}} \kappa y_{\mathrm{SRR}} + \sqrt{P_{\mathrm{I}}} h_{\mathrm{ID}} x_{\mathrm{I}} + n_{\mathrm{D}}, \tag{3.2}$$

where $h_{\mathrm{RD}}$ and $h_{\mathrm{ID}}$ are the channel coefficients for the information (R-D) and co-channel interference-destination (I-D) links, respectively. In addition, $P_{\mathrm{I}}$ is the transmitted power of the

interfering signal, $n_{\mathrm{D}}$ is the AWGN at D with zero mean and variance $N_{\mathrm{o}}$, and $\kappa$ is the amplification factor at R which satisfies $\kappa \leq \sqrt{P_{\mathrm{R}}/(P_{\mathrm{S}}\left|h_{\mathrm{SR}}\right|^2 + P_{\mathrm{R}}\left|h_{\mathrm{RR}}\right|^2 + N_{\mathrm{o}})}$ Eshteiwi *et al.* (2019). Here, perfect CSI is considered available at the destination node Alghorani & Seyfi (2017); Alghorani *et al.* (2015a); Tassi *et al.* (2017). This assumption is justified since a feedback channel could be used to send pilot signals to acquire knowledge about the channel properties before the transmission Caire *et al.* (2010).

### 3.4 Performance Analysis

Given the aforementioned scenario, the equivalent instantaneous SINR of the received signal at D can be written as

$$\gamma_{\mathrm{eq}} = \frac{\gamma_1 \gamma_2}{\gamma_1 + \gamma_2 + 1} \tag{3.3}$$

where $\gamma_1 = \gamma_{\mathrm{SR}}/(\gamma_{\mathrm{RR}} + 1)$ and $\gamma_2 = \gamma_{\mathrm{RD}}/(\gamma_{\mathrm{ID}} + 1)$. Moreover, $\gamma_{\mathrm{SR}} = P_{\mathrm{S}}\left|h_{\mathrm{SR}}\right|^2/N_{\mathrm{o}}$, $\gamma_{\mathrm{RR}} = P_{\mathrm{R}}\left|h_{\mathrm{RR}}\right|^2/N_{\mathrm{o}}$, $\gamma_{\mathrm{RD}} = P_{\mathrm{R}}\left|h_{RD}\right|^2/N_{\mathrm{o}}$, and $\gamma_{\mathrm{ID}} = P_{\mathrm{I}}\left|h_{\mathrm{ID}}\right|^2/N_{\mathrm{o}}$ correspond to the instantaneous signal-to-noise ratio (SNR) of the S-R, relay-relay (R-R), R-D, and I-D links, respectively. Since the channel coefficients are i.n.i.d Nakagami$-m$ random variables, $\left|h_{\mathrm{ij}}\right|^2$ follows a gamma distribution. The probability density function (PDF) of $\gamma_{\mathrm{ij}}$ can be written as

$$f_{\gamma_{\mathrm{ij}}}(x) = \frac{C_{\mathrm{ij}}^{m_{\mathrm{ij}}}}{\Gamma(m_{\mathrm{ij}})} x^{m_{\mathrm{ij}}-1} \exp(-xC_{\mathrm{ij}}), \tag{3.4}$$

where $\Gamma(z) = \int_0^\infty \exp(-t)t^{z-1}dt$ is the Gamma function Jeffrey & Zwillinger (2007), $m_{\mathrm{ij}} > 0.5$ is the shape parameter, $C_{\mathrm{ij}} = \frac{m_{\mathrm{ij}}}{\bar{\gamma}_{\mathrm{ij}}}$, and $\bar{\gamma}_{\mathrm{ij}} = E(\left|h_{\mathrm{ij}}\right|^2)P_{\mathrm{i}}/N_{\mathrm{o}}$ is the average SNR.

#### 3.4.1 Exact Outage Probability

The outage probability is defined as the probability that the rate is below a certain threshold and can be evaluated as the probability that the SINR falls bellow a corresponding threshold $\gamma_{\mathrm{th}} = 2^{R_{\mathrm{T}}} - 1$, where $R_{\mathrm{T}}$ is the target rate in bits/sec/Hz Eshteiwi *et al.* (2019). In this context,

considering the aforementioned system, the cumulative distribution function (CDF) of the end-to-end SINR is expressed as

$$F_{\gamma_{\rm eq}}(\gamma_{\rm th}) = Pr\left(\frac{\gamma_1\gamma_2}{\gamma_1+\gamma_2+1} \leq \gamma_{\rm th}\right) \tag{3.5}$$

which can be evaluated as Amarasuriya, G., Tellambura, C. & Ardakani, M. (2012)

$$F_{\gamma_{\rm eq}}(\gamma_{\rm th}) = 1 - \int_0^{\infty} \overline{F}_{\gamma_2}\left(\gamma_{\rm th}\left(1+\frac{\gamma_{\rm th}+1}{y}\right)\right) f_{\gamma_1}(\gamma_{\rm th}+y)dy \tag{3.6}$$

where $\overline{F}_{\gamma_2}(\cdot)$ is the complementary CDF of $\gamma_2$ and $f_{\gamma_1}(\cdot)$ is the PDF of $\gamma_1$.

**Theorem 1**: The exact outage probability expression of full duplex AF cooperative relaying systems with CCI at the destination is given in (3.7), at the top of next page, where $G^{0,1,1,1,1}_{0,[1,1],1,[1,1]}(\cdot|\cdot)$ is the extended generalized bivariate Meijer's G-function Ansari, I. S., Al-Ahmadi, S., Yilmaz, F., Alouini, M.-S. & Yanikomeroglu, H. (2011); Verma, R. (1966).

$$\begin{aligned}
F_{\gamma_{\rm eq}}(\gamma_{\rm th}) = 1 &- \frac{C_{\rm RR}^{m_{\rm RR}} C_{\rm SR}^{m_{\rm SR}} C_{\rm ID}^{m_{\rm ID}}}{\Gamma(m_{\rm RR})\Gamma(m_{\rm SR})\Gamma(m_{\rm ID})} \exp\left[-\gamma_{\rm th}(C_{\rm SR}+C_{\rm RD})\right] \sum_{j=0}^{m_{\rm RD}-1} \frac{(C_{\rm RD})^j}{j!} \sum_{k=0}^{j} \binom{j}{k} \\
&\times (k+m_{\rm ID}-1)! \sum_{l=0}^{m_{\rm SR}} \binom{m_{\rm SR}}{l} \Gamma(m_{\rm RR}+l) \sum_{r=0}^{j} \binom{j}{r} \frac{(\gamma_{\rm th}+1)^{j-r}}{(\gamma_{\rm th}C_{\rm RD}+C_{\rm ID})^{k+m_{\rm ID}}} \\
&\times \sum_{f=0}^{m_{\rm SR}-1} \binom{m_{\rm SR}-1}{f} \gamma_{\rm th}^{j+m_{\rm SR}-f-1} \frac{1}{(C_{\rm SR})^{m_{\rm RR}+l}} \sum_{q=0}^{\infty} \frac{(-C_{\rm SR})^q}{q!} \frac{1}{\Gamma(k+m_{\rm ID})} \frac{1}{\Gamma(l+m_{\rm RR})} \\
&\times \left(\frac{\gamma_{\rm th}C_{\rm RD}+C_{\rm ID}}{\gamma_{\rm th}^2 C_{\rm RD}+\gamma_{\rm th}C_{\rm RD}}\right)^{k+m_{\rm ID}} \left(\frac{C_{\rm SR}}{\gamma_{\rm th}C_{\rm SR}+C_{\rm RR}}\right)^{l+m_{\rm RR}} \\
&\times \frac{G^{0,1,1,1,1}_{0,[1,1],1,[1,1]}\left(\begin{matrix}-;(k+m_{\rm ID});(l+m_{\rm RR}) \\ 1+(r+k+m_{\rm ID}+f+q-j);0;0\end{matrix}\middle| \frac{\gamma_{\rm th}C_{\rm RD}+C_{\rm ID}}{(\gamma_{\rm th}^2 C_{\rm RD}+\gamma_{\rm th}C_{\rm RD})^2}, \frac{C_{\rm SR}}{(\gamma_{\rm th}C_{\rm SR}+C_{\rm RR})(\gamma_{\rm th}^2 C_{\rm RD}+\gamma_{\rm th}C_{\rm RD})}\right)}{\left(\gamma_{\rm th}^2 C_{\rm RD}+\gamma_{\rm th}C_{\rm RD}\right)^{r+k+f+q+m_{\rm ID}-j+1}}
\end{aligned} \tag{3.7}$$

**Proof**: The proof is provided in **Appendix I**

Obtaining an exact analytical expression for outage probability for MIMO system and also using imperfect channel estimation appears to be intractable and cumbersome problem. Therefore, we have performed simulations to evaluate the outage performance in Section IV.

### 3.4.2 Asymptotic Outage Probability

Here, we seek to derive the asymptotic outage probability expression which provides a simplified expression for the evaluation of the system's performance in the high SINR regime. In this context, at high SINR, the equivalent SINR in (4.3) can be approximated as

$$\gamma_{\text{asy}} \approx \frac{\gamma_{1_{\text{asy}}}\gamma_{2_{\text{asy}}}}{\gamma_{1_{\text{asy}}} + \gamma_{2_{\text{asy}}}} \tag{3.8}$$

where $\gamma_{1_{\text{asy}}} \approx \frac{\gamma_{\text{SR}}}{\gamma_{\text{RR}}}$ and $\gamma_{2_{\text{asy}}} \approx \frac{\gamma_{\text{RD}}}{\gamma_{\text{ID}}}$.
For mathematical tractability of the derivation, we first derive the PDF of $\gamma_{1_{\text{asy}}}$ and the CDF of $\gamma_{2_{\text{asy}}}$ and then an asymptotic outage probability is obtained.

#### 3.4.2.1 PDF of the Asymptotic SINR

**Lemma 1**: For a full duplex relay with SI, the PDF of the asymptotic SINR at the relay can be written as

$$f_{\gamma_{1_{\text{asy}}}}(x) \approx \frac{C_{\text{SR}}^{m_{\text{SR}}} C_{\text{RR}}^{m_{\text{RR}}} x^{m_{\text{SR}}-1}}{\Gamma(m_{\text{SR}})\Gamma(m_{\text{RR}})} \frac{\Gamma(m_{\text{SR}}+m_{\text{RR}})}{(xC_{\text{SR}}+C_{\text{RR}})^{m_{\text{SR}}+m_{\text{RR}}}} \tag{3.9}$$

**Proof**: The proof is provided in **Appendix I**

Similarly, at the destination side, taking into account the CCI, the PDF of the asymptotic SINR for the R-D link ($\gamma_{2_{\text{asy}}}$) is obtained by substituting $m_{\text{SR}} \to m_{\text{RD}}$ and $m_{\text{RR}} \to m_{\text{ID}}$ in Eq. (3.9).

#### 3.4.2.2 CDF of Asymptotic SINR

**Lemma 2**: Assuming full duplex relaying and CCI at the destination side, the CDF of the asymptotic SINR at the destination node is obtained as

$$F_{\gamma_{2_{\text{asy}}}}(x) \approx 1-\frac{C_{\text{ID}}^{m_{\text{ID}}}}{\Gamma(m_{\text{ID}})}\sum_{k=0}^{m_{\text{RD}}-1}\frac{(xC_{\text{RD}})^k}{k!}(m_{\text{ID}}+k-1)!(C_{\text{ID}}+xC_{\text{RD}})^{-(m_{\text{ID}}+k)} \tag{3.10}$$

**Proof**: The proof is provided in **Appendix I**

Similarly, we can write the CDF of the asymptotic SINR ($\gamma_{1_{\text{asy}}}$) at the relay node including SI by replacing $m_{\text{RD}} \rightarrow m_{\text{SR}}$ and $m_{\text{ID}} \rightarrow m_{\text{RR}}$ in Eq. (3.10).

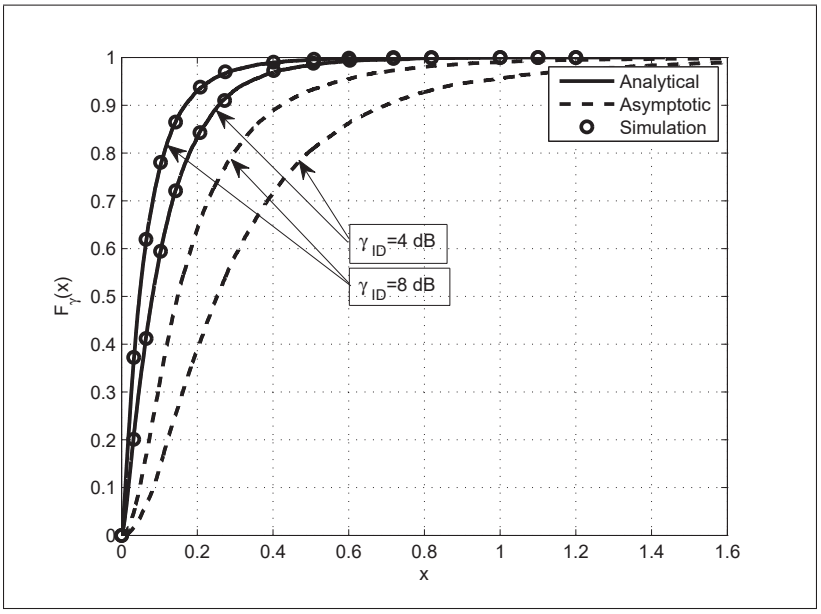


Figure 3.2 Analytical and simulation results for the exact CDF ($F_{\gamma_{\text{eq}}}(x)$) compared to asymptotic CDF ($F_{\gamma_{\text{asy}}}(x)$) of V2V wireless communications in the presence of SI and CCI over Nakagami-*m* fading channels for different values of $\overline{\gamma}_{\text{ID}}$, $\overline{\gamma}_{\text{SR}} = 2$ dB, $\overline{\gamma}_{\text{RR}} = 4$ dB, $\overline{\gamma}_{\text{RD}} = 2$ dB, $m_{\text{ij}} = 2$

#### 3.4.2.3 Asymptotic outage Probability of approximated SINR

Following a similar approach to Section 3.4.1, the asymptotic outage probability of the approximate SINR in (3.8) is evaluated as Almradi & Hamdi (2017a); Amarasuriya *et al.* (2012)

$$F_{\gamma_{\text{asy}}}(\gamma_{\text{th}}) \approx 1 - \int_0^{\infty} \overline{F}_{\gamma_{2\text{asy}}}\left(\frac{\gamma_{\text{th}}(\gamma_{\text{th}}+y)}{y}\right) f_{\gamma_{1\text{asy}}}(\gamma_{\text{th}}+y)dy \tag{3.11}$$

**Theorem 2**: The asymptotic outage probability of the equivalent SINR is obtained in (3.12), at the top of the next page, where $G_{\cdot,\cdot}^{\cdot,\cdot}(\cdot|\cdot)$ is Meijer's G-function (Jeffrey & Zwillinger, 2007, Eq. (9.301))

$$\begin{aligned} F_{\gamma_{\text{asp}}}(\gamma_{\text{th}}) \approx 1 &- \frac{C_{\text{RR}}^{m_{\text{RR}}} C_{\text{SR}}^{m_{\text{SR}}} C_{\text{ID}}^{m_{\text{ID}}}}{\Gamma(m_{\text{RR}})\Gamma(m_{\text{SR}})\Gamma(m_{\text{ID}})} \Gamma(m_{\text{SR}}+m_{\text{RR}}) \sum_{k=0}^{m_{\text{RD}}-1} \frac{(C_{\text{RD}})^k}{k!}(k+m_{\text{ID}}-1)! \\ &\times \sum_{l=0}^{m_{\text{SR}}-1} \binom{m_{\text{SR}}-1}{l} x^{m_{\text{SR}}-1-l} \sum_{p=0}^{k} \binom{k}{p} \gamma_{\text{th}}^{2k-p} \frac{1}{\Gamma(m_{\text{SR}}+m_{\text{RR}})} \left(\frac{1}{\gamma_{\text{th}}C_{\text{SR}}+C_{\text{RR}}}\right)^{m_{\text{SR}}+m_{\text{RR}}} \\ &\times \frac{1}{\Gamma(k+m_{\text{ID}})} \left(\frac{1}{\gamma_{\text{th}}^2 C_{\text{RD}}}\right)^{k+m_{\text{ID}}} \left(\frac{C_{\text{SR}}}{\gamma_{\text{th}}C_{\text{SR}}+C_{\text{RR}}}\right)^{-(l+p+m_{\text{RR}}+1)} \\ &\times G_{2,2}^{2,2}\left(\begin{matrix} 1-(k+m_{\text{ID}}),-(l+p+m_{\text{RR}}) \\ 0,-(l+p+m_{\text{RR}}+1)+(m_{\text{SR}}+m_{\text{RR}}) \end{matrix} \middle| \frac{C_{\text{ID}}+\gamma_{\text{th}}C_{\text{RD}}}{\gamma_{\text{th}}^2 C_{\text{RD}}} \frac{\gamma_{\text{th}}C_{\text{SR}}+C_{\text{RR}}}{C_{\text{SR}}} \right) \end{aligned} \tag{3.12}$$

**Proof**: The proof is provided in **Appendix I**

Fig. 3.2 shows the analytical $F_{\gamma_{\text{eq}}}(x)$ and $F_{\gamma_{\text{asy}}}(x)$ obtained in (3.7) and (3.12) compared to the Monte-Carlo simulation results for different values of $\overline{\gamma}_{\text{ID}}$. It is noticed that our analytical curves perfectly match the corresponding simulation results.

### 3.4.3 End-to-End Outage Probability

Assuming that there are two obstacles present between S and D, as shown in Fig. 3.1, the end-to-end outage probability can be formulated as

$$P_{\mathrm{e2e}}(\gamma_{\mathrm{th}}) = \prod_{\mathrm{p}=1}^{2} P_{\mathrm{p}}(\mathrm{LOS}_{\mathrm{OBS}}/\Lambda_{\mathrm{S}}, \Lambda_{\mathrm{D}}) F_{\gamma_{\mathrm{eq}}/\gamma_{\mathrm{asy}}}(\gamma_{\mathrm{th}}), \tag{3.13}$$

where $P(\mathrm{LOS}_{\mathrm{OBS}}/\Lambda_{\mathrm{S}}, \Lambda_{\mathrm{D}})$ is the probability that the source-destination (S-D) link is obstructed, while $F_{\gamma_{\mathrm{eq}}}(\gamma_{\mathrm{th}})$ and $F_{\gamma_{\mathrm{asy}}}(\gamma_{\mathrm{th}})$ correspond to the exact and asymptotic outage probabilities defined in (3.7) and (3.12), respectively. Based on the assumption that the vehicles' heights follow a normal distribution, the probability of LOS obstruction for the S-D link is evaluated as Akhtar *et al.* (2015); Boban *et al.* (2011)

$$P(\mathrm{LOS}_{\mathrm{OBS}}/\Lambda_{\mathrm{S}}, \Lambda_{\mathrm{D}}) = Q\Big(\frac{\Lambda_{\mathrm{EF}} - \chi}{\sigma_{\mathrm{OBS}}}\Big), \tag{3.14}$$

where $\Lambda_{\mathrm{S}}$ and $\Lambda_{\mathrm{D}}$ are the the source and destination heights, respectively. Moreover, $\chi$ and $\sigma_{\mathrm{OBS}}$ denote the mean and standard deviation of the obstacles' height and $Q(z)$ is the Q-function ($Q(z) = \int_z^{\infty} \frac{1}{\sqrt{2\pi}} \exp(\frac{-x^2}{2}) dx$)(Goldsmith, A., 2005, Eq.(5.39)). $\Lambda_{\mathrm{EF}}$ is the effective height of the straight line between S and D at the obstacle's location when the first Fresnel ellipsoid is considered, which can be expressed as

$$\Lambda_{\mathrm{EF}} = (\Lambda_{\mathrm{D}} - \Lambda_{\mathrm{S}}) \frac{d_{\mathrm{OBS}}}{d_{\mathrm{SD}}} + \Lambda_{\mathrm{S}} - 0.6 r_{\mathrm{F}} + \Lambda_{\mathrm{A}}, \tag{3.15}$$

where $d_{\mathrm{OBS}}$ is the distance between the source and the obstacle, $d_{\mathrm{SD}}$ is the distance between the source and destination, $\Lambda_{\mathrm{A}}$ is the height of the antenna, and $r_{\mathrm{F}}$ is the radius of the first Fresnel zone ellipsoid which is given by

$$r_{\mathrm{F}} = \sqrt{\frac{\lambda d_{\mathrm{OBS}}(d_{\mathrm{SD}} - d_{\mathrm{OBS}})}{d_{\mathrm{SD}}}} \tag{3.16}$$

where $\lambda$ is the wavelength.

### 3.4.4 Throughput

In this subsection, we evaluate the throughput of the aforementioned FD AF vehicular cooperative relaying network. In this context, it is recalled that the throughput can be defined as the total number of error free packets successfully delivered during a given period of time, which can be evaluated as Khafagyx, M. G., Alouini, M. S. & Aïssa, S. (Sep. 2015)

$$G = R_{\mathrm{S}}(1 - P_{\mathrm{e2e}}(\gamma_{\mathrm{th}})), \tag{3.17}$$

where $R_{\mathrm{S}}$ is the fixed rate of the transmitter in bits/sec/Hz.

### 3.4.5 Average Symbol Error Rate

In this subsection, we analyze the average symbol error rate ($\overline{\mathrm{SER}}$) performance of the proposed system. The $\overline{\mathrm{SER}}$ can be calculated as Li *et al.* (2017c)

$$\overline{\mathrm{SER}} = \alpha \mathbb{E}\left[Q\left(\sqrt{\beta x}\right)\right] = \frac{\alpha\sqrt{\beta}}{2\sqrt{2\pi}} \int_0^{\infty} \frac{\exp\left(-\beta x/2\right) F_{\gamma_{\mathrm{eq}}}(x)}{\sqrt{x}} dx \tag{3.18}$$

where $F_{\gamma_{\mathrm{eq}}}(.)$ is the SINR CDF. The parameters $\alpha$ and $\beta$ depend on the modulation scheme, e.g., $\alpha = 1$ and $\beta = 2$ for BPSK modulation. The derivation of the exact $\overline{\mathrm{SER}}$ which involves an integration of the CDF in (3.7) is intractable. Therefore, we proceed to derive a $\overline{\mathrm{SER}}$ lower bound ($\overline{\mathrm{SER}}_{\mathrm{LB}}$) based on the outage probability lower bound.

**Theorem 3**: The average SER lower bound expression for full duplex AF cooperative relaying systems with CCI at the destination is obtained in (3.19).

**Proof**: The proof is provided in **Appendix I**

$$\overline{\mathrm{SER}}_{\mathrm{LB}} = \frac{\alpha\sqrt{\beta}}{2\sqrt{2\pi}}\left(\sqrt{\frac{2\pi}{\beta}} - \frac{1}{\Gamma(m_{\mathrm{RR}})\Gamma(m_{\mathrm{ID}})}\sum_{l=0}^{m_{\mathrm{SR}}-1}\frac{(C_{\mathrm{SR}})^l}{l!}\sum_{t=0}^{l}\binom{l}{t}\sum_{j=0}^{m_{\mathrm{RD}}-1}\frac{(C_{\mathrm{RD}})^j}{j!}\right.$$
$$\sum_{k=0}^{j}\binom{j}{k}\frac{(C_{\mathrm{SR}}+C_{\mathrm{RD}}+\frac{\beta}{2})^{-(l+j+1/2)}}{C_{\mathrm{RR}}^{t+m_{\mathrm{RR}}}C_{\mathrm{ID}}^{k+m_{\mathrm{ID}}}\Gamma(t+m_{\mathrm{RR}})\Gamma(k+m_{\mathrm{ID}})}$$
$$\left.G_{1,[1,1],0,[1,1]}^{1,1,1,1,1}\left(\begin{matrix}(j+l+1/2);1-(t+m_{\mathrm{RR}});1-(k+m_{\mathrm{ID}})\\ -;0;0\end{matrix}\middle|\frac{C_{\mathrm{SR}}}{C_{\mathrm{RR}}(C_{\mathrm{SR}}+C_{\mathrm{RD}}+\frac{\beta}{2})},\frac{C_{\mathrm{RD}}}{C_{\mathrm{ID}}(C_{\mathrm{SR}}+C_{\mathrm{RD}}+\frac{\beta}{2})}\right)\right) \tag{3.19}$$

### 3.4.6 End-to-End Average Symbol Error Rate

The end-to-end average symbol error rate ( $\overline{\mathrm{SER}}_{\mathrm{e2e}}$) is evaluated as

$$\overline{\mathrm{SER}}_{\mathrm{e2e}} = \prod_{\mathrm{p}=1}^{2} P_{\mathrm{p}}(\mathrm{LOS}_{\mathrm{OBS}}/\Lambda_{\mathrm{S}},\Lambda_{\mathrm{D}})\overline{\mathrm{SER}}_{\mathrm{LB}} \tag{3.20}$$

where $\overline{\mathrm{SER}}_{\mathrm{LB}}$ is obtained Eq. (3.19).

## 3.5 Simulation Results

This section seeks to validate the accuracy of the derived analytical expressions and provide insights into the performance of practical V2V full duplex wireless networks. To this end, we consider a V2V network where the source communicates with the destination via a full duplex relay. The considered normalized distances separating the nodes are $d_{\mathrm{SR}} = 0.4$, $d_{\mathrm{RD}} = 0.6$, $d_{\mathrm{OBS}_1} = 0.2$, and $d_{\mathrm{OBS}_2} = 0.7$. All the channel are assumed to follow i.n.i.d Nakagami-$m$ distributions. Without loss of generality, the noise at all the nodes is assumed to follow a complex Gaussian distribution with zero mean and variance $N_{\mathrm{o}}$. In addition, a pathloss exponent of $\eta = 3.18$ is considered and we set $\chi = 0.04$, $\Lambda_{\mathrm{A}} = 0.0052$, $\Lambda_{\mathrm{S}} = 0.028$, $\Lambda_{\mathrm{D}} = 0.034$, $\sigma_{\mathrm{OBS}} = 0.006$, $R_{\mathrm{T}} = 1$bit/sec/Hz, and $m_{\mathrm{ij}} = 2$. Finally, we assume that the carrier frequency is

5.9 GHz, which is appropriate for DSRC standard vehicular communications. It is noted that the considered parameters have been extensively employed in the related literature, e.g. Boban *et al.* (2011); Eshteiwi *et al.* (2019,2); Khafagy *et al.* (2015b) and the references therein.

Unless otherwise stated, the derived analytical expressions are represented by solid lines whereas the markers depict the corresponding simulation results. In this context, Figs. 3.3-3.15 show the derived exact and asymptotic $P_{\mathrm{e2e}}$, throughput, and $\overline{\mathrm{SER}}_{\mathrm{LB}}$, where a perfect match between the exact and the corresponding simulation results is observed. Moreover, the derived asymptotic and lower bound expressions provide a tight approximation to the actual performance of the system.

Fig. 3.3 illustrates the end-to-end outage probability of FDR and HDR in dual-hop vehicular wireless cooperative communications. Here, the presented results show the destructive influence of the CCI at the destination on the end-to-end outage probability of the system. Moreover, we notice the superiority of the FD scheme compared to HD relaying in terms of lower outage probability which is because the outage probability is evaluated at $\gamma_{\mathrm{th}} = 2^{2R_{\mathrm{T}}} - 1$ for HD relaying and at $\gamma_{\mathrm{th}} = 2^{R_{\mathrm{T}}} - 1$ for FDR. This means that HD needs two time slots to accomplish the transmission while one time slot is enough in the case of FDR. For instance, for $\overline{\gamma}_{\mathrm{ID}} = 5$ dB, an outage probability of $10^{-2}$ appears at 11 dB in FDR while it occurs at 14 dB in HDR. Moreover, it is observed that the performance of HDR with $\overline{\gamma}_{\mathrm{ID}} = 5$ dB is quite comparable to that of FDR with $\overline{\gamma}_{\mathrm{ID}} = 10$ dB, which implies that a 5 dB gain can be achieved by using FDR. The detrimental effects of CCI are also observed here. This is in line with our results in (3.3) which indicates that the received signal at the destination is negatively affected by any increase in the CCI.

Fig. 3.4 depicts the end-to-end outage probability as a function of $P_{\mathrm{S}}/N_{\mathrm{o}}$ for different obstacles mean height ($\chi$). The average strength of the self and co-channel interference links were set to 5 and 15 dB, respectively. Meanwhile, the height of the source and destination are set to 0.028 and 0.034, respectively. Different types of blockers, such as small blocker (personal vehicle) and large blocker (van, bus), were investigated. The results show that the blockage

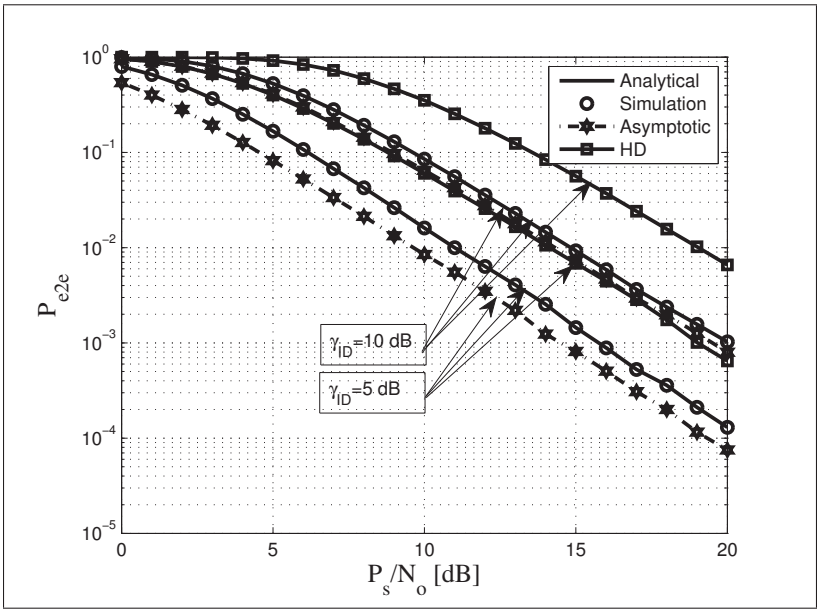


Figure 3.3 End-to-end outage probability vs. $P_S/N_o$ for different values of $\overline{\gamma}_{ID}$ with $m_{ij}$=2, $\overline{\gamma}_{RR}$=5 dB, and $R_T$=1 bit/sec/Hz

probability is signicantly impacted by the blocker size. It is observed that the average height of the obstacles negatively impacts the $P_{e2e}$ of both FD and HD relaying. For instance, for a target $P_{e2e}$ of $10^{-2}$ in FDR, there is a 4 dB loss when the $\chi$ goes from 0.026 to 0.06. This can be explained by the fact that increasing the obstacles' average height impedes the strength of the transmitted signal at both the source and relay, which increases the outage probability, therefore degrading the system's performance. Moreover, the difference between small and large blocker is also noticeable, where large blocker impact the outage probability more significantly than the small ones. Another interesting point is that FDR with a high obstacle ($\chi$=0.06) outperforms HDR with a shorter obstacle ($\chi$=0.03).

Fig. 3.5 plots the end-to-end outage probability as a function of $P_S/N_o$ for different target rates $R_T$ bit/sec/Hz. It is observed that, for FDR, an outage probability of $10^{-2}$ appears at $\approx$ 15 dB when $R_T$ =1 bit/sec/Hz and at $\approx$ 19.5 when $R_T$ =2 bit/sec/Hz. Meanwhile, in HDR, there is a 7 dB loss when $R_T$ goes from 1 to 2 bit/sec/Hz at $P_{e2e} = 10^{-1}$. This is because the low target rate $R_T$ allows the relay to participate in forwarding the information to the destination node which improves the end-to-end SINR, therefore reducing the outage probability.

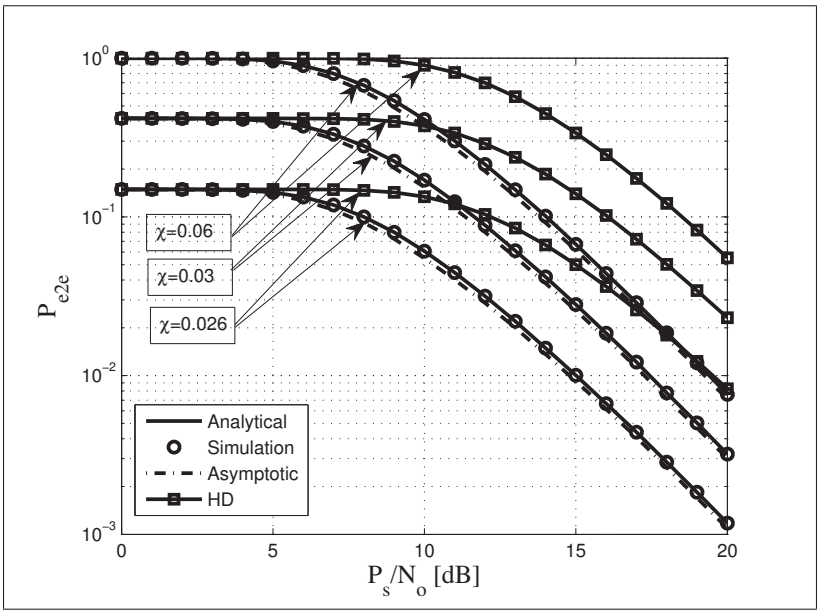


Figure 3.4 End-to-end outage probability vs. $P_S/N_o$ for different values of $\chi$ with $\overline{\gamma}_{ID}$=15dB, $m_{ij}$=2, $\overline{\gamma}_{RR}$=5dB and $R_T$=1 bit/sec/Hz

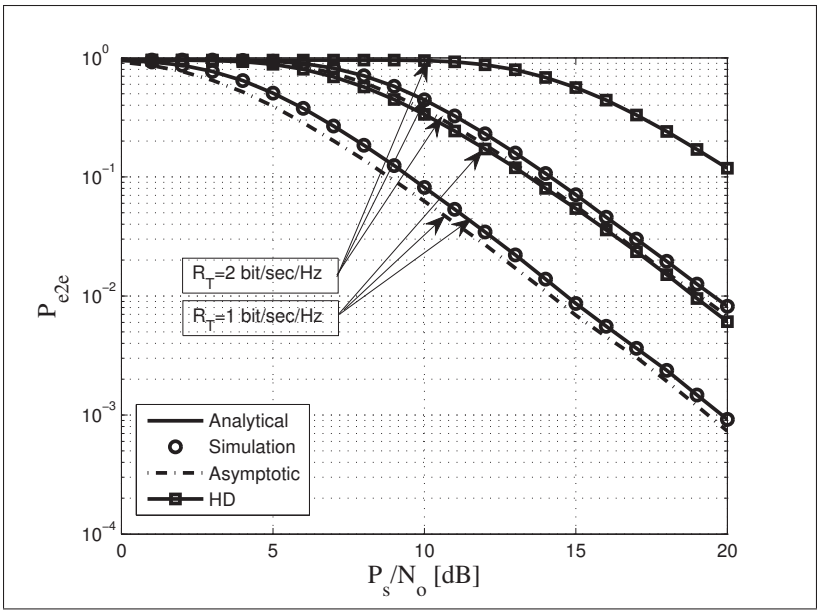


Figure 3.5 End-to-end outage probability vs. $P_S/N_o$ for different values of $R_T$ with $\overline{\gamma}_{ID}$=10dB, $m_{ij}$=2 and $\overline{\gamma}_{RR}$=5dB

Fig. 3.6 depicts the end-to-end outage probability for different source heights ($\Lambda_S$). Here, it is observed that the performance of the system improves by increasing the height of the source. This is because for a high transmitter, especially when it is higher than the mean height of the obstacle $\chi$, the strong LOS component is not blocked either at the relay or the destination which improves the system's performance. Concretely, for a target $P_{e2e}$ of $10^{-1}$, this results in approximately a 3 dB loss when the antenna height goes from 0.046 and 0.026 in both FD and HD relaying. Moreover, the difference between small and large source heights is also noteworthy, where an increase in the source heights causes a decrease in the outage probability due to an increase in the received power is high at the destination node. Once more, FDR with a short source ($\Lambda_S$=0.026) outperforms HDR with a high source ($\Lambda_S$=0.04).

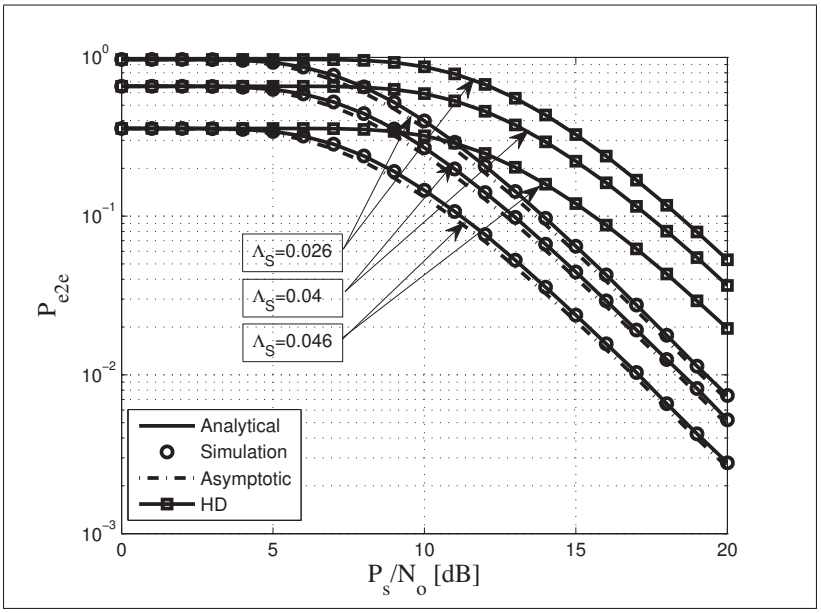


Figure 3.6 End-to-end outage probability vs. $P_S/N_o$ for different values of $\Lambda_S$ with $m_{ij}$=2, $R_T$=1 bit/sec/Hz, $\overline{\gamma}_{ID}$=15 dB and $\overline{\gamma}_{RR}$=5 dB

Fig. 3.7 presents the end-to-end outage probability versus $P_S/N_o$ for different distances between the source and the two obstacles. It is noticed that when the obstacles are close to the source, the effective height of the straight line between the source and the destination decreases, and consequently the probability of obstruction increases which degrades the $P_{e2e}$. On the other

hand, when the obstacles are close to the destination, this increases the effective height and decreases the probability of obstruction between the source and the destination which improves the $P_{\mathrm{e2e}}$. For example, in both FD and HD relaying, there is a 1 dB loss at $P_{\mathrm{S}}/N_{\mathrm{o}} = 15$ dB when the obstacles are closer to the source than the destination. We can see that when the obstacles are close to the source node the system performance is degraded since the received signal at the relay is weaker and the blockage probability is increased. In order to improve the SINR of the received signal at the relay, the transmission power at the source needs to be increased.

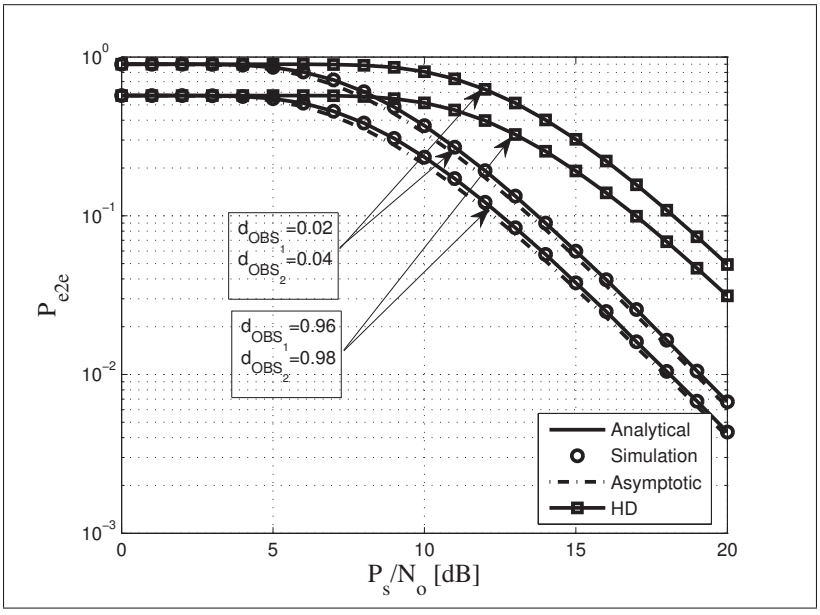


Figure 3.7 End-to-end outage probability vs. $P_{\mathrm{S}}/N_{\mathrm{o}}$ for different values of $d_{\mathrm{OBS}_1}$ and $d_{\mathrm{OBS}_2}$ with $\overline{\gamma}_{\mathrm{ID}}$=15 dB, $m_{\mathrm{ij}}$=2, $\overline{\gamma}_{\mathrm{RR}}$=5 dB and $R_{\mathrm{T}}$=1 bit/sec/Hz

Furthermore, in Fig. 3.8, our results are compared to the vehicular full duplex dual-hop (VDH) scheme presented in Eshteiwi *et al.* (2019); Mafra *et al.* (2016). In this scheme, the source-destination link is considered as interference at the destination node. It is observed that the VDH scheme is associated to a slightly higher outage probability, which is due to the interference from the direct link at the destination node. For example, an outage probability of $10^{-2}$ occurs at $\approx$ 15 dB and at $\approx$ 15.8 dB for $\overline{\gamma}_{\mathrm{ID}} = 10$ dB for the proposed system and the VDH scheme respectively, while, for $\overline{\gamma}_{\mathrm{ID}} = 15$ dB, it occurs at $\approx$ 19.5 dB and at $\approx$ 19.8 dB for the

proposed system and VDH, respectively. In addition, in this figure we notice a performance degradation when the CCI is increased. This is because, as pointed out in (4.3), the end-to-end SINR is deteriorated when this interference is increased, which negatively affects on the outage probability.

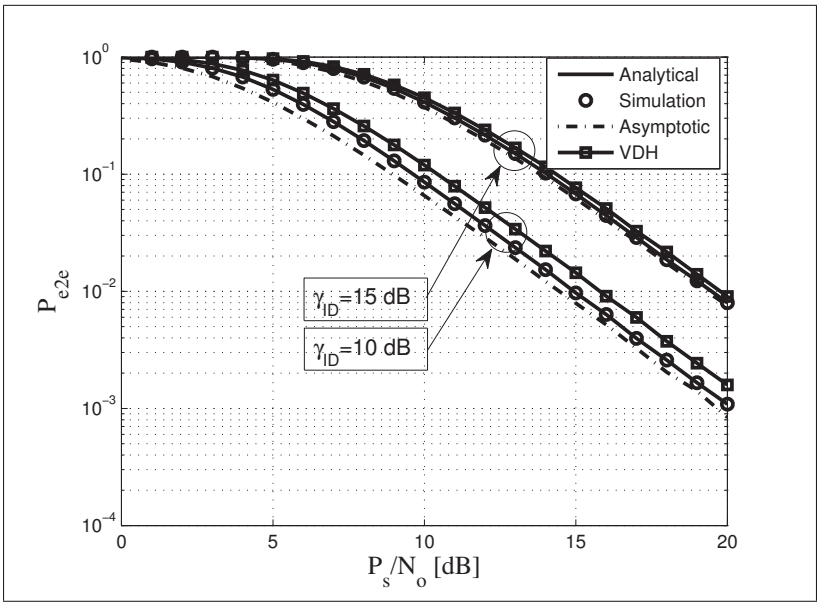


Figure 3.8 End-to-end outage probability vs. $P_S/N_o$ for different values of $\overline{\gamma}_{ID}$ with $m_{ij}$=2, $\overline{\gamma}_{RR}$=5 dB, $\overline{\gamma}_{SD}$=4dB, and $R_T$=1 bit/sec/Hz

Fig. 3.9 shows the performance degradation incurred by the distortion noise caused by hardware impairments on the end-to-end outage probability. Besides the aggregate hardware impairments, we also consider the impact of RSI due to imperfect cancellation at the FD relay node. The distortion noise is modeled using a complex Gaussian variable with zero mean and a variance of $k_R^2 P_R$, where $k_R$ is the aggregate level of the hardware distortion at the relay as represented in Nguyen & Tran (2019); Tran, X. N., Nguyen, B. C. & Tran, D. T. (2019). In this context, we consider $k_R = 0.1$ and $P_R = 5$ dB where it is observed that hardware distortion negatively affects the system performance by increasing the outage probability. For instance, for a target $P_{e2e}$ of $10^{-1}$, the required transmit SNR is 13 dB when hardware distortion is taken into account at the relay node against 12 dB for the ideal case.

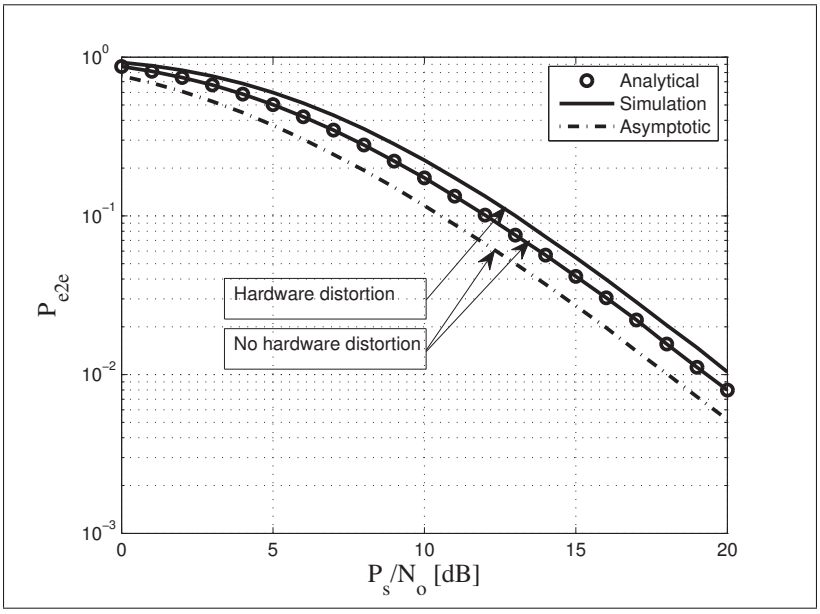


Figure 3.9 End-to-end outage probability vs. $P_S/N_o$ with $\overline{\gamma}_{ID}$=5 dB with $m_{ij}$=2, and $R_T$=1 bit/sec/Hz

Fig. 3.10 depicts the end-to-end outage probability as a function of $P_S/N_o$ with perfect and imperfect channel estimation. The channel estimation error is defined as $e_{h_i} = h_i - \hat{h}_i$, where $h_i$ and $\hat{h}_i$ denote the actual and estimated channels, respectively. The estimation errors are assumed to be Gaussian distributed with zero mean and variance $\sigma_{e_i}^2 = 0.002$. It is noted that $\sigma_{e_i}^2$ is a parameter that captures the quality of the channel estimation and depends on the channel dynamics and the considered estimation schemes. It is shown that imperfect channel state information (ICSI) degrades the outage probability of the system, especially in the high SNR regime.

Considering multiple antennas to the relay can substantially increase the capacity, link reliability and generally improve the quality of service in wireless communications. Considering multiple antennas at the relay, Fig. 3.11 shows the outage performance of the considered V2V FD AF relaying for various receiving $N_R$ and transmitting $N_T$ antennas at the relay. Here, selection combining is used to select the best receiving and transmitting antenna at the relay node. In this context, although only one receive antenna is used at S and D, it is noticed that, by increasing the number of antennas at R, the outage probability is improved and the diversity

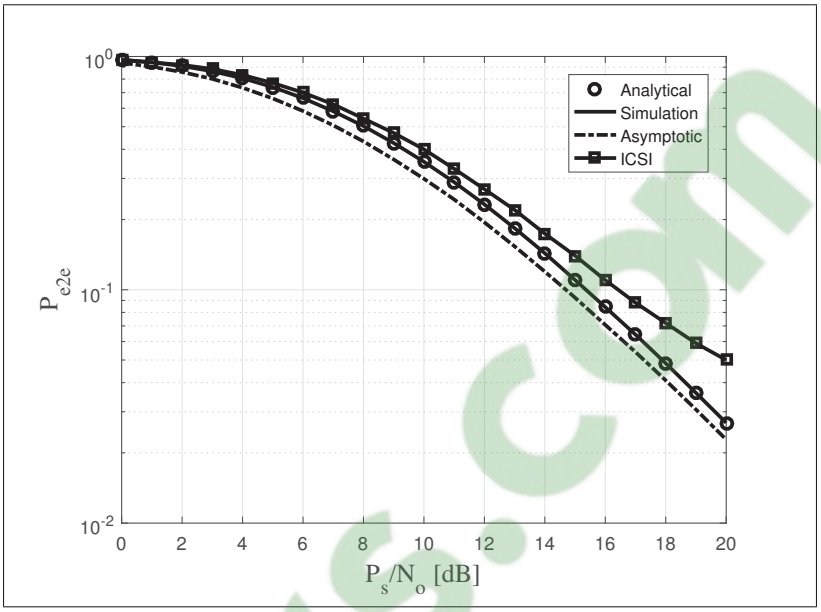


Figure 3.10 End-to-end outage probability vs. $P_S/N_o$ with $m_{ij}$=2, $\overline{\gamma}_{RR}$=5 dB, $\overline{\gamma}_{ID}$=10 dB, and $R_T$=1 bit/sec/Hz

order is increased. For instance, 7 dB could be gained from using three antennas at the relay node instead of one, where, for an SNR of 15 dB, we achieve an outage probability of $\approx 10^{-3}$ and $\approx 10^{-1}$ for $N_R = N_T = 3$ and $N_R = N_T = 1$, respectively.

In addition, Figs. 3.12-3.13 depict the throughput of FD and HD AF relaying V2V communication versus $P_S/N_o$. Fig. 3.12 shows the detrimental effect of the CCI on the throughput of the system, while in Fig. 3.13, the improvement of the throughput when the average height of the obstacles is decreased is shown. The lower the obstacles' height, the lower the blockage of the communication link between the source and destination which enables the source to transmit the signal with appropriate power to the destination through the relay node. For example, for $\chi = 0.04$, a throughput of 0.5 bit/sec/Hz is achieved when $P_S/N_o = 9$ dB and 13 dB in FD and HD relaying, respectively. Moreover, in FDR, when the average height of the obstacles is $\chi = 0.03$, the system accomplishes $\approx 85\%$ of the throughput at 10 dB while increasing the average height of the obstacles to $\chi = 0.04$ decreases this value to $\approx 61\%$ of the throughput. Moreover, when increasing the average height of the obstacles $\chi$ from 0.03 to 0.04, the blockage probability increases from $\approx 42\%$ to $\approx 96\%$ which consequently degrades the system

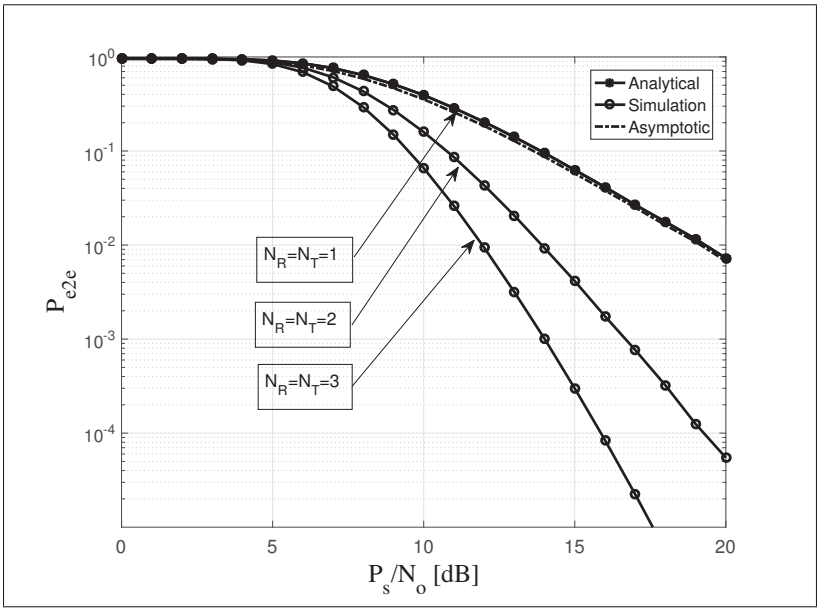


Figure 3.11 End-to-end outage probability vs. $P_S/N_o$ for different numbers of transmitting ($N_T$) and receiving ($N_R$) antennas at the relay node with $m_{ij}$=2, $\overline{\gamma}_{RR}$=5 dB, $\overline{\gamma}_{ID}$=15 dB, and $R_T$=1 bit/sec/Hz

performance and disrupts the communication link between the source and destination nodes.

Figs. 3.14- 3.15 depict the average end-to-end SER as a function of $P_S/N_o$. Precisely, in Fig. 3.14, it is observed that, for different mean height of the obstacle ($\chi$), it is once again noted that the $\overline{\text{SER}}_{\text{e2e}}$ performance improves with the decrease of the average height of the obstacles in both HD and FD. For instance, for a target $\overline{\text{SER}}_{\text{e2e}}$ of $10^{-2}$, there is a 3 dB loss when the $\chi$ goes from 0.028 to 0.06. Moreover, it is noticed that HDR outperforms FDR by approximately 2 dB. This is because SI affects the SER performance of FDR only. Different types of vehicle blockers were investigated such as small blocker (personal vehicle) and large blocker (van, bus). The results show that the blockage probability, and consequently the SER, is signicantly impacted by the blocker.

Finally, in Fig. 3.15 shows that for different source heights, it is noticed that the performance of the system improves when the source height in increased. Here, for a target $\overline{\text{SER}}_{\text{e2e}}$ of $10^{-2}$,

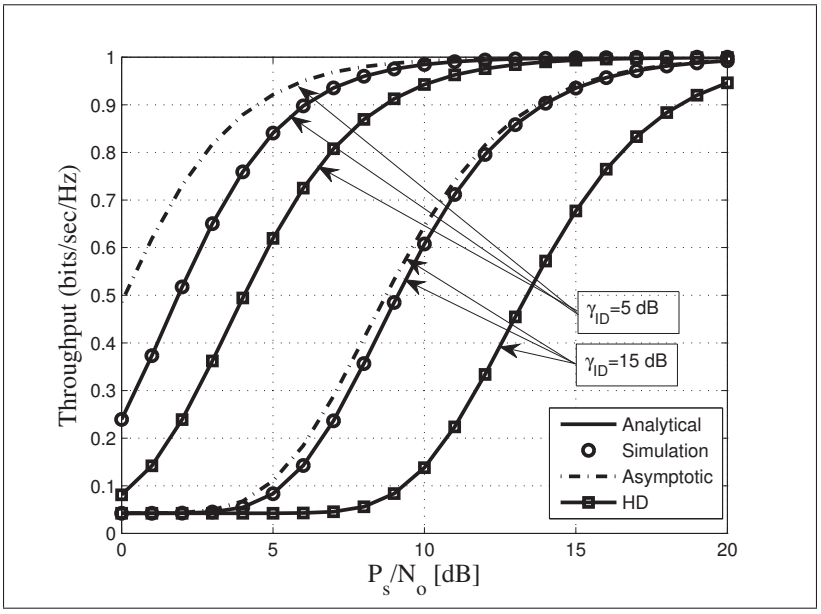


Figure 3.12 Throughput vs. $P_S/N_o$ for different values of $\overline{\gamma}_{ID}$ with $m_{ij}$=2, $\overline{\gamma}_{RR}$=5 dB and $R_S$=$R_T$=1 bit/sec/Hz

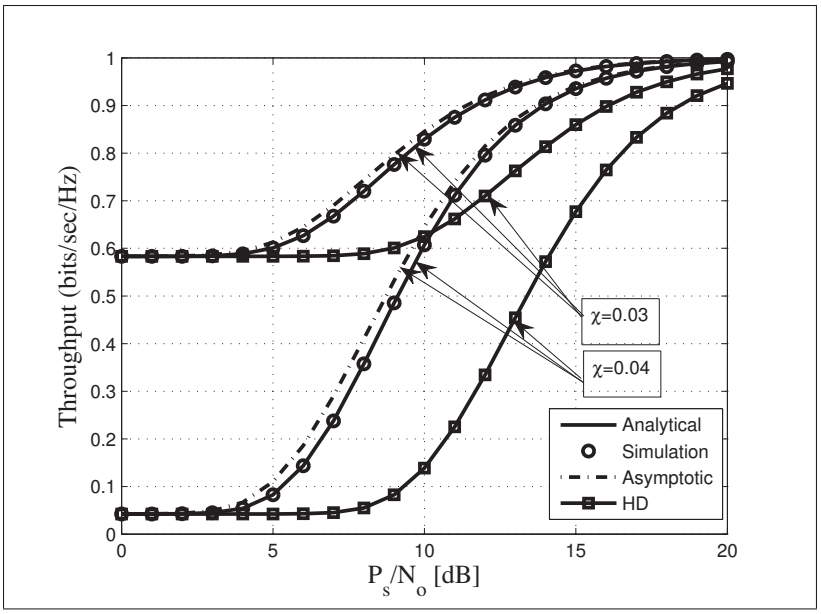


Figure 3.13 Throughput vs. $P_S/N_o$ for different values of $\chi$ with $\overline{\gamma}_{ID}$=15dB, $m_{ij}$=2, $\overline{\gamma}_{RR}$=5dB and $R_S$=$R_T$=1 bit/sec/Hz

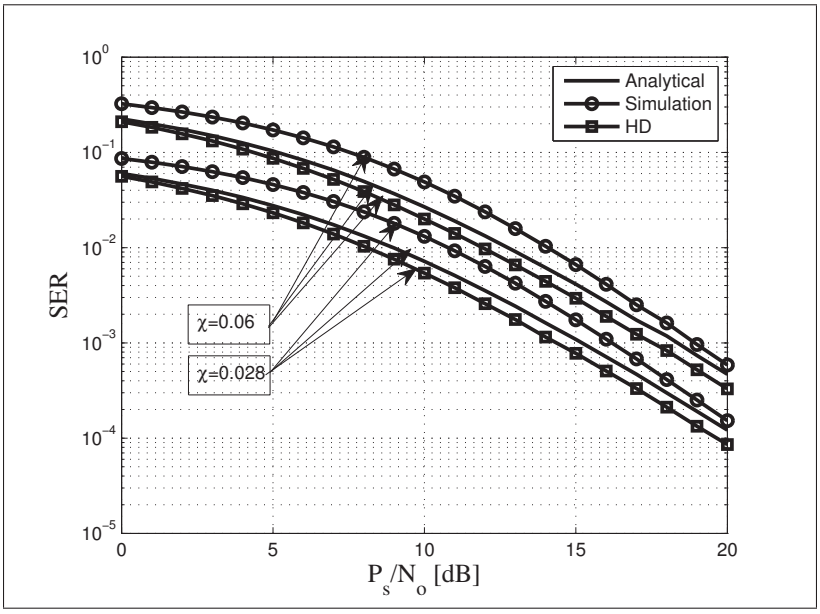


Figure 3.14 End-to-end symbol error rate vs. $P_S/N_o$ for different values of $\chi$ with $\overline{\gamma}_{ID}$=15 dB, $m_{ij}$=2 and $\overline{\gamma}_{RR}$=15 dB

when the antenna height is increased from 0.028 to 0.048, a gain of approximately 3 dB and 4 dB is observed in FDR and HDR, respectively. Moreover, the difference between small and large source heights is observable, with the large source heights cause a decrease in the end-to-end SER compared to smaller source heights. Here, FDR with a source height $\chi$=0.026 outperforms HDR with $\chi$=0.04).

## 3.6 Conclusions

In this paper, we presented a comprehensive framework for the performance analysis of AF-based FDR in vehicular communications. Both self-interference at the relay and co-channel interference at the destination were taken into account and exact and asymptotic outage probability, throughput, and symbol error rate lower bound expressions were derived over i.n.i.d Nakagami-*m* fading channels. In addition, the impact of blockage from obstacles on the outage probability was analyzed and evaluated. These expressions enable the assessment of practical dual-hop FDR systems. The influence of key system parameters such as CCI at the destination, the target rate, the mean height of the obstacles, the source's height, the distance between the

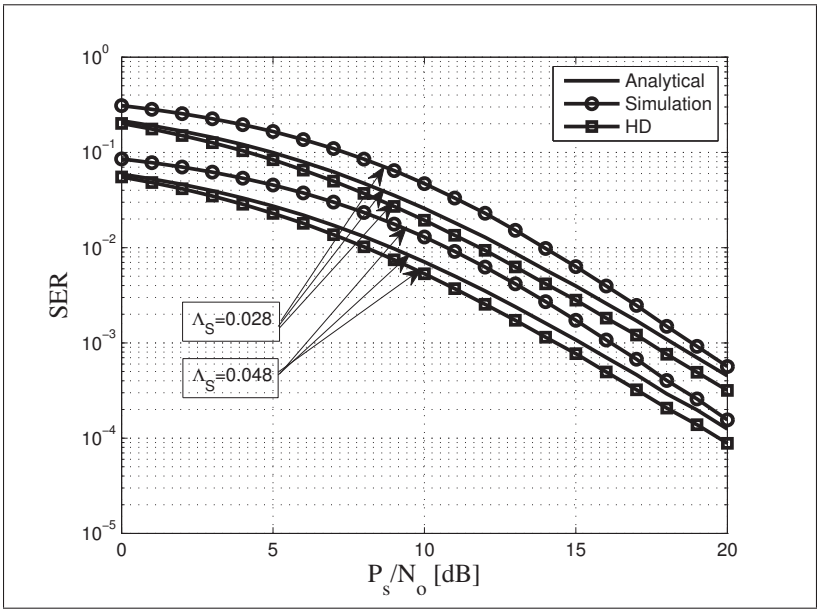


Figure 3.15 End-to-end symbol error rate vs. $P_S/N_o$ for different values of $\Lambda_S$ with $\overline{\gamma}_{ID}$=10, $m_{ij}$=2, $\chi$=0.04 dB, and $\overline{\gamma}_{RR}$=15 dB

source and the obstacles on the system's performance were investigated. It was demonstrated that, in both FD and HD relaying, the effect of vehicles as obstacles cannot be neglected even in the case of relatively sparse vehicular networks. Furthermore, we showed that the obstructing vehicles significantly increase the outage probability and decrease the throughput which highlights the importance of taking into account these phenomena in order to provide pragmatic information to the system designer.

# CHAPTER 4

# ERGODIC CAPACITY ANALYSIS OF FULL DUPLEX RELAYING IN THE PRESENCE OF CO-CHANNEL INTERFERENCE IN V2V COMMUNICATIONS

Khaled Eshteiwi [1], Georges Kaddoum[1], and Md Sahabul Alam [1]

[1] Département de Génie Electrique, École de technologie supérieure,
1100 Notre-Dame Ouest, Montréal, Québec, H3C 1K3, Canada
Article published in MDPI sensors Journal, December, 2019.

## 4.1 Abstract

We analyze the ergodic capacity of a dual-hop full duplex amplify-and-forward (AF) vehicle-to-vehicle (V2V) cooperative relaying system over Nakagami-*m* fading channels. In this context, the impacts of self-interference (SI) at the relay and co-channel interference (CCI) at the destination are taken into account in this analysis. Precisely, based on the analysis of the moment generating function (MGF) of the signal-to-interference-plus-noise ratio (SINR), new exact and lower bound expressions for the ergodic capacity are derived. The ergodic capacity upper bound is also derived based on the asymptotic outage probability of the approximated SINR. Monte-Carlo simulation results are presented to corroborate the derived analytical results. Our results show the significant impact of the considered interferences on the system performance. It is shown that the ergodic capacity is degraded when the average SI at the relay and/or the average CCI at the destination is increased. This highlights the importance of taking these phenomena into account in the performance evaluation in order to assess the practical limit of full duplex relaying (FDR) cooperative wireless communications. Interestingly, it is also observed that FDR with SI and CCI still shows a higher ergodic capacity than the interference-free half duplex relaying, especially at medium to high signal-to-noise ratios (SNRs).

## 4.2 Introduction

Full duplex relaying techniques have recently become an interesting research area due to their ability to increase the spectral efficiency compared to half duplex relaying Kim *et al.* (2015). This increased efficiency is achieved because it allows the relays to avoid any spectral efficiency loss by transmitting and receiving over the same band simultaneously. However, the performance of full duplex relaying (FDR) systems is affected by the self-interference at the relay nodes which arises due to the simultaneous transmission and reception. Although the received signal is significantly weaker than the transmitted signal due to heavy path loss and fading Duarte & Sabharwal (Nov. 2010); Jain *et al.* (2011), this effect cannot be perfectly eliminated. Meanwhile, in half duplex relaying (HDR), the relays are subject to a spectral efficiency loss as they transmit and receive in different time slots or over different frequency bands.

In the context of traditional HDR networks, the impact of co-channel interference (CCI) due to frequency reuse on the system performance has been extensively studied in the literature Ikki & Aissa (2012b); Lee *et al.* (2014); Trigui *et al.* (2013a,1); Zhu *et al.* (2014b). However, it has been noted that FDR networks, which are characterized by more frequency reuse, are more susceptible to CCI than their conventional HDR counterparts Almradi *et al.* (2018). Therefore, in practical FDR protocol designs, the impact of CCI should be taken into account for a more accurate system analysis.

In this paper, we present a comprehensively analytical method in obtaining closed-form expressions for the exact, lower and upper bonds of ergodic capacity of V2V FDR cooperative wireless networks used AF relaying technique over i.n.i.d Nakagami$-m$ fading channels. Such closed form expressions are extremely desirable because they allow for prompt and adequate evaluation of the system performance. Monte-Carlo simulation results are presented to corroborate and validate the derived analytical results.Thus, giving an exact analysis for ergodic capacity of FDR which is valid for all SNR regimes is the main objective of this paper. To the best of our knowledge, the effect of CCI on full duplex (FD) with AF relaying over Nakagami-

*m* fading channels has not been addressed in the available literature. We analyze the impact of CCI on FDR using variable gain AF relaying over independent but not necessarily identically distributed (i.n.i.d) Nakagami-*m* fading channels.

The main contributions of this paper are summarized below.

- We derive a closed form expression of the exact ergodic capacity of the equivalent end-to-end signal-to-interference-plus-noise ratio (SINR) of FD AF relaying over Nakagami-*m* fading channels under the effects of SI at the relay and of CCI at the destination.
- We also derive a closed form lower bound of the corresponding ergodic capacity. It should be noted that both the exact and the lower bound ergodic capacity expressions are derived based on the derivation of the SINR moment generating function (MGF) of the proposed system.
- We further derive a closed form expression for the ergodic capacity upper bound based on the asymptotic outage probability of the aforementioned system.

The remainder of this paper is organized as follows: Section 4.3 discusses the related work on ergodic capacity. Section 4.4 presents the system model. The exact, lower bound, and upper bound of the ergodic capacity expressions of the proposed system are derived in Section 4.5, and Section 4.6 presents the corresponding simulation results. Finally, closing remarks are discussed in Section 4.7.

## 4.3 Related Work

In this section, we present the works which mainly focus on the ergodic capacity analysis of FDR networks. FDR networks are often evaluated in terms of the ergodic capacity due to their ability to double the spectral efficiency compared to HDR. Recently, multiple-input multiple-output (MIMO) FDR techniques have attracted significant attention due to their ability to extend the network coverage, connectivity, and attain higher capacity without any requirement for extra power resources. Zero forcing (ZF) beamforming for MIMO FDR and HDR systems with

CCI using amplify-and-forward (AF) relaying over Rayleigh fading channels was investigated in Almradi *et al.* (2018). In Almradi & Hamdi (2017a), the impact of CCI at the relay node was investigated in terms of ergodic capacity for a one-way MIMO FDR system over Rayleigh fading channels. FDR systems with a non-orthogonal multiple access (NOMA) based communication system with two source-destination pairs were also investigated and analysed over Rayleigh fading channels in Kader, M. F., Shin, S. Y. & Leung, V. C. (2018). The impact of antenna correlation and imperfect channel state information (ICSI) on one-way MIMO FDR was analyzed in Almradi, A. & Hamdi, K. A. (2017b). Similarly, the influence of antenna correlation on two-way massive MIMO FDR was considered in Feng, J., Ma, S., Yang, G. & Poor, H. V. (2018), where the achievable sum-rate was derived. The authors in Shojaeifard, A., Wong, K.-K., Di Renzo, M., Zheng, G., Hamdi, K. A. & Tang, J. (2017a) analyzed the spectral efficiency of massive MIMO FDR systems where the main channels and the self-interference (SI) channels follow Rayleigh and Rician distributions, respectively. In Uddin, M. B., Kader, M. F. & Shin, S. Y. (2019); Zhong, C. & Zhang, Z. (2016), the authors analyzed the ergodic capacity of FD cooperative NOMA employing the DF relaying protocol over Rayleigh fading channels. The authors in Gohary, R. H. & Yanikomeroglu, H. (2014) presented the ergodic capacity of non-coherent MIMO Grassmannian modulation using DF over frequency flat block Rayleigh fading FDR. In Arifin, A. S. & Ohtsuki, T. (2015), the authors evaluated the asymptotic ergodic capacity of AF FD relaying MIMO using Tracy-Widom distribution. In addition, they showed that increasing the number of source antennas can reduce the capacity, especially when the number of destination antennas is fixed. The authors in Cui *et al.* (2014) studied the ergodic capacity of relay selection for two way FD AF relaying over Rayleigh fading channels. In Yang, K., Cui, H., Song, L. & Li, Y. (2015), the authors proposed FDR with joint antenna relay selection and SI elimination over block Rayleigh fading channels, where an ergodic capacity closed expression form was derived. The authors in You, J., Zhong, Z., Dou, Z., Dang, J. & Wang, G. (2016) introduced the ergodic capacity of FDR for high speed railway using both DF and AF relaying over Rayleigh fading channels and compared its performance with HDR. In Jebur, B. A., Tsimenidis, C. C. & Chambers, J. A. (2016), the authors analyzed the upper bound ergodic capacity of two-way AF FDR of orthogonal frequency division multiplex-

ing (OFDM) using physical layer network coding (PLNC). In Hu, R., Hu, C., Jiang, J., Xie, X. & Song, L. (2014a), a two way AF FDR over Rayleigh fading channels is considered, and the ergodic capacity closed form is provided where self-interference is simplified to be AWGN channel.

All of the above cited works were carried out assuming Rayleigh fading channels for ergodic capacity of FDR cooperative wireless networks. However, there are certain circumstances where the assumption of Rayleigh fading fails to represent the actual channel behavior of particular communication scenarios. For instance, if the suppression is not sufficient at the relay node, a line-of-sight (LOS) component may persist between the transmitter and receiver antennas at the relay and, hence, Rayleigh-fading is no longer a suitable model. Meanwhile, the Nakagami$-m$ distribution is a more general model that can describe many fading distributions such as Rician and Rayleigh Cheng *et al.* (2007). Furthermore, the Nakagami-*m* fading channel was shown to be the most accepted model for vehicular communications and short-range communications Eshteiwi *et al.* (2019); He *et al.* (2014); Mafra *et al.* (2016); Tassi *et al.* (2017). Motivated by these attributes, we consider the Nakagami-*m* fading channel model in this article.

Earlier works have mainly investigated the performance of FDR over Nakagami-*m* fading channels in terms of outage probability Ai, Y. & Cheffena, M.; Airod *et al.* (2017); Koç, A., Altunbas, I. & Yongaçoglu, A. (2016); Xu, Y., Wang, Y., Wang, C. & Xu, K. (2014). In Shi *et al.* (2015), the authors studied the performance of FDR over Nakagami-*m* fading channels in terms of outage probability and asymptotic capacity. A similar performance analysis was carried out in Gaafar, M., Khafagy, M. G., Amin, O., Schaefer, R. F. & Alouini, M.-S. (2017) for FDR with decode-and-forward (DF) relaying , in which the impact of improper Gaussian signaling was investigated. Although instructive, these works were built upon the classical assumption that there is no CCI from adjacent cells.

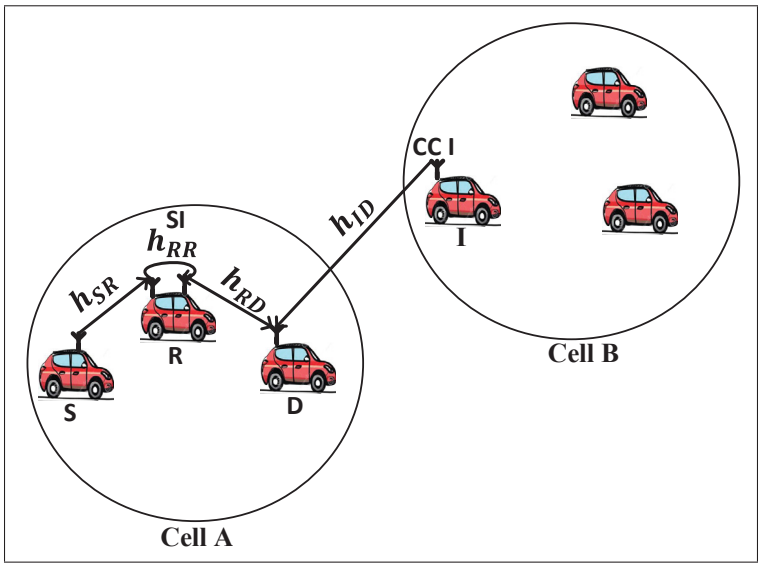


Figure 4.1 FDR with co-channel interference in vehicular communications

## 4.4 System model

We consider a vehicle-to-vehicle (V2V) FDR scenario, where, in a single cell A, a source $S$ communicates with a destination $D$ via an AF relay $R$, as shown in Fig. 4.1. It is assumed that the direct link between $S$ and $D$ is unavailable. In addition, we consider that $D$ experiences CCI resulting from the spectrum re-usage of an adjacent user $I$ in cell B. In this context, all the nodes are assumed to be equipped with a pair of antennas, one serving the purpose of transmitting while the other is for receiving. Thus, the received signal at $R$ is corrupted by self-interference due to the simultaneous transmission/reception which characterizes the full duplex transmission mode.

In this vein, we list our system model assumptions below:

**Assumption 1**: The direct link between $S$ and $D$ is assumed absent. This is a realistic assumption in many cases especially when the distance between $S$ and $D$ is larger than the coverage of the source Soliman, S. S. & Beaulieu, N. C. (2013).

**Assumption 2**: In the proposed system model, full duplex relaying (FDR) networks, which are characterized by more frequency reuse, are more susceptible to co-channel interference (CCI) than their conventional half duplex relaying (HDR) counterparts Almradi *et al.* (2018). Therefore, in practical FDR protocol designs, the impact of CCI should be taken into account for a more accurate system analysis.

**Assumption 3**: The Nakagami-*m* fading channel model is considered as it is widely used to model cooperative vehicular communication and short-range communications Mafra *et al.* (2016); Tassi *et al.* (2017). On the other hand, self-interference and its fading model heavily depend on the employed isolation/cancellation techniques. For instance, if the suppression is not sufficiently employed, line-of-sight (LOS) effects will persist and, hence, Rayleigh-fading will not be a suitable model since it does not count the LOS component. Moreover, the Nakagami$-m$ fading is able to span a wide range of fading distributions that can also capture either scenarios in case of absence/presence of LOS effects. Furthermore, the Nakagami$-m$ distribution is a more general model which can be used to describe many fading distributions such as Rician, Rayleigh or fading environment that is more severe than Rayleigh fading distribution Cheng *et al.* (2007). Furthermore, the Nakagami-*m* fading channel was shown to be the most accepted model for vehicular communications and short-range communications Eshteiwi *et al.* (2019); He *et al.* (2014); Mafra *et al.* (2016); Tassi *et al.* (2017). A benefit of the Nakagami$-m$ fading model is that it can be used when the received signal has contributions from both diffuse and specular scattering. It also offers greater flexibility and accuracy in fitting to experimental data He *et al.* (2014). Motivated by this, in this article, we considered the Nakagami-*m* fading channel model. We further assume that all underlying channels are quasi-static and remain constant during one slot, but change independently from one slot to another (this assumption is commonly used in the context of cooperative networks; see for example da Costa & Aissa (2009); Jalil *et al.* (2010); Krikidis *et al.* (2008)) and the received signal undergoes slow fading (i.e., the symbol period of the received signal is smaller than the coherence time of the channel), which can be justified for V2V communications scenarios in rush-hour traffic.

In this context, the received signal at $R$ is given as

$$y_{SRR} = \sqrt{P_S} h_{SR} x_S + \sqrt{P_R} h_{RR} x_R + n_R, \tag{4.1}$$

where $x_S$ and $x_R$ are the transmitted binary phase shift keying (BPSK) signals while $P_S$ and $P_R$ denote the transmit powers at $S$ and $R$, respectively. Moreover, $h_{SR}$ and $h_{RR}$ are the channel coefficients of the $S$-$R$ and the self-interference $R$-$R$ links, respectively. These are modeled as mutually i.n.i.d Nakagami$-m$ random variables. All the channels are assumed to be quasi-static and remain constant during one slot, but change independently from one slot to another, which is typically the case for V2V communications scenarios in rush-hour traffic da Costa & Aissa (2009); Jalil *et al.* (2010); Krikidis *et al.* (2008). The term $n_R$ corresponds to the additive white Gaussian noise (AWGN) at $R$ with variance $N_o$. At the destination side, the received signal from $R$ is obtained as

$$y_D = \sqrt{P_R} h_{RD} \kappa y_{SRR} + \sqrt{P_I} h_{ID} x_I + n_D, \tag{4.2}$$

where $h_{RD}$ and $h_{ID}$ are the channel coefficients of the $R$-$D$ (information link) and $I$-$D$ (CCI link), respectively. In addition, $P_I$ is the transmitted power of the interference signal, $n_D$ is the AWGN at $D$ with variance $N_o$, and $\kappa$ is the amplification factor at $R$ which satisfies $\kappa \leq \sqrt{P_R/(P_S |h_{SR}|^2 + P_R |h_{RR}|^2 + N_o}$ Eshteiwi *et al.* (2019). Here, perfect CSI is considered available at the destination node Alghorani & Seyfi (2017); Alghorani *et al.* (2015a); Tassi *et al.* (2017). This assumption is valid since a feedback channel could be used to send pilot signals before the transmission to acquire knowledge about the channel properties Caire *et al.* (2010). In this study, we employ the normalized distance model Ikki & Ahmed (Spring 2009); Laneman *et al.* (Dec. 2004); Lateef *et al.* (June 2010) to take into account the impact of pathloss which implies that $\mathbb{E}(|h_{ij}|^2) = (d_{SD}/d_{ij})^{\eta}$, where $d_{ij}$ is the relative distance from $i$ to $j$, $ij \in \{SR, RR, RD, ID\}$, and $\eta$ is the pathloss exponent.

## 4.5 Performance Analysis

Considering the AF relaying strategy while taking into account the impact of SI at R and CCI at D, the instantaneous SINR of the received signal at $D$ can be written as Hasna, M. O. & Alouini, M.-S. (2003)

$$\gamma_{eq} = \frac{\gamma_1 \gamma_2}{\gamma_1 + \gamma_2 + 1}, \tag{4.3}$$

where $\gamma_1 = \frac{\gamma_{SR}}{\gamma_{RR}+1}$ and $\gamma_2 = \frac{\gamma_{RD}}{\gamma_{ID}+1}$. Here $\gamma_{SR} = P_S |h_{SR}|^2 / N_o$, $\gamma_{RR} = P_R |h_{RR}|^2 / N_o$, $\gamma_{RD} = P_R |h_{RD}|^2 / N_o$, and $\gamma_{ID} = P_I |h_{ID}|^2 / N_o$ denote the instantaneous SNRs of the *S-R*, *R-R*, *R-D* and *I-D* links, respectively. For the considered scenario, since the channel coefficients are modelled as Nakagami$-m$ distributions, $\left|h_{ij}\right|^2$ follows a Gamma distribution. Moreover, since the channels are i.n.i.d, the PDF of $\gamma_{ij}$ can be written as Simon, M. K. & Alouini, M.-S. (2005)

$$f_{\gamma_{ij}}(x) = \frac{C_{ij}^{m_{ij}}}{\Gamma(m_{ij})} x^{m_{ij}-1} \exp(-xC_{ij}), \tag{4.4}$$

where $\Gamma(z)$=$\int_0^\infty \exp(-t)t^{z-1}dt$ denotes the Gamma function (Jeffrey & Zwillinger, 2007, Eq. (8.310.1)), $m_{ij} > 0.5$ is the shape parameter, $C_{ij}$=$\frac{m_{ij}}{\bar{\gamma}_{ij}}$, $\bar{\gamma}_{ij}$=$\mathbb{E}(\left|h_{ij}\right|^2)P_i/N_o$ is the average SNR, and $\mathbb{E}(.)$ is the expectation operator.

### 4.5.1 Exact Ergodic Capacity

The ergodic capacity is defined as the expected value of the instantaneous mutual information between the source and destination, which is given as

$$\mathrm{EC} = \mathbb{E}\left[\log_2(1+\gamma_{eq})\right]. \tag{4.5}$$

Substituting $\gamma_{eq}$ from Eq. (4.3) into Eq. (4.5), we get

$$\mathrm{EC} = \frac{1}{\ln(2)} \mathbb{E}\left[\ln\left(1+\frac{\gamma_1\gamma_2}{\gamma_1+\gamma_2+1}\right)\right]. \tag{4.6}$$

**Theorem 1**: Assuming full duplex mode, the exact closed-form ergodic capacity expression of AF cooperative relaying systems with SI at the relay and CCI at the destination is given by Eq. (4.7).

$$\begin{aligned}
\mathrm{EC} = & \frac{1}{\ln(2)} \sum_{s=0}^{q} \binom{q}{s} (C_{SR})^s \sum_{w=0}^{r} \binom{r}{w} (C_{RD})^w \Gamma(q+r+2-s-w) \left( \frac{C_{RR}^{m_{RR}}}{\Gamma(m_{RR})} \sum_{j=0}^{m_{SR}-1} \sum_{k=0}^{j} \sum_{q=0}^{\infty} \binom{j}{k} \right. \\
& \times \frac{(C_{SR})^{j-k-m_{RR}}}{j!} (k+m_{RR}-1)! \frac{(-1)^q}{q!} \sum_{f=0}^{j+q} \binom{j+q}{f} (-1)^{j+q-f} (\frac{C_{RR}}{C_{SR}})^{j+q-f} \\
& \left. \times \left[ \frac{(f-k-m_{RR}+1) - (\frac{C_{RR}}{C_{SR}})^{f-k-m_{RR}+1}}{f-k-m_{RR}+1} \right] \right) \left( \frac{C_{ID}^{m_{ID}}}{\Gamma(m_{ID})} \sum_{l=0}^{m_{RD}-1} \sum_{t=0}^{l} \sum_{r=0}^{\infty} \binom{l}{t} \frac{(C_{RD})^{l-t-m_{ID}}}{l!} \right. \\
& \times (t+m_{ID}-1)! \frac{(-1)^r}{r!} \sum_{e=0}^{l+r} \binom{l+r}{e} (-1)^{l+r-e} (\frac{C_{ID}}{C_{RD}})^{l+r-e} \\
& \left. \times \left[ \frac{(e-t-m_{ID}+1) - (\frac{C_{ID}}{C_{RD}})^{e-t-m_{ID}+1}}{e-t-m_{ID}+1} \right] \right).
\end{aligned} \tag{4.7}$$

*Proof*: The proof is provided in **Appendix II**

### 4.5.2 Ergodic Capacity Lower Bound

To simplify the derivation of the ergodic capacity lower bound expression, let us re-write Eq. (4.6) as follows

$$\begin{aligned}
\mathrm{EC} &= \mathbb{E}\left[\log_2\left(\frac{(1+\gamma_1)(1+\gamma_2)}{\gamma_1+\gamma_2+1}\right)\right] \\
&= \mathrm{EC}_{\gamma_1} + \mathrm{EC}_{\gamma_2} - \mathrm{EC}_{\gamma_T},
\end{aligned} \tag{4.8}$$

where $\mathrm{EC}_{\gamma_i}$=$\mathbb{E}[\log_2(1+\gamma_i)]$, $i \in \{1,2\}$, and $\mathrm{EC}_{\gamma_T}$=$\mathbb{E}[\log_2(1+\gamma_1+\gamma_2)]$. Here, a lower bound for $\mathrm{EC}_{\gamma_T}$ is obtained by utilizing the Jensen's inequality as follows

$$\mathrm{EC}_{\gamma_T} \leq \log_2\left(1+\mathbb{E}(\gamma_1)+\mathbb{E}(\gamma_2)\right). \tag{4.9}$$

**Theorem 2**: Assuming full duplex mode, the ergodic capacity lower bound of an AF cooperative relaying system with SI at the relay and CCI at the destination is given by Eq. (4.10).

$$\begin{aligned}
\mathrm{EC}_{lower} &= \Bigg( \frac{1}{\ln(2)} \frac{C_{RR}^{m_{RR}}}{\Gamma(m_{RR})} \sum_{j=0}^{m_{SR}-1} \sum_{k=0}^{j} \sum_{q=0}^{\infty} \binom{j}{k} \frac{(C_{SR})^{j-k-m_{RR}}}{j!} (k+m_{RR}-1)! \frac{(-1)^q}{q!} \sum_{f=0}^{j+q} \binom{j+q}{f} \\
&\times (-1)^{j+q-f} \left(\frac{C_{RR}}{C_{SR}}\right)^{j+q-f} \sum_{s=0}^{q} \binom{q}{s} (C_{SR})^{q-s} \Gamma(s+1) \left[ \frac{(f-k-m_{RR}+1) - \left(\frac{C_{RR}}{C_{SR}}\right)^{f-k-m_{RR}+1}}{f-k-m_{RR}+1} \right] \Bigg) \\
&+ \Bigg( \frac{1}{\ln(2)} \frac{C_{ID}^{m_{ID}}}{\Gamma(m_{ID})} \sum_{l=0}^{m_{RD}-1} \sum_{t=0}^{l} \sum_{r=0}^{\infty} \binom{l}{t} \frac{(C_{RD})^{l-t-m_{ID}}}{l!} (t+m_{ID}-1)! \frac{(-1)^r}{r!} \sum_{e=0}^{l+r} \binom{l+r}{e} (-1)^{l+r-e} \\
&\times \left(\frac{C_{ID}}{C_{RD}}\right)^{l+r-e} \sum_{u=0}^{r} \binom{r}{u} (C_{RD})^{r-u} \Gamma(u+1) \left[ \frac{(e-t-m_{ID}+1) - \left(\frac{C_{ID}}{C_{RD}}\right)^{e-t-m_{ID}+1}}{e-t-m_{ID}+1} \right] \Bigg) \\
&- \log_2 \Bigg( 1 + \frac{C_{SR}^{m_{SR}} C_{RR}^{m_{RR}}}{\Gamma(m_{SR})\Gamma(m_{RR})} \sum_{l_1=0}^{m_{SR}} \binom{m_{SR}}{l_1} \frac{\Gamma(m_{RR}+l_1)}{C_{SR}^{m_{RR}+l_1}} \exp(C_{RR}) \sum_{l_2=0}^{m_{SR}} (-1)^{m_{SR}-l_2} \left(\frac{C_{RR}}{C_{SR}}\right)^{m_{SR}-l_2} \\
&\times (C_{SR})^{-(l_2-m_{RR}-l_1+1)} \Gamma(l_2-m_{RR}-l_1+1, C_{RR}) + \frac{C_{RD}^{m_{RD}} C_{ID}^{m_{ID}}}{\Gamma(m_{RD})\Gamma(m_{ID})} \sum_{j_1=0}^{m_{RD}} \binom{m_{RD}}{j_1} \frac{\Gamma(m_{ID}+j_1)}{C_{RD}^{m_{ID}+j_1}} \\
&\times \exp(C_{ID}) \sum_{j_2=0}^{m_{RD}} (-1)^{m_{RD}-j_2} \left(\frac{C_{ID}}{C_{RD}}\right)^{m_{RD}-j_2} (C_{RD})^{-(j_2-m_{ID}-j_1+1)} \Gamma(j_2-m_{ID}-j_1+1, C_{ID}) \Bigg).
\end{aligned} \tag{4.10}$$

*Proof*: The proof is provided in **Appendix II**

### 4.5.3 Ergodic Capacity Upper Bound

In order to provide further insights into the system performance, we also derive an upper bound ergodic capacity expression in the following theorem.

**Theorem 3**: Assuming full duplex mode, the ergodic capacity upper bound of AF cooperative relaying systems with SI at the relay and CCI at the destination is given by Eq. (4.11), where $G_{1,[1,1],1,[1,1]}^{1,1,1,1,1}(.|.)$ is the extended generalized bivariate Meijer's G-function Ansari *et al.* (2011); Verma (1966).

$$\begin{aligned}\mathrm{EC}_{upper} =& \frac{C_{RR}^{m_{RR}} C_{ID}^{m_{ID}}}{\ln(2)\Gamma(m_{RR})\Gamma(m_{ID})} \sum_{j=0}^{m_{SR}-1} \frac{(C_{SR})^j}{j!} \sum_{k=0}^{j} \binom{j}{k} (k+m_{RR}-1)! \sum_{l=0}^{m_{RD}-1} \frac{(C_{RD})^l}{l!} \sum_{t=0}^{l} \\ & \times \binom{l}{t} (t+m_{ID}-1)! \sum_{q=0}^{\infty} \frac{(-1)^q (C_{SR}+C_{RD})^q}{q!\Gamma(k+m_{RR}) C_{RR}^{k+m_{RR}} \Gamma(t+m_{ID}) C_{ID}^{t+m_{ID}}} \\ & \times G_{1,[1,1],1,[1,1]}^{1,1,1,1,1} \left( \begin{matrix} -(j+l+q);(k+m_{RR});(t+m_{ID}) \\ 1+j+l+q;0;0 \end{matrix} \middle| \frac{C_{SR}}{C_{RR}}, \frac{C_{RD}}{C_{ID}} \right)\end{aligned} \tag{4.11}$$

*Proof*: The proof is provided in **Appendix II**

## 4.6 Simulation Results

This section seeks to validate the accuracy of the derived analytical expressions and to provide more insights into the performance of practical FDR networks. To this end, we consider a FDR network where the source communicates with the destination via an AF full duplex relay including SI and CCI at the relay and destination nodes, respectively. Without loss of generality, all AWGN terms are assumed to be zero-mean complex Gaussian random variables with variance $N_o$. In addition, a pathloss exponent of $\eta = 3.18$ and a shape parameter of $m_{ij} = 2$ are considered. Unless otherwise stated, the derived analytical expressions are represented by solid lines whereas the markers depict the corresponding simulation results. In this context, Figs. 4.2-4.5 show the exact as well as the lower and upper bounds of the ergodic capacity obtained in Eq. (4.7), Eq. (4.10), and Eq. (4.11), respectively, where a perfect match is observed between the analytical and the corresponding simulation results, while the derived lower

and upper bound expressions provide a close approximation to the actual performance of the system.

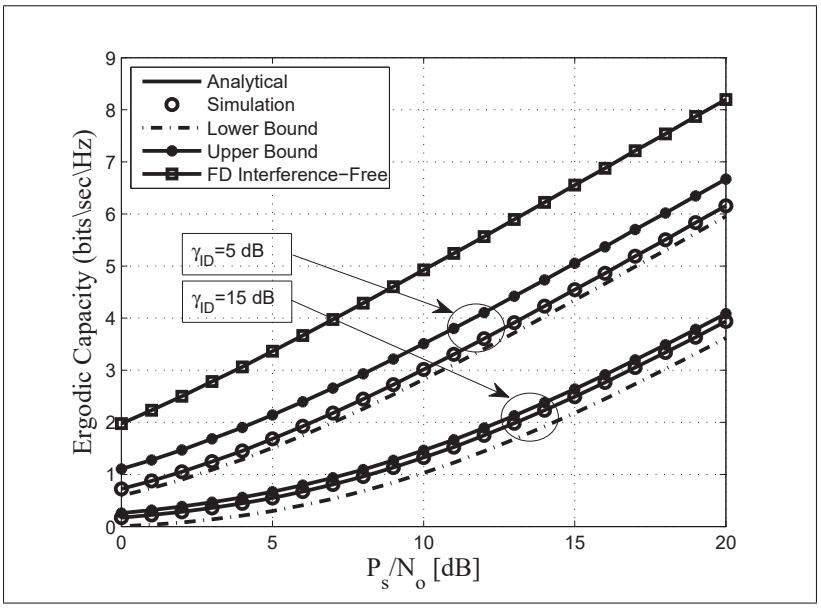


Figure 4.2 Ergodic capacity vs. $P_S/N_o$ for different values of $\overline{\gamma}_{ID}$, $m_{ij}$=2, $d_{SR}$= 0.45, $d_{RD}$= 0.55, $\overline{\gamma}_{RR}$=5 dB, and $\eta = 3.18$

Specifically, Fig. 4.2 illustrates the ergodic capacity of the considered dual-hop FDR cooperative communication system versus $P_S/N_o$ for different levels of CCI. From the obtained results it is seen that when $\overline{\gamma}_{ID}$ goes from 5 dB to 15 dB, the upper bound becomes closer to the exact ergodic capacity while the lower bound is 0.5 dB lower than the exact value. Moreover, our results are compared to FDR systems assuming that both the relay and the destination nodes are interference-free, which provides a significant ergodic capacity improvement. The simulation results in this figure are consistent with our theoretical analysis where the destructive impact of the co-channel interferences on the system performance are clearly indicated. For instance, in the ideal case (FD interference-free) the ergodic capacity =5.6 bits/sec/Hz at $P_S/N_o$=12 dB and for $\overline{\gamma}_{ID}$=5 dB, the corresponding ergodic capacity values are 3.6, 3.4, and 4.1 bits/sec/Hz for the exact, lower, and upper bounds respectively at $P_S/N_o$=12 dB, while the ergodic capacity values at $\overline{\gamma}_{ID}$=15 dB are 1.7, 1.4, and 1.9 bits/sec/Hz for the exact, lower, and upper

bounds respectively. Hence, the considered interferences impose severe constraints on the system's ergodic capacity, which highlights the need for system characterization and the design of suitable interference cancellation techniques for the efficient implementation of the vehicular communication paradigm.

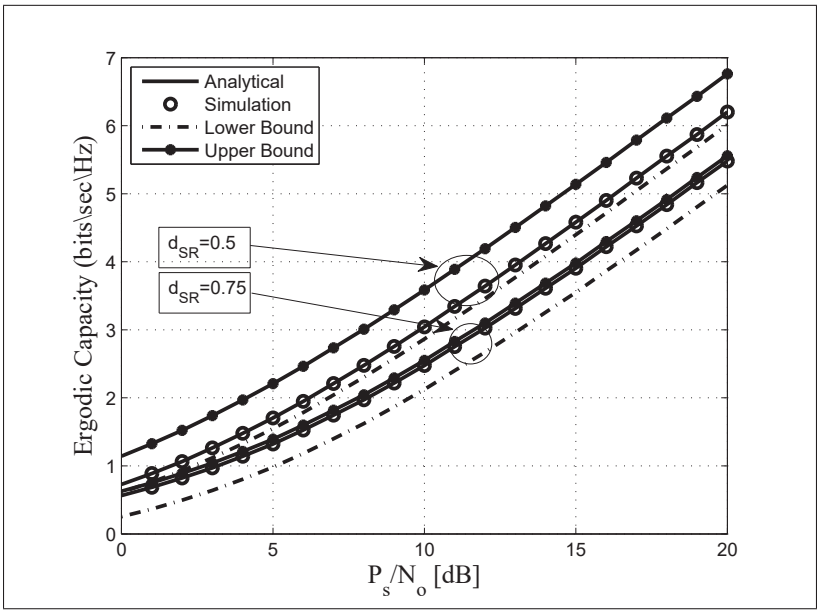


Figure 4.3 Ergodic capacity vs. $P_S/N_o$ for different values of $d_{SR}$ and $d_{RD}$, $\overline{\gamma}_{ID}$= $\overline{\gamma}_{RR}$=5 dB, $m_{ij}$=2, and $\eta = 3.18$

Fig. 4.3 exhibits the performance of the proposed system in terms of ergodic capacity for different relay locations. From the figure, it is seen that the ergodic capacity of the system improves if the relay is placed in the middle of the source-destination pair (i.e., $d_{SR}$= 0.5 and $d_{RD}$= 0.5, with $d_{SD}$=1), which corresponds to a balanced average channel gain between the $S-R$ and $R-D$ links. On the other hand, the ergodic capacity is decreased when the relay is located close to the destination node ($d_{SR}$= 0.75 and $d_{RD}$= 0.25). For instance, for $d_{RD}$= 0.5, at 10 dB, the exact, lower, and upper bound of the ergodic capacity values are 3, 2.8, and 3.6 bits/sec/Hz, respectively. While for $d_{RD}$= 0.75, the corresponding exact, lower, and upper bound are 2.5, 2.1, and 2.6 bits/sec/Hz, respectively.

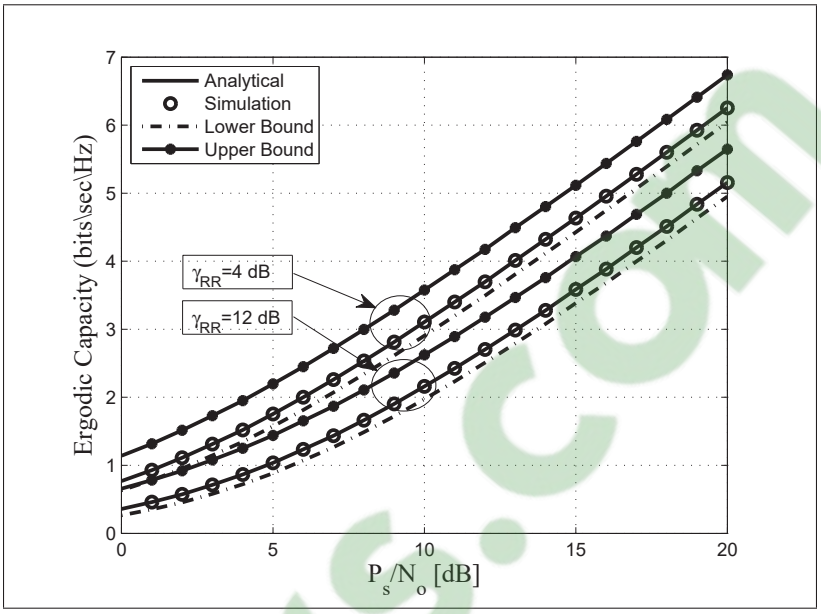


Figure 4.4 Ergodic capacity vs. $P_S/N_o$ for different values of $\overline{\gamma}_{RR}$, $m_{ij}$=2, $d_{SR}$= 0.45, $d_{RD}$= 0.55, $\overline{\gamma}_{ID}$=5 dB, and $\eta = 3.18$

Fig. 4.4 shows the ergodic capacity of dual-hop FDR systems for different levels of self-interference at the relay. From the obtained results, it is observed that when the average self-interference at the relay increases, the system's performance is deteriorated. For example, an ergodic capacity of 5.3 and 4.2 bits/sec/Hz appears at 17 dB for $\overline{\gamma}_{RR} = 4$ and $\overline{\gamma}_{RR} = 12$ dB, respectively. This figure validates the theoretical results obtained in Eq. (4.6), where the destructive influence of the self-interference on the ergodic capacity performance is formulated. This can be explained by the fact that increasing the average SI at the relay degrades the relay transmitted signal to the destination node which decreases the ergodic capacity, therefore affecting the system's performance.

Fig. 4.5 depicts the ergodic capacity of FDR and HDR in the presence/absence of interference. We observe that when there are no interferences at both the relay and the destination nodes in both FDR and HDR schemes, FDR can achieve twice the capacity of HDR. For instance, at the SNR range of 20 dB, the obtained ergodic capacity of the FDR system is 8.2 bits/sec/Hz, whereas the ergodic capacity of HDR is only 4.1 bits/sec/Hz. This is because the transmission

and reception in HDR is accomplished in two time slots while one time slot is enough in the case of FDR. In addition, the performance of both FDR and HDR is degraded in the presence of interferences at the relay and destination nodes. Interestingly, from the figure, it is also seen that FDR with SI and CCI still achieves higher ergodic capacity compared to the interference free HDR case, especially at medium and high $P_S/N_o$.

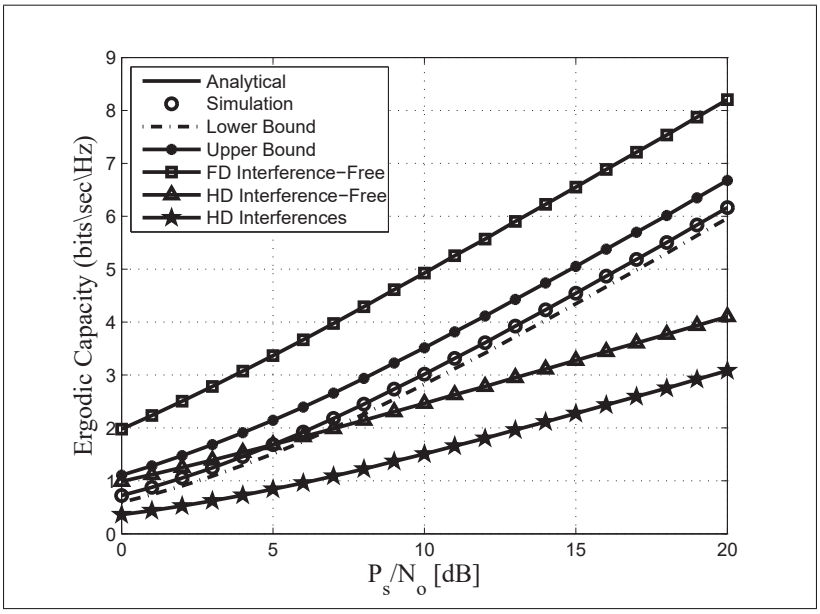


Figure 4.5 Ergodic capacity vs. $P_S/N_o$ for different relaying techniques, $\overline{\gamma}_{RR} = \overline{\gamma}_{ID}$=5 dB, $m_{ij}$=2, $d_{SR}$= 0.45, $d_{RD}$= 0.55, and $\eta = 3.18$

Fig. 4.6 plots the ergodic capacity as a function of the $P_S/N_o$ for different values of the distance between user $I$ and the destination node ($d_{ID}$) where $P_I/N_o$ was set to 2 dB. It is clear that when the user $I$ is close to the destination, the effective SNR between the user $I$ and the destination increases, and consequently the ergodic capacity decreases, which degrades the system's performance. For instance, for a target of ergodic capacity of 3 bits/sec/Hz, the required transmit $P_S/N_o$ is 11 dB and 17 dB when $d_{ID}$=0.7 and 0.45, respectively.

Fig. 4.6 plots the ergodic capacity as a function of the $P_S/N_o$ for different values of the distance between user $I$ and the destination node ($d_{ID}$) where $P_I/N_o$ was set to 2 dB. It is clear that when the user $I$ is close to the destination, the effective SNR between the user $I$ and the destination

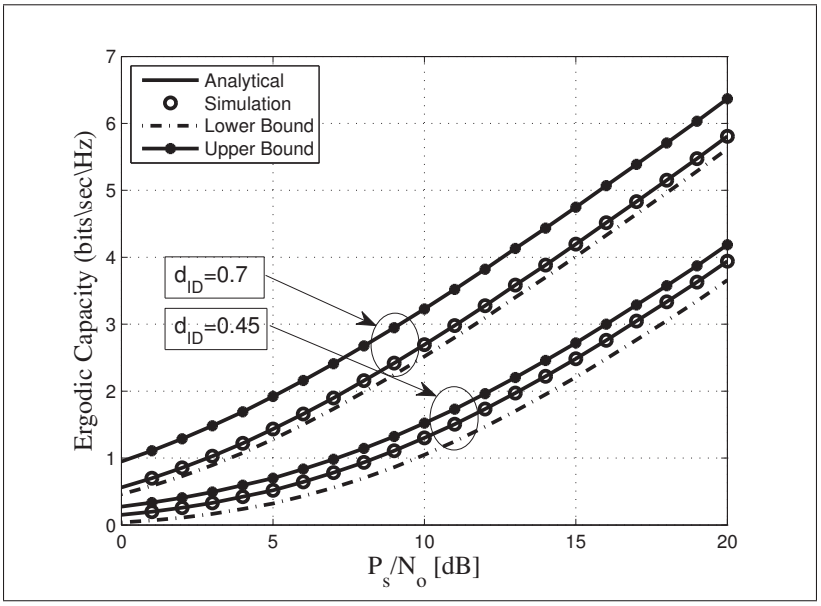


Figure 4.6 Ergodic capacity vs. $P_S/N_o$ for different values of $d_{ID}$ with $\overline{\gamma}_{RR} = 8$ dB, $m_{ij} = 2$, $d_{SR} = 0.45$, $d_{RD} = 0.55$, and $\eta = 3.18$

increases, and consequently the ergodic capacity decreases, which degrades the system's performance. For instance, for a target of ergodic capacity of 3 bits/sec/Hz, the required transmit $P_S/N_o$ is 11 dB and 17 dB when $d_{ID}$=0.7 and 0.45, respectively.

As for the ergodic capacity, Fig. 4.7 shows the ergodic capacity as a function of the $P_S/N_o$. The obtained results are compared to the exact simulation under different values of $m_{ij}$ in full duplex mode and under the impact of self-interference over Nakagami$-m$ fading channels. It is clear that, as $m_{ij}$ increases, the ergodic capacity increases and the performance improves. Moreover, this figure clearly exhibits a perfect match between our analytical expressions and the corresponding simulation results. Meanwhile, it can be observed that the derived lower and upper bounds are close to the exact simulation results where a gap of approximately 1 dB is observed between the lower and upper bounds and the exact expression.

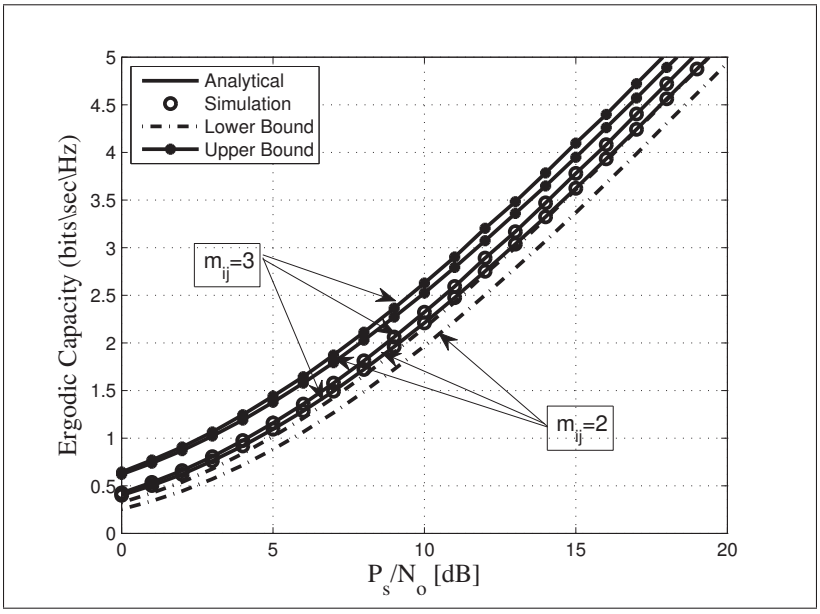


Figure 4.7 Ergodic capacity vs. $P_S/N_o$ for different values of $m_{ij}$ with $\overline{\gamma}_{RR} = 5$ dB, $\overline{\gamma}_{ID} = 10$ dB, $d_{SR} = 0.45$, $d_{RD} = 0.55$, and $\eta = 3.18$

## 4.7 Conclusions

In this paper, we presented a comprehensive framework for the ergodic capacity evaluation of FDR in vehicular communications. Both SI at the relay and CCI at the destination were taken into account. In particular, we evaluated the performance of V2V wireless cooperative communications with an FD non-regenerative AF relaying system over i.n.i.d Nakagami-$m$ fading channels. Moreover, we derived closed form expressions for exact, lower bound, and upper bound expressions of the ergodic capacity. These expressions offer an efficient way to assess the ergodic capacity of the considered dual-hop FDR systems with SI and CCI. In this context, the influences of key system parameters such as the average CCI at the destination, the average SI at the relay node, and the relay position between the source and destination on the system performance were investigated. Our results showed that the system performance is significantly degraded by an increase in the average CCI at the destination or average SI at the relay. We Also found that the best location for the relay is in the middle of the source-destination link. Furthermore, we showed that when the user $I$ is close to the destination node,

the ergodic capacity decreases and the system's performance degrades. This insight reveals the importance of taking into account these phenomena in order to provide pragmatic information with which to assess the practical limits of V2V FDR cooperative wireless communications to the system designer.

# CHAPTER 5

# PERFORMANCE ANALYSIS OF FULL-DUPLEX VEHICLE RELAY-BASED SELECTION IN DENSE MULTI-LANE HIGHWAYS

Khaled Eshteiwi [1], Georges Kaddoum[1], Kais Ben Fredj[2], Ebrahim Soujeri [1],
, and François Gagnon [1]

[1] Département de Génie Electrique, École de technologie supérieure,
1100 Notre-Dame Ouest, Montréal, Québec, H3C 1K3, Canada
[2] Département de Génie Electrique, Institut National de La Recherche Scientifique (INRS),
490 rue de la Couronne, Montréal, Québec, G1K 9A9, Canada
Article published in IEEE Access, March, 2019.

## 5.1 Abstract

This article considers a dual-hop vehicle-to-vehicle (V2V) communication system equipped with full duplex relays (FDR) in millimeter-wave (mmWave) networks. The performance of this network is studied in a dense multi-lane highway considering cooperative best vehicular relay selection strategy. In fact, two different FDR schemes are analyzed for the given network. In the first scheme that is called self-interference (SI) vehicle relaying selection, the FDR models the source-relay and the relay-relay links by one channel state information (CSI) coefficient (i.e. a single channel estimation of the two links) while in the second scheme that is called individual self-interference (ISI) vehicle relaying selection, the CSI of the source-relay and the relay-relay links are estimated separately. Moreover, relay-destination link is modeled by one CSI coefficient in both aforementioned schemes. Dissimilar to traditional V2V schemes where either line-of-sight (LOS) or non-line-of-sight (NLOS) propagation is considered, and the effect of the blockage on V2V communications is not taken into account when analyzing the performance, in this paper, we propose a probabilistic model capturing the occurrences of LOS and NLOS propagations, which depend on the movement of the vehicles between the central and adjacent lanes. Thus, the movement of the vehicles between any two adjacent lanes is assumed to take place independently and is deemed to be according to Poisson distribution. This vehicle movement model considers the blockage between the source and destination links.

In this vein, a LOS link is considered available when the center lane is clear of vehicles between the source and destination nodes, an NLOS link is assumed otherwise. Furthermore, a Nakagami-*m* fading channel model is considered due to its excellent representation of the V2V communication environment. The LOS/NLOS probabilities combined together with the probability of blockage are used to analyze the system performance. The cumulative density function (CDF) expression of the signal-to-interference-plus-noise ratio (SINR) at the relay is derived for both relaying schemes. Moreover, lower bound expressions of the end-to-end outage probabilities are developed and used to express throughput. Lastly, the theoretical results postulated and presented here are verified by numerical simulation for a variety of parameters.

## 5.2 Introduction

The growth and expansion of intelligent transportation technologies for the next generation vehicular communications have brought with them a few key challenges. Focusing on inter-vehicle congestions during heavy traffic or accidents, an ultra-low latency transmission is vital to send ultra-fast warning messages within an extremely short time frame Yang *et al.* (2004). This is because the inter-connected and autonomous vehicles of the future will need to exchange information at a high data rate and low latency. In this context, emerging technologies have recently used mmWave frequency bands between 30 GHz and 300 GHz to provide an alternative solution in order to offer both high data rates, of up to 7 Gbps, and low latency of less than 10 msec Ghosh *et al.* (2014); Tassi *et al.* (2017). Some of the key features of advanced vehicular applications under the umbrella of intelligent transportation systems (ITSs) can be exploited to offer passengers smart applications, including vehicle parking, accident response, traffic congestion and accident avoidance tools Qureshi & Abdullah (2013). Based on the aforementioned applications, the enhancement of the currently ongoing systems capacity and the incremental growth of data rates are extremely important, and are therefore, being explored as part of the fifth-generation (5G) standardization effort by third Generation Partnership Project (3GPP). One of the key areas to explore under 5G is vehicular cooperative wireless Campolo *et al.* (2017), wherein the objectives are to reduce the aftermath of multi-path fading

and signal degradation within the vehicular wireless communications space. Likewise, cooperative relaying systems based on V2V communications, also known as inter-vehicular communications (IVC), increase the diversity and generally improve the performance of wireless communication systems.

In addition, the cooperation mechanism between vehicles and infrastructure can be improved by extending the technology to enhance the coverage area, thereby offering improved road safety and better network connectivity Silva *et al.* (2017). One of the key solutions to this requirement is the implementation of full duplex relaying in order to reduce the end-to-end delay and to concurrently double the spectral efficiency when self-interference is eliminated Kim *et al.* (2015). This is because with full duplex, also known as in-band full duplex, the relays avoid any spectral efficiency loss by transmitting and receiving over the same band simultaneously. However, a full duplex relaying performance could be severely degraded, because of the self-interference at the relay node due to the simultaneous transmission and reception over the same channel, which cannot be perfectly eliminated Duarte & Sabharwal (Nov. 2010); Jain *et al.* (2011). Meanwhile, in the half duplex relaying, also known as out-of-band full duplex, the relays encounter a spectral efficiency loss as they transmit and receive in different time slots and over different frequency bands. As a result, in practical FDR protocol designs, the impact of self-interference should be taken into account for a more accurate system analysis. Recently, $N^*$ Nakagami fading channels in cooperative wireless communications have been proposed and analysed in many scenarios and under different cooperative relaying techniques. The authors in Qin, D., Wang, Y. & Zhou, T. (2018) studied the average symbol error probability for a cooperative system that contains a single source node, a single destination node and a single relay for amplify-and-forward (AF) relaying over Nakagami-$m$ fading channels by implementing various modulation techniques. The cellular multiuser two-way relay network has been evaluated in terms of the outage probability under Nakagami-$m$ fading Shukla, M. K., Yadav, S. & Purohit, N. (2018), where a multi-antenna base station communicates bidirectionally, i.e. in a full duplex mode, with several single-antenna mobile stations via a single-antenna relay node. Such systems can accomplish both multi-user diversity and multi-antenna diversity. The

outage probability and average symbol error rate are derived for orthogonal frequency division multiplexing (OFDM) over independent but non-identical Nakagami-*m* distributed fading channels Kumar, N., Singya, P. K. & Bhatia, V. (2017). Moreover, cooperative AF relaying with a non-linear power amplifier is considered at the relay terminal. The authors in Qian, S., Zhou, X., He, X., He, J., Juntti, M. & Matsumoto, T. (2017) have shown that the lossy forward (LF) relaying scheme outperforms the conventional decode-and-forward (DF) relaying in terms of outage probability over Nakagami-*m* fading environments.

Recent works on full duplex unidirectional and bidirectional wireless cooperative relaying schemes, including self-interference were studied and analysed in different communication scenarios in Almradi & Hamdi (2017b); Alves *et al.* (2012, June 2013); Khafagy *et al.* (2015b); Krikidis *et al.* (2012); Kwon *et al.* (Sep. 2010); Li *et al.* (2017c); Sharma & Garg (Feb. 2013). In addition, a bidirectional full duplex mode is investigated for a single relay in Kothapalli *et al.* (2016) and for multi-relays in Cui *et al.* (2014). The performance of full duplex DF relay selection over Nakagami-*m* fading channels is investigated and analysed in term of outage probability in Wang *et al.* (2016).

A study of FDR with improper Gaussian signaling (IGS) is presented in Gaafar, M., Khafagy, M. G., Amin, O., Schaefer, R. F. & Alouini, M.-S. (2018), in which the authors show that IGS is superior to proper Gaussian signalling (PGS) in terms of interference-limited settings. Moreover, the outage probability and the ergodic rate are derived to evaluate the system performance. The performances of FDR over a Nakagami-*m* fading environment is presented in Ai & Cheffena, where, the outage probability of hybrid automatic repeat requests (ARQs) is derived. In Fu, H., Roy, S. & Cheng, J. (2018), the authors have derived approximate probability density functions (PDFs) for double-Nakagami fading and Gamma-Gamma fading channels. The approximated PDF is then used to determine the outage probability, the ergodic capacity and the symbol error rate for the equal-gain and selection combining diversity techniques.

From the vehicular communication perspective, several V2V half-duplex relaying (HDR) techniques have been studied and investigated in the literature. The communication between

source-destination (*S*-*D*) nodes could be established by a road access point (AP) Ilhan *et al.* (2008), a mobile vehicle Li *et al.* (2010) and multiple mobile vehicles in Akin *et al.* (2015). The authors in Ilhan *et al.* (2009) studied two different cooperative relaying schemes. In the first scheme, V2V is assisted by an AP, and in the second one, V2V is assisted by relaying vehicles. Moreover, the authors in Nguyen & Kong (2016) present a V2V dual-hop cooperative network under DF relaying scheme, where the communication between the two vehicles is assisted by the vehicles within one cluster and by APs in adjacent clusters, where the APs act as relays. Within the scope of V2V cooperative communications, the impacts of co-channel interference and imperfect channel estimation are studied in Bithas *et al.* (Kuala Lumpur, Malaysia 2016); Ilhan (2015). The performance of multi-hop V2V wireless cooperative communications over $n^*$ Rayleigh fading channels is considered in Alghorani *et al.* (2016), and a V2V multiple-input and multiple-output (MIMO) channel model is investigated in Alghorani & Seyfi (2017). Additionally, a two-way HDR V2V wireless communication scheme over double-Rayleigh fading channels is proposed in Shakeri *et al.* (2014), and over mixed Nakagami$-m$ and double Nakgamai$-m$ channels in Hu *et al.* (2014b). The performance of V2V communication in a single dense lane topology is examined in Pitsiladis *et al.* (2015), while Farooq *et al.* (2016) proposes a multi-lane topology with different packet forwarding schemes. In Eshteiwi *et al.* (Sep. 2017), an exact expression for the PDF of peer-to-peer V2V communication including the impact of interference is derived and used to obtain the bit error rate (BER).

Overall, *full duplex relaying* in vehicular communication is still in its infancy and very few works have been published, especially from the physical layer and performance analysis perspectives. Therefore, the current literature is limited to the V2V half-duplex scenario, except for the case of Mafra *et al.* (2016), where the authors present the simulation results of a V2V full duplex relay selection wireless cooperative communication by using joint decoding as proposed in Khafagy *et al.* (2013), however, a mathematical analysis of the system performance is not included. In Bazzi *et al.* (2015), the authors investigate the long term evolution (LTE) technique for V2V beaconing services by exploiting full duplex direct communications, while the joint resource assignment and power allocation problems are analyzed for full duplex ve-

hicular communication from a medium access control (MAC) layer perspective in Yang *et al.* (2016).

Our paper is a continuation, as well as an update, of the recent progress of IVC-based full duplex relaying. Thus, we consider a dual-hop full duplex V2V wireless cooperative communication in which a source vehicle ($S$) communicates with a destination vehicle ($D$) both directly and with the help of multiple cooperative vehicles-based on the full duplex relays present in the network. The analysis is performed for a dense multi-lane highway scenario in a non-regenerative AF relaying mode. Two relaying selection schemes are considered for such networks, and the availability of the CSI at the receiver side is assumed. Thereupon, to ensure good cooperation, the FDR represents the source-relay and the relay-relay links by one CSI coefficient for estimation process in the first scheme, which is the SI vehicle relaying selection, while for the second scheme[1], which is the ISI vehicle relaying selection, the CSIs of the source-relay and of the relay-relay are estimated separately. In addition, a selection combining (SC) technique is employed to select the best vehicle relay that achieves the highest signal-to-noise ratio (SNR).

To create more realistic V2V communication scenarios, LOS and NLOS propagations between $S$ and $D$ are considered and the dependence of the probabilistic model on the movement of the vehicle between the central and adjacent lanes is studied. In fact, due to the unceasing movement of vehicles between adjacent lanes, which can be modelled based on independent vehicles Poisson distribution, the LOS is attainable *only* if the central lane between the source and the destination nodes is free of vehicles, otherwise, the NLOS dominates. It should be mentioned that the channels are modelled as Nakagami$-m$ fading channels for accuracy in modelling short-range highway vehicular communications. For the considered network model, the CDF expression of the source-relay link including self-interference is first derived, then the end-to-end lower bound outage probability is expressed in terms of the blockage probability in the central lane, and then the throughput is calculated and presented accordingly.

[1] In our terminology, we use the term *individual* for the second selection scheme to distinguish between the two proposed selection schemes, as will be mentioned in upcoming sections

Based on the results obtained, the concept of multiple vehicular relays both offers diversity and significantly boosts performance by reducing the outage probability, which motivates its use in V2V environments. On the other hand, the essential differences between this work and the related work done in Farooq *et al.* (2016) are that in our work we consider a two-hop full duplex relaying over mmWave including a blockage model between $S$ and $D$, while Farooq *et al.* (2016) considers a multi-hop half duplex over dedicated short range communications (DSRC). In addition, we analyse the outage probability and the throughput, while Farooq *et al.* (2016) studies routing strategies for packet forwarding. Finally, the channels are modeled as Nakagami-$m$ fading channels in our analysis. To the best of the authors' knowledge, no previous work has presented a mathematical model for V2V full duplex communications considering the aforementioned scenario. Taking these parameters into consideration, it is clear that the present work differs significantly from previous studies that neither provide analytical outage probability nor throughput expressions. Our main contributions in this work can be summarized as follows:

- Consider the performance analysis of an FDR V2V system over Nakagami$-m$ fading channels.
- Develop a new CDF expression of the ratio of two Gamma distribution random variables (RVs) for the source-relay ($S$-$R$) link including self-interference.
- Analyzes and compares two cooperative schemes with full duplex relaying: i) SI vehicle relaying selection and ii) ISI vehicle relaying selection.
- Present the probability of a blockage model between the source and the destination nodes according to independent vehicles Poisson distribution.
- Derive the outage probability with respect to the occurrence of LOS and NLOS probabilistic models, and then obtaining the throughput of the proposed system.

The remainder of this paper is organized as follows: Section 5.3 represents the system model. A deep performance analysis of the proposed system is introduced in Section 5.4. Section 5.5

contains numerical and simulation results, and concluding remarks are presented in Section 5.6. Proofs are provided in appendices.

## 5.3 V2V Full Duplex Communication System Model

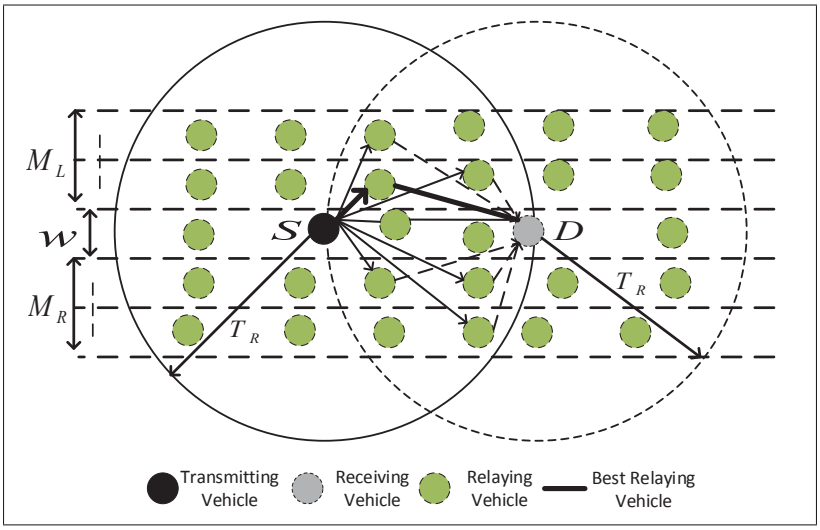


Figure 5.1 A schematic diagram of the V2V full duplex wireless cooperation multi-lane highway with a transmitter and a receiver located at the central lane, at the existence of left and right lanes

In this paper, we consider a system model composed of one source vehicle $S$, one destination vehicle $D$ and multiple relay vehicles that are distributed in each lane inside the transmission range $T_R$. In our model, all vehicles such as cars, vans, lorries, and buses are located on $M$ parallel traffic lanes with a fixed width of $w$ for each lane. Homogeneous traffic lanes are assumed for simplicity of the analysis, i.e. each traffic lane has an infinite length and an equal number of vehicles. The transmitting vehicle under the analysis has $M_L$ and $M_R$ traffic lanes on its left-hand and right-hand sides respectively, where $M = M_L + M_R + 1$ as shown in Fig. 5.1. Moreover, the source and the destination are assumed to be placed on the same traffic lane that is called the central lane[2]. Without loss of generality, each vehicle has the same transmitted

[2] The central lane means that the transmitting vehicle and the receiving vehicle are located in the same lane to allow direct communication where possible

power $P$ within $T_R$ and the intensity of vehicles in each traffic lane is $\delta$ vehicles/lane/unit length.

All the nodes including $S$, $D$ and the relays are supplied with two antennas, where the transmitter uses only the transmit antenna, the receiver uses only the receive antenna and the vehicle relay nodes use both transmit and receive antennas concurrently to accomplish full duplex relaying.

In the *S-D* communication link, we consider two cases. The first case assumes the availability of LOS and a direct link is attained. The second case assumes NLOS because the *S-D* link is obstructed. In our model, it is possible for vehicles to change lane according to independent Poisson distribution. For the cooperation process, a one-way full duplex transmission, taking into account the effect of the self-interference at the relay nodes is considered helping $S$ to convey data to $D$. In addition, we assume that CSIs are also known at the destination node and SC technique is employed to select the best vehicle relay that achieves the highest SNR. Therefore, the best relaying vehicle cooperates only in relaying and one channel is required regardless of the number of vehicle relays.

As mentioned in Ikki & Ahmed (2008), the SC technique has two important advantages over regular cooperative diversity network i) it reduces the inefficient amount of used channel resources to the best relay node ii) it maintains the full diversity order. Moreover, the SC is implemented in vehicular communication to decrease the number of costly radio frequency (RF) chains at the receiver side, where only a single RF chain needs to be employed at both the transmitter and the receiver nodes Alghorani & Seyfi (2017).

In this vein, we list our system model assumptions

**Assumption 1**: A dense network in a single direction highway situation at rush hours or in an accident/congestion scenario is considered. Hence, the effect of mobility and the Doppler phenomenon are justifiably ignored. As such, the whole system compromised of the transmitter, the receiver, and the vehicular relays, all move along the same direction on the highway. Any

occurrence of a non-zero bias in the Doppler spectrum is compensated by using an automatic frequency control loop at the receiver side Tassi *et al.* (2017).

**Assumption 2**: As shown in Fig. 5.1, transmitters (source and relays) have a range, $T_R$, much higher than the highway width, as they should be able to communicate with various infrastructures such as road signs and buildings located across the highway.

**Assumption 3**: In particular, mmWave is very sensitive to blockage, therefore, LOS is lost if at least one vehicle obstructs the *S*-*D* link.

**Assumption 4**: The Nakagami-*m* fading channel model is considered as it is widely used to model cooperative vehicular communication and short-range communications Mafra *et al.* (2016); Tassi *et al.* (2017). On the other hand, self-interference and its fading model heavily depend on the employed isolation/cancellation techniques. For instance, if the suppression is not sufficiently employed, LOS effects will persist and, hence, Rayleigh-fading will not be a suitable model since it does not count the LOS component. Moreover, the Nakagami$-m$ fading is able to span a wide range of fading distributions that can also capture either scenarios in case of absence/presence of LOS effects. Furthermore, the Nakagami$-m$ distribution is a more general model which can be used to describe many fading distributions such as Rician, Rayleigh or fading environment that is more severe than Rayleigh fading distribution Cheng *et al.* (2007).

Furthermore, the number of relaying vehicles in the highway inside the $T_R$ surrounding the source *S* can be written as Farooq *et al.* (2016)

$$\lfloor N \rfloor = \delta \left( T_R + \sum_{f=1}^{M_R} \sqrt{T_R^2 - (fw)^2} + \sum_{k=1}^{M_L} \sqrt{T_R^2 - (kw)^2} \right), \tag{5.1}$$

where $\lfloor . \rfloor$ is roundup operator.

In the proposed system model, both $R_i$, where $i \in \{1, ..., \lfloor N \rfloor\}$ and $D$ receive the message transmitted from *S*, where $R_i$ employs the AF technique and then forwards the message to the

destination node. Thus, the received signal at the relay node is composed of the signal emitted by the source plus self-interference. This is expressed as

$$y_{SR_iR_i} = \sqrt{P_S} h_{SR_i} x_S + \sqrt{P_{R_i}} h_{R_iR_i} x_{R_i} + n_{R_i}, \tag{5.2}$$

where $x_S$ and $x_{R_i} \in \{+1, -1\}$ are the transmitted BPSK symbol signal with unit power, while $P_S$ and $P_{R_i}$ are the transmitted signal power at $S$ and $R_i$, respectively. The parameters $h_{SR_i}$ and $h_{R_iR_i}$ represent the channel coefficients in the $S$-$R_i$ link and the self-interference $R_i$-$R_i$, respectively. The term $n_{R_i}$ represents white Gaussian noise (AWGN) at $R_i$ with a variance of $N_o$. The channels are modelled as mutually independent Nakagami$-m$ fading channels and are not necessarily identically distributed (i.n.i.d).

Thus, the communication process can be summarized as follows; 1) The transmitted signal reaches the destination $D$ directly and via cooperative relay nodes. This can be modelled as

$$y_{D_{R_i}} = (1-\varepsilon) y_{D_{R_{i_{\text{dir}}}}} + \varepsilon y_{D_{R_{i_{\text{ind}}}}}, \tag{5.3}$$

with

$$\varepsilon = \begin{cases} 0 \text{ , Presence of LOS ,} \\ 1 \text{ , Absence of LOS} \end{cases} \tag{5.4}$$

where the received signal $y_{D_{R_i}}$ is the resultant of the signal arriving directly $y_{D_{R_{i_{\text{dir}}}}}$ on the $S$-$D$ link plus the relayed signal $y_{D_{R_{i_{\text{ind}}}}}$. In addition, $y_{D_{R_{i_{\text{ind}}}}}$ and $y_{D_{R_{i_{\text{dir}}}}}$ can be individually expressed as

$$y_{D_{R_{i_{\text{ind}}}}} = \sqrt{P_{R_i}} h_{R_iD} \kappa_i y_{SR_iR_i} + n_D, \tag{5.5}$$

$$y_{D_{R_{i_{\text{dir}}}}} = \sqrt{P_S} h_{SD} x_S + y_{D_{R_{i_{\text{ind}}}}}, \tag{5.6}$$

where $h_{SD}$, $h_{R_iD}$ are the channel coefficients in the $S$-$D$ and $R_i$-$D$ links respectively, $n_D$ is white Gaussian noise (AWGN) at $D$ with a variance of $N_o$ and $\kappa_i \leq \sqrt{P_{R_i}/(P_S |h_{SR_i}|^2 + P_{R_i} |h_{R_iR_i}|^2 + N_o)}$ is the amplification factor for AF relaying.

Finally, to capture the impact of path loss on the system performance, the widely normalized distances model is used as in literature e.g. Ikki & Ahmed (Spring 2009); Laneman *et al.* (Dec. 2004); Lateef *et al.* (June 2010) with $\mathbb{E}(|h_{SR}|^2) = (d_{SD}/d_{SR})^{\eta}$, $\mathbb{E}(|h_{RD}|^2) = (d_{SD}/d_{RD})^{\eta}$, $\mathbb{E}(|h_{RR}|^2) = (d_{SD}/d_{RR})^{\eta}$ and $\mathbb{E}(|h_{SD}|^2) = 1$, where $\mathbb{E}(.)$ is expectation operator, $\eta$ is the path loss exponent and $d_{pq}$ is the distance between vehicle $p$ and $q$. Due to the high density of vehicles in each lane, the vehicles act as relays and are divided into two groups between source and destination inside the $T_R$ with different source-relay and relay-destination distances.

## 5.4 Performance Analysis

In this section, we present an analysis on the end-to-end outage performance and the throughput of the proposed system. First, we recall the PDF expression for the *S*-$R_i$ link including self-interference from Eshteiwi *et al.* (Sep. 2017) to derive the cumulative distribution function (CDF). Once the CDF is obtained, it is used to derive the outage probability expression for our proposed model in two distinct cases, namely the absence or the presence of a direct *S*-*D* link.

1. **PDF of the *S*-*R* link including self interference**

   Here, we derive the PDF expression for the *S*-*R* link including self-interference. According to Eq. (5.2), the received SINR at the relay node is formulated as

$$\gamma_{SR_iR_i} = \frac{P_S\,|h_{SR_i}|^2}{P_{R_i}\,|h_{R_iR_i}|^2 + N_o} = \frac{\frac{P_S|h_{SR_i}|^2}{N_o}}{\frac{P_{R_i}|h_{R_iR_i}|^2}{N_o} + 1} = \frac{\gamma_{SR_i}}{\gamma_{R_iR_i} + 1}, \qquad (5.7)$$

   where $\gamma_{SR_i} = P_S\,|h_{SR_i}|^2/N_o$ and $\gamma_{R_iR_i} = P_{R_i}\,|h_{R_iR_i}|^2/N_o$ are the instantaneous SNR of *S*-$R_i$ and $R_i$-$R_i$ (loop interference) links respectively. The channel coefficients in the proposed system are modelled as Nakagami$-m$ distribution, therefore, $\left|h_{ij}\right|^2$ follows gamma distribution. Since the channels are independent and not identically distributed (i.n.i.d), the PDF of $\gamma_{SR_i}$ and $\gamma_{R_iR_i}$ can be respectively written as

$$f_{\gamma_{SR_i}}(x) = \frac{C_{SR_i}^{m_{SR_i}}}{\Gamma(m_{SR_i})} x^{m_{SR_i}-1} \exp(-xC_{SR_i}), \qquad (5.8)$$

$$f_{\gamma_{R_iR_i}}(x) = \frac{C_{R_iR_i}^{m_{R_iR_i}}}{\Gamma(m_{R_iR_i})} x^{m_{R_iR_i}-1} \exp(-xC_{R_iR_i}), \tag{5.9}$$

where $\Gamma(z)$ denotes the Gamma function and is given by $\Gamma(z) = \int_0^\infty \exp(-t)t^{z-1}dt$ (Jeffrey & Zwillinger, 2007, Eq. (8.310.1)), $m_i > 0.5$ is the shape parameter, $C_{ij} = \frac{m_{ij}}{\bar{\gamma}_{ij}}$, $\gamma_{ij} = |h_{ij}|^2 P_i/N_o$ is the instantaneous SNR and $\bar{\gamma}_{ij} = \mathbb{E}(|h_{ij}|^2)P_i/N_o$ is the average SNR. The PDF of the total SINR which is stated in Eq. (5.7) can be written as Eshteiwi *et al.* (Sep. 2017)

$$f_{\gamma_{SR_iR_i}}(x) = \frac{C_{SR_i}^{m_{SR_i}} C_{R_iR_i}^{m_{R_iR_i}} x^{m_{SR_i}-1} \exp(-xC_{SR_i})}{\Gamma(m_{SR_i})\Gamma(m_{R_iR_i})} \sum_{j=0}^{m_{SR_i}} \binom{m_{SR_i}}{j} \frac{\Gamma(m_{R_iR_i}+j)}{(xC_{SR_i}+C_{R_iR_i})^{m_{R_iR_i}+j}}, \tag{5.10}$$

where $\bar{\gamma}_{SR_i}$ and $\bar{\gamma}_{R_iR_i}$ are the average SNR of the $S$-$R_i$ and $R_i$-$R_i$ channels, respectively.

2. **CDF of the $S$-$R$ link including self interference**

We derive the CDF expression for the $S$-$R_i$ link including self-interference by using Eq. (5.10).

**Theorem 1**: The CDF of $\gamma_{SR_iR_i}$ which represents the ratio of two Gamma-distributed RVs can be written as

$$\begin{aligned} F_{\gamma_{SR_iR_i}}(x) = 1 - \frac{\exp(C_{R_iR_i})}{\Gamma(m_{SR_i})\Gamma(m_{R_iR_i})} \sum_{j=0}^{m_{SR_i}} \binom{m_{SR_i}}{j} \Gamma(m_{R_iR_i}+j) \sum_{q=0}^{m_{SR_i}-1} \binom{m_{SR_i}-1}{q} \\ \times (-1)^{m_{SR_i}-q-1} (C_{R_iR_i})^{m_{SR_i}+m_{R_iR_i}-q-1} \Gamma(q-m_{R_iR_i}-j+1, (C_{SR_i}x+C_{R_iR_i})), \end{aligned} \tag{5.11}$$

where $\Gamma(x,y)$ is the upper incomplete Gamma function (Jeffrey & Zwillinger, 2007, Eq. (8.350.2))

**Proof**: See **Appendix III**

Fig. 5.2 depicts the CDF results for different values of the fading parameter $m_{SR_i}$ and $m_{R_iR_i}$ at $\overline{\gamma}_{SR_i} = 2$ dB dB and $\overline{\gamma}_{R_iR_i} = 0$ dB, where a perfect match between theoretical expressions

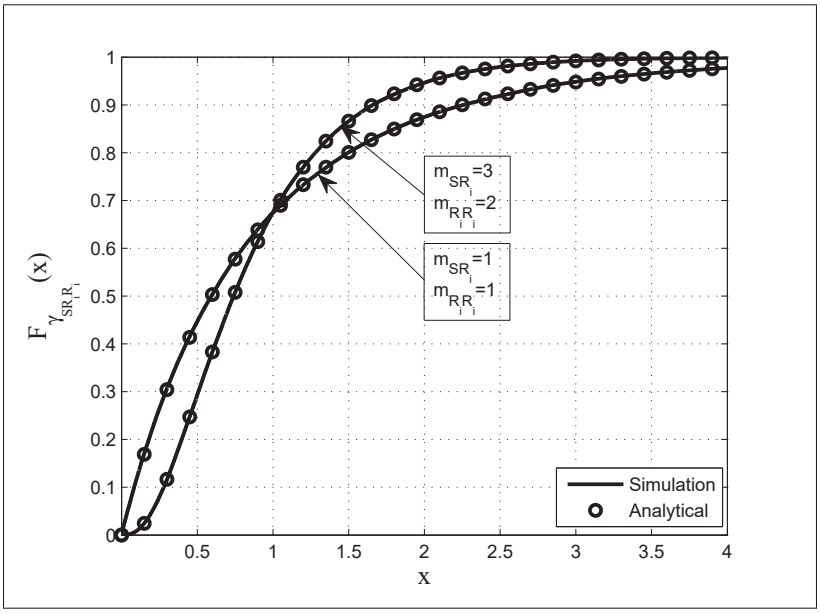


Figure 5.2 Analytical and simulation results for the CDF of SNR of V2V wireless communications in the presence of interference over Nakagami$-m$ fading channels for different values of $m_{SR_i}$ and $m_{R_iR_i}$ with $\overline{\gamma}_{SR_i} = 2$ dB and $\overline{\gamma}_{R_iR_i} = 0$ dB

and simulation is observed.

### 3. Outage Probability

In this article, we analyse the outage probability of the best vehicular relaying selection of FDR cooperative wireless communications in a dense multi-lane highway situation. We define the outage probability as the probability that the end-to-end SNR between the transmitted signal at the source and the received signal at the destination is smaller than a predefined threshold $\gamma_{th} = 2^{R_T} - 1$, where $R_T$ is the fixed source transmission rate in bit-s/sec/Hz. The end-to-end outage probabilities are combination of the outage probabilities of the cooperative V2V network in the presence or absence of a direct *S-D* link which are derived in the following subsections 5.4.1, 5.4.2, and 5.4.3.

### 5.4.1 Indirect Link Outage Probability

In this subsection, a direct link between source and destination nodes is assumed unavailable, a practical situation which arises when at least one vehicle in the central lane blocks a direct *S-D* communication. In addition, a selection combining technique is applied at the destination node to select the best relaying vehicle which offers the highest SNR. Therefore, The instantaneous SNR of the received signal at the destination and using AF relaying technique at the relay node can be written as Hasna & Alouini (2003)

$$\gamma_i = \frac{\frac{\frac{P_S\left|h_{SR_i}\right|^2}{N_o}}{\frac{P_{R_i}\left|h_{R_iR_i}\right|^2}{N_o}+1}\frac{P_{R_i}\left|h_{R_iD}\right|^2}{N_o}}{\frac{\frac{P_S\left|h_{SR_i}\right|^2}{N_o}}{\frac{P_{R_i}\left|h_{R_iR_i}\right|^2}{N_o}+1}+\frac{P_{R_i}\left|h_{R_iD}\right|^2}{N_o}+1} = \frac{\gamma_{SR_iR_i}\gamma_{R_iD}}{\gamma_{SR_iR_i}+\gamma_{R_iD}+1} \quad (5.12)$$

where $\gamma_{R_iD} = P_{R_i}\left|h_{R_iD}\right|^2/N_o$. In addition, a selection combining technique is applied at the destination node to select the best relaying vehicle which offers the highest SINR. Therefore, the total SINR at the destination can be written as Soliman, S. S. & Beaulieu, N. C. (2012)

$$\gamma^{\text{sc}}_{\text{ind}_{\text{exact}}} = \max_{i\in\{1,\ldots,\lfloor N\rfloor\}}(\gamma_i), \quad (5.13)$$

Since the derivation of the exact outage probability of the two FDR schemes, SI and ISI, is difficult to obtain directly from Eq. (5.13), then max-min criteria will be used as an alternative to derive the outage probabilities bounds of these latter schemes

#### 5.4.1.1 Max-min criteria of SI scheme (MMSI) when the S-D link is blocked

The overall SNR in Eq. (5.13) can be written mathematically as an upper bound expression to calculate the total SNR simply as

$$\gamma^{\text{sc}}_{\text{ind}_{\text{MMSI}}} = \max_{i\in\{1,\ldots,\lfloor N\rfloor\}}(\min(\gamma_{SR_iR_i},\gamma_{R_iD})), \quad (5.14)$$

where $\gamma^{sc}_{\text{ind}_{\text{MMSI}}}$ represents the total SNR at $D$ for indirect links using selection combining technique and $\gamma^{sc}_{\text{ind}_{\text{MMSI}}} \geq \gamma^{sc}_{\text{ind}_{\text{exact}}}$, its accurate to catch the system performance at medium and high SNR. Also, $\gamma_{SR_iR_i}$ represents the SINR at the relay node including the FD loop interference.

**Theorem 2**: The lower bound of the outage probability for the proposed system including indirect links can be written as

$$P_{\text{ind}_{\text{MMSI}}}(\gamma_{th}) = \sum_{k=0}^{\lfloor N \rfloor} \binom{\lfloor N \rfloor}{k} (-1)^{\lfloor N \rfloor - k} (T_1)^{\lfloor N \rfloor - k} \left[ \exp(-\gamma_{th} C_{R_iD}) \sum_{h=0}^{m_{R_iD}-1} \frac{(\gamma_{th} C_{R_iD})^h}{h!} \right]^{\lfloor N \rfloor - k}$$

$$T_1 = \frac{\exp(C_{R_iR_i})}{\Gamma(m_{SR_i})\Gamma(m_{R_iR_i})} \sum_{j=0}^{m_{SR_i}} \binom{m_{SR_i}}{j} \Gamma(m_{R_iR_i}+j) \sum_{q=0}^{m_{SR_i}-1} \binom{m_{SR_i}-1}{q} (-1)^{m_{SR_i}-q-1}$$

$$\times (C_{R_iR_i})^{m_{SR_i}+m_{R_iR_i}-q-1} \Gamma\left(q - m_{R_iR_i} - j + 1, (C_{SR_i}\gamma_{th} + C_{R_iR_i})\right). \tag{5.15}$$

Note, all the parameters are defined previously.

**Proof**: See **Appendix III**

#### 5.4.1.2 Max-min criteria of ISI scheme (MMISI) when the S-D link is blocked

This technique requires the knowledge of the CSI for the source-relay, relay-relay and relay-destination links separately. The SNR given in Eq. (5.13) can be further simplified to ease the computation of the PDF of SNR, and can be approximated as

$$\gamma^{sc}_{\text{ind}_{\text{MMISI}}} = \max_{i \in \{1,\ldots,\lfloor N \rfloor\}} (\min(\gamma_{SR_i}, \gamma_{R_iR_i}, \gamma_{R_iD})). \tag{5.16}$$

The SNR in Eq. (5.16) represents the lower bound on SNR of MMSI and $\gamma^{sc}_{\text{ind}_{\text{MMISI}}} \geq \gamma^{sc}_{\text{ind}_{\text{MMSI}}} \geq \gamma^{sc}_{\text{ind}_{\text{exact}}}$. As mentioned earlier, the self-interference can not be perfectly eliminated but can be estimated, therefore $\gamma_{R_iR_i}$ represents the residual self-interference (loop interference) after the mitigation process.

**Theorem 3**: The lower bound of the outage probability for the proposed system including

indirect links can be written as

$$P_{\text{ind}_{\text{MMISI}}}(\gamma_{th}) = \sum_{k=0}^{\lfloor N \rfloor} \binom{\lfloor N \rfloor}{k} (-1)^{\lfloor N \rfloor - k} (T_2)^{\lfloor N \rfloor - k}$$
$$T_2 = \frac{\Gamma(m_{SR_i}, \gamma_{th} C_{SR_i})}{\Gamma(m_{SR_i})} \frac{\Gamma(m_{R_iR_i}, \gamma_{th} C_{R_iR_i})}{\Gamma(m_{R_iR_i})} \frac{\Gamma(m_{R_iD}, \gamma_{th} C_{R_iD})}{\Gamma(m_{R_iD})}. \tag{5.17}$$

Following the same steps as in Appendix B, the lower bound on the outage probability of the MMISI when *S*-*D* is blocked in Eq. (5.17) can be derived.

### 5.4.2 Direct Link Outage Probability

In this subsection, a direct *S*-*D* link is assumed available, a situation that occurs if there is no vehicle in the central lane between the source and destination nodes. In addition, a selection combining technique is applied at the destination node for the two schemes MMSI and MMISI, to choose the best relaying vehicle. Therefore, the total SNR at the destination can be written as

$$\gamma^{\text{sc}}_{\text{dir}_{\text{exact}}} = \max_{i \in \{1,\ldots,\lfloor N \rfloor\}} (\gamma_{SD}, \gamma_i). \tag{5.18}$$

The total outage probability may be derived for two cases as follows

#### 5.4.2.1 Max-min criteria of SI scheme (MMSI) when the S-D link is available

The overall SNR in Eq. (5.18) can be expressed as an upper bound to calculate the total SNR as

$$\gamma^{\text{sc}}_{\text{dir}_{\text{MMSI}}} = \max_{i \in \{1,\ldots,\lfloor N \rfloor\}} (\gamma_{SD}, \min(\gamma_{SR_iR_i}, \gamma_{R_iD})), \tag{5.19}$$

where $\gamma^{\text{sc}}_{\text{dir}_{\text{MMSI}}}$ is the total SNR at the destination node for selection combining and $\gamma^{\text{sc}}_{\text{dir}_{\text{MMSI}}} \geq \gamma^{\text{sc}}_{\text{dir}_{\text{exact}}}$. In addition, the SNR in (5.19) represents an upper bound which is more attractable than the exact SNR in (5.18).

**Theorem 4**: The lower bound of the outage probability for the proposed system including direct and indirect links may be written as

$$P_{\mathrm{dir}_{\mathrm{MMSI}}}(\gamma_{th}) = \left[1-\exp(-\gamma_{th}C_{SD})\sum_{l=0}^{m_{SD}-1}\frac{(\gamma_{th}C_{SD})^{l}}{l!}\right]\sum_{k=0}^{\lfloor N\rfloor}\binom{\lfloor N\rfloor}{k}(-1)^{\lfloor N\rfloor-k} \times (T_1)^{\lfloor N\rfloor-k}\left[\exp(-\gamma_{th}C_{R_iD})\sum_{h=0}^{m_{R_iD}-1}\frac{(\gamma_{th}C_{R_iD})^{h}}{h!}\right]^{\lfloor N\rfloor-k} \tag{5.20}$$

where $T_1$ is defined previously in Eq. (5.15)

**Proof**: See **Appendix III**

#### 5.4.2.2 Max-min criteria of ISI scheme (MMISI) when the S-D link is available

This technique requires the knowledge of all CSI pertinent to source-destination, source-relay, relay-relay and relay-destination links separately for estimation process. The SNR in Eq. (5.18) can be reformulated to simplify the calculation of the PDF of SNR and can be expressed as

$$\gamma^{\mathrm{sc}}_{\mathrm{dir}_{\mathrm{MMISI}}} = \max_{i\in\{1,\ldots,\lfloor N\rfloor\}}(\gamma_{SD},\min(\gamma_{SR_i},\gamma_{R_iR_i},\gamma_{R_iD})). \tag{5.21}$$

The SNR in Eq. (5.21) represents a lower bound on the SNR of MMSI and $\gamma^{\mathrm{sc}}_{\mathrm{dir}_{\mathrm{MMISI}}} \geq \gamma^{\mathrm{sc}}_{\mathrm{dir}_{\mathrm{MMSI}}} \geq \gamma^{\mathrm{sc}}_{\mathrm{dir}_{\mathrm{exact}}}$

**Theorem 5**: Following the same steps as in Appendix C, the lower bound on the outage probability of the proposed system including direct *S-D* and indirect links can be written as

$$P_{\mathrm{dir}_{\mathrm{MMISI}}}(\gamma_{th}) = \left(1-\exp(-\gamma_{th}C_{SD})\sum_{l=0}^{m_{SD}-1}\frac{(\gamma_{th}C_{SD})^{l}}{l!}\right)\sum_{k=0}^{\lfloor N\rfloor}\binom{\lfloor N\rfloor}{k}(-1)^{\lfloor N\rfloor-k}(T_2)^{\lfloor N\rfloor-k}, \tag{5.22}$$

where $T_2$ is defined previously in Eq. (5.17).

### 5.4.3 End-to-End Outage Probability

**Theorem 6**: The end-to-end outage probability of MMIS or MMISI systems can be found using the combination of direct and indirect links including the probability of blockage $P_{\mathrm{c}}$ as follows

$$P_{\mathrm{e2e}_{\mathrm{MMSI/MMISI}}}(\gamma_{th}) = P_{\mathrm{c}} P_{\mathrm{ind}_{\mathrm{MMSI/MMISI}}}(\gamma_{th}) + (1-P_{\mathrm{c}}) P_{\mathrm{dir}_{\mathrm{MMSI/MMISI}}}(\gamma_{th}), \tag{5.23}$$

where $P_{\mathrm{ind}_{\mathrm{MMSI}}}(\gamma_{th})$, $P_{\mathrm{dir}_{\mathrm{MMSI}}}(\gamma_{th})$, $P_{\mathrm{ind}_{\mathrm{MMISI}}}(\gamma_{th})$, and $P_{\mathrm{dir}_{\mathrm{MMISI}}}(\gamma_{th})$ are defined in Eq. (5.15), Eq. (5.20), Eq. (5.17) and Eq. (5.22) respectively and $P_c$ represents the probability that there exists a vehicle inside the central lane (probability of blockage) that can be calculated as follows

$$\begin{aligned} P_{\mathrm{c}} &= P[\text{At least one vehicle in the central lane}] \\ &= 1 - P[\text{No vehicle in the central lane}] \\ &= 1 - \exp(-\delta T_R). \end{aligned} \tag{5.24}$$

Substituting Eq. (5.15), Eq. (5.20) and Eq. (5.24) into Eq. (5.23), $P_{\mathrm{e2e}_{\mathrm{MMSI}}}(\gamma_{th})$ can be written as in Eq. (5.25).

**Theorem 7**: In order to find the end-to-end outage probability of MMISI system, Eq. (5.17), Eq. (5.22) and Eq. (5.24) are simply plugged into Eq. (5.23) to yield $P_{\mathrm{e2e}_{\mathrm{MMISI}}}(\gamma_{th})$ as in Eq. (5.26) shown on the next page.

$$P_{\mathrm{e2e_{MMSI}}}(\gamma_{th}) = \sum_{k=0}^{\lfloor N \rfloor} \binom{\lfloor N \rfloor}{k} (-1)^{\lfloor N \rfloor - k} \left[ \frac{\exp(C_{R_iR_i})}{\Gamma(m_{SR_i})\Gamma(m_{R_iR_i})} \right]^{\lfloor N \rfloor - k}$$
$$\times \left[ \sum_{j=0}^{m_{SR_i}} \binom{m_{SR_i}}{j} \Gamma(m_{R_iR_i}+j) \right]^{\lfloor N \rfloor - k} \left[ \sum_{q=0}^{m_{SR_i}-1} \binom{m_{SR_i}-1}{q} (-1)^{m_{SR_i}-q-1} \right.$$
$$\left. \times (C_{R_iR_i})^{m_{SR_i}+m_{R_iR_i}-q-1} \Gamma(q - m_{R_iR_i} - j + 1, (C_{SR_i}\gamma_{th} + C_{R_iR_i})) \right]^{\lfloor N \rfloor - k} \tag{5.25}$$
$$\times \left[ \exp(-\gamma_{th}C_{R_iD}) \sum_{h=0}^{m_{R_iD}-1} \frac{(\gamma_{th}C_{R_iD})^h}{h!} \right]^{\lfloor N \rfloor - k} \left[ (1 - \exp(-\delta T_R)) + \exp(-\delta T_R) \right.$$
$$\left. \times \left( 1 - \exp(-\gamma_{th}C_{SD}) \sum_{l=0}^{m_{SD}-1} \frac{(\gamma_{th}C_{SD})^l}{l!} \right) \right]$$

$$P_{\mathrm{e2e_{MMISI}}}(\gamma_{th}) = \sum_{k=0}^{\lfloor N \rfloor} \binom{\lfloor N \rfloor}{k} (-1)^{\lfloor N \rfloor - k} \left( \frac{\Gamma(m_{SR_i}, \gamma_{th}C_{SR_i})}{\Gamma(m_{SR_i})} \frac{\Gamma(m_{R_iR_i}, \gamma_{th}C_{R_iR_i})}{\Gamma(m_{R_iR_i})} \right.$$
$$\left. \times \frac{\Gamma(m_{R_iD}, \gamma_{th}C_{R_iD})}{\Gamma(m_{R_iD})} \right)^{\lfloor N \rfloor - k} \left[ (1 - \exp(-\delta T_R)) + \exp(-\delta T_R)\,(1 - \exp(-\gamma_{th}C_{SD}) \right. \tag{5.26}$$
$$\left. \times \sum_{l=0}^{m_{SD}-1} \frac{(\gamma_{th}C_{SD})^l}{l!} \right]$$

## 4. **Throughput**

In this subsection, we present the throughput performance of FD V2V wireless cooperative AF relaying. The throughput of the MMIS and MMISI systems are defined as the total number of packets that are successfully delivered to the receiver with no error for a given period of time in bits/sec/Hz and can be written as Khafagyx *et al.* (Sep. 2015)

$$G = R_S(1 - P_{\mathrm{e2e_{MMSI/MMISI}}}(\gamma_{th})), \tag{5.27}$$

where $R_S$ is the fixed rate of the transmitter in bits/sec/Hz.

## 5.5 Simulation Results

Analytical and simulation results for the outage probability and throughput of the proposed system are delivered in this section. The system simulation setup includes the transmission of $10^6$ bits, a lane width of $w = 0.04$, $M = 5$ traffic lanes with $M_R = M_L = 2$, a transmission range of $T_R = 1$, and a path loss exponent of $\eta = 3.18$. Moreover, the vehicles in each lane are distributed with the intensity of $\delta = 2$ vehicles/lane/unit length. Hence, vehicles acting as relays inside the transmission range are assumed to be present in symmetrical locations around the central lane. As mentioned earlier, relaying vehicles are divided into two groups between $S$ and $D$ within the range $T_R$ with different distances. The distances of the first group are $d_{SR_i} = 0.4$ and $d_{R_iD} = 0.6$, respectively, and that of the second group are $d_{SR_i} = 0.7$ and $d_{R_iD} = 0.3$, respectively, with $d_{SD} = 1$ and $d_{R_iR_i} = 0.01$. Therefore, we have $d_{SR_i} + d_{R_iD} = 1$. For simplicity, the transmission power is set to $P_S = P_R = P$. All the exact simulation results are compared to MMSI and MMISI schemes in Eq. (5.25) and Eq. (5.26) respectively in the case of outage probability and also compared to the throughput in Eq. (5.27). Furthermore, some corresponding case-specific system parameters are included in the caption of each figure, where applicable.

Fig. 5.3 depicts the evaluation of the outage probability for the best vehicle relaying selection as a function of $P_S/N_o$ with a different number of highway lanes. As can be seen, the performance improvement is proportional to the number of highway lanes . For instance, an outage probability of $10^{-10}$ appears at $\approx 0$ dB when the total number of lanes $M = 5$, while it occurs at $\approx 3.5$ dB for $M = 3$ lanes in the MMISI scheme. For the MMSI structure, however, an outage probability of $10^{-10}$ appears at $\approx 1.5$ dB for $M = 5$ lanes, while it occurs at $\approx 5.2$ dB for $M = 3$. For exact simulation, the outage probability of $10^{-10}$ occurs at $\approx 2.3$ dB for $M = 5$ and at $\approx 5.3$ dB for $M = 3$ lanes. This behaviour is mathematically described in Eq. (1) in the paper, where expanding the highway to contain more lanes increases the number of vehicular relays inside the transmission range and improves performance.

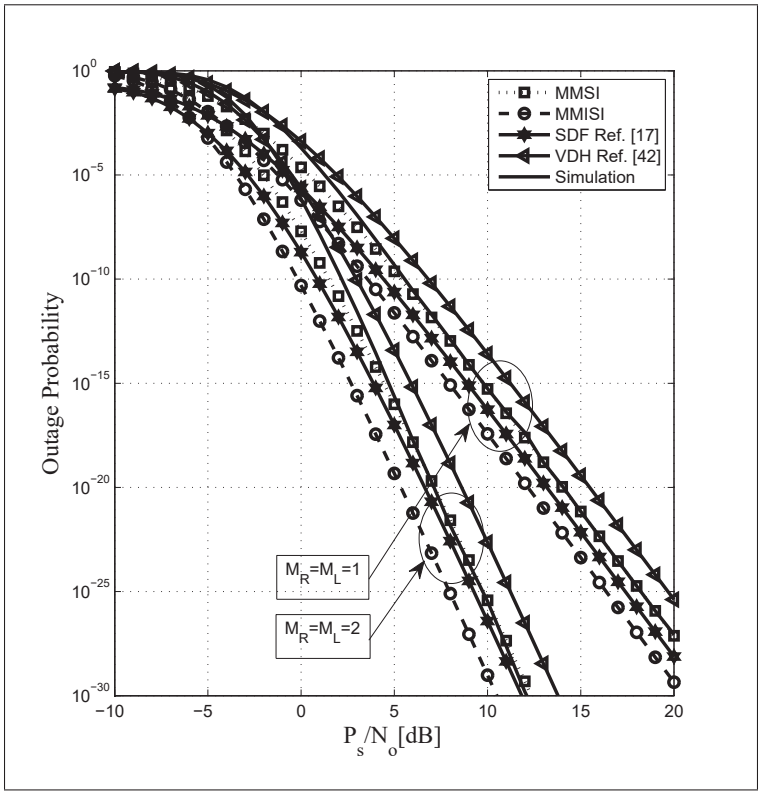


Figure 5.3 Analytical and simulation results for the outage probability vs. $P_S/N_o$ of V2V wireless communications in the presence of interference over Nakagami$-m$ fading channels for different values of $M_R$ and $M_L$, $m_{ij}=2$, where $i,j\in\{S,R,D\}$, $\delta=2$ vehicles/lane/unit length, $w=0.04$, $T_R=d_{SD}=1$, $d_{SR_i}=0.4$ and 0.7, $d_{R_iD}=0.6$ and 0.3, respectively, $d_{R_iR_i}=0.01$, $\overline{\gamma}_{R_iR_i}=0$ dB, $R_T=1$ bit/sec/Hz and $\eta=3.18$

Furthermore, our results in Fig. 5.3 are compared to vehicular full duplex dual hop scheme (VDH) which represented in Mafra *et al.* (2016). It is clear that the outage probability derived in this paper is better than that proposed in Mafra *et al.* (2016) [3] with $\approx 1$ dB diversity gain at medium and high $P_S/N_o$ in both cases of $M=5$ and $M=3$ lanes for MMSI and simulation results. The degradation of VDH scheme due to the self-interference at the relay node and also because the direct link is seen as interference at the destination node. For example, an outage

[3] [42]: S. B. Mafra, E. M. Fernandez, and R. D. Souza, "Performance analysis of full-duplex cooperative communication in vehicular ad-hoc networks," IFAC-Papers OnLine, vol. 49, no. 30, pp. 227–232, 2016.

probability of $10^{-15}$ occurs at $\approx 4.5$ dB and at $\approx 10$ dB for for $M = 5$ and for $M = 3$ lanes respectively, while it occurs at $\approx 5.6$ dB and at $\approx 11$ dB for the same number of lanes in VDH scheme Mafra *et al.* (2016). Moreover, our results are also compared to selective DF (SDF) full duplex relaying Khafagy *et al.* (2015b)[4] which is also known as vehicular full duplex joint decoding (VJD) Mafra *et al.* (2016). As observed, SDF has a better outage probability performance compared to the MMSI scheme. This degradation in MMSI scheme is due to the effect of blockage probability on the system performance as shown in Eq. (25).

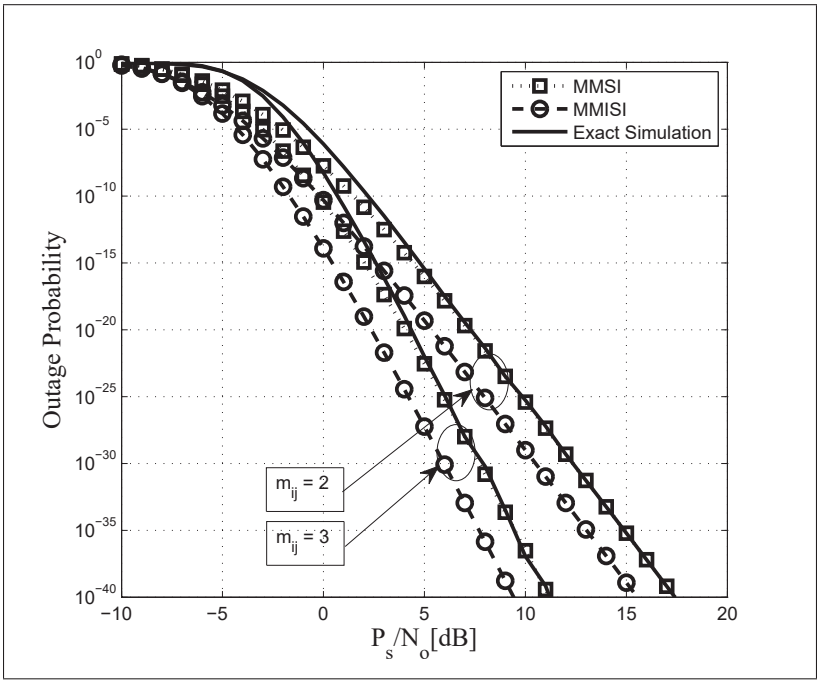


Figure 5.4 Analytical and simulation results for the outage probability vs. $P_S/N_o$ of V2V wireless communications in the presence of interference over Nakagami$-m$ fading channels for different values of $m_{ij}$, where $i, j \in \{S, R, D\}$, $R_T = 1$ bit/sec/Hz, $\delta = 2$ vehicles/lane/unit length, $w = 0.04$ , $M_R = M_L = 2$, $T_R = d_{SD} = 1$, $d_{SR_i} = 0.4$ and 0.7, $d_{R_iD} = 0.6$ and 0.3, respectively, $d_{R_iR_i} = 0.01$, $\overline{\gamma}_{R_iR_i} = 0$ dB and $\eta = 3.18$

[4] [17]: M. G. Khafagy, A. Ismail, M.-S. Alouini, and S. Aïssa, "Efficient cooperative protocols for full-duplex relaying over Nakagami$-m$ fading channels," IEEE Trans. Wireless Commun., vol. 14, no. 6, pp. 3456–3470, 2015.

As for the outage probability, Fig. 5.4 shows the outage probability of the best relaying vehicle as a function of the $P_S/N_o$. The obtained results are compared to exact simulation under different fading values $m_{ij}$ in full duplex mode including self-interference, over i.n.i.d Nakagami$-m$ fading channels. It is clear that as $m_{ij}$, where $i, j \in \{S, R, D\}$ values increase, the outage probability decreases significantly and the performance improves. On the other hand, higher $m_{SD}$ values do not enhance the system performance due to the high density of vehicles in the central lane that also causes a high blockage probability of the direct link. More, it can be observed that the derived lower bound on MMSI is close enough to the exact simulation result, especially at medium and high $P_S/N_o$ values, and is valid for different values of $m_{ij}$. For example, the outage probability for the exact simulation for $m_{ij} = 2$ at $P_S/N_o = 8$ dB is equal to $4.2 \times 10^{-22}$ while the outage probability for the MMSI is equal to $2.6 \times 10^{-22}$ and for MMISI $7.9 \times 10^{-26}$. At the same time the outage probability at $m_{ij} = 3$ for exact simulation equals to $6.1 \times 10^{-31}$, for MMSI is equal to $1.5 \times 10^{-31}$ and for MMISI is $1.3 \times 10^{-36}$. On the other hand, a gap of approximated 2 dB is observed at high SNR between the simulation results and the MMISI scheme. This gap is because the MMISI takes into account the effect of the self-interference individually and does not mingle it into the relay input as represented in Eq. (5.16) and Eq. (5.21).

Fig. 5.5 plots the outage probability in Eq. (5.25) and Eq. (5.26) as a function of $P_S/N_o$ for different source transmission rates $R_T$. Also, the results of the lower bounds are verified by the exact simulation for the parameters indicated in the caption. While this figure clearly exhibits the closeness of our analytical expressions and simulation results for medium and high $P_S/N_o$ values, an important point we could deduce from it is that the performance improves with less $R_T$ as expected. As an example, the outage probability of $10^{-10}$ occurs at $\approx 1.5$ dB in the case of $R_T = 1$ bit/sec/Hz, while it occurs at $\approx 6.3$ dB in the case of $R_T = 2$ bit/sec/Hz for the MMSI scheme. However, the outage probability of $10^{-10}$ occurs at $\approx 0$ dB in the case of $R_T = 1$ bit/sec/Hz, while it occurs at $\approx 4.5$ dB in the case of $R_T = 2$ bit/sec/Hz for the MMISI scheme. For the exact simulation result, the outage probability of $10^{-10}$ occurs at $\approx 2.3$ dB and $\approx 6.8$ dB in the case of $R_T = 1$ and $R_T = 2$ bit/sec/Hz respectively. This behaviour can

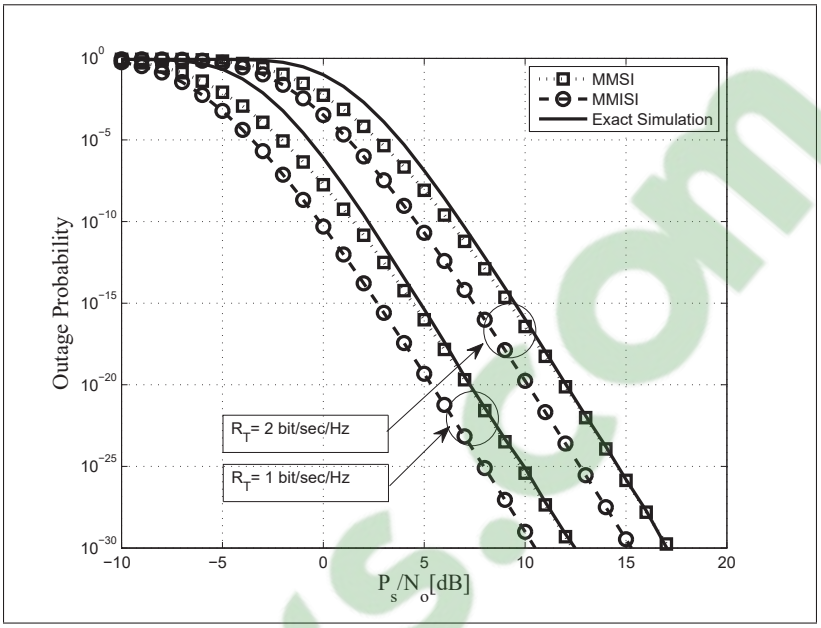


Figure 5.5 Analytical and simulation results for the outage probability vs. $P_S/N_o$ of V2V wireless communications in the presence of interference over Nakagami$-m$ fading channels for different values of $R_T$, $m_{ij} = 2$, where $i, j \in \{S, R, D\}$, $\delta = 2$ vehicles/lane/unit length, $w = 0.04$, $M_R = M_L = 2$, $T_R = d_{SD} = 1$, $d_{SR_i} = 0.4$ and 0.7, $d_{R_iD} = 0.6$ and 0.3, respectively, $d_{R_iR_i} = 0.01$, $\overline{\gamma}_{R_iR_i} = 0$ dB and $\eta = 3.18$

be explained as follows: Decreasing the source transmission rate $R_T$ cuts back the threshold value, which allows more relays to participate in forwarding the information to the destination node and improve the performance by reducing the outage probability. In addition, it can be seen in Fig. 5.4 and Fig. 5.5 that the lower bound on MMSI and the exact simulation approach are close enough to each other as $P_S/N_o$ increases while the two curves dissociate at low $P_S/N_o$ values. In consequence, the total SNR expressions provided in Eq. (5.14) and Eq. (5.19) have a higher accuracy for larger $P_S/N_o$ values.

Fig. 5.6 shows the performance of the best vehicle relaying scheme under several values of the average self-interference at relay nodes. We observe a deterioration of the system performance, i.e. an augmentation of the outage probability while the average self-interferences at the relays

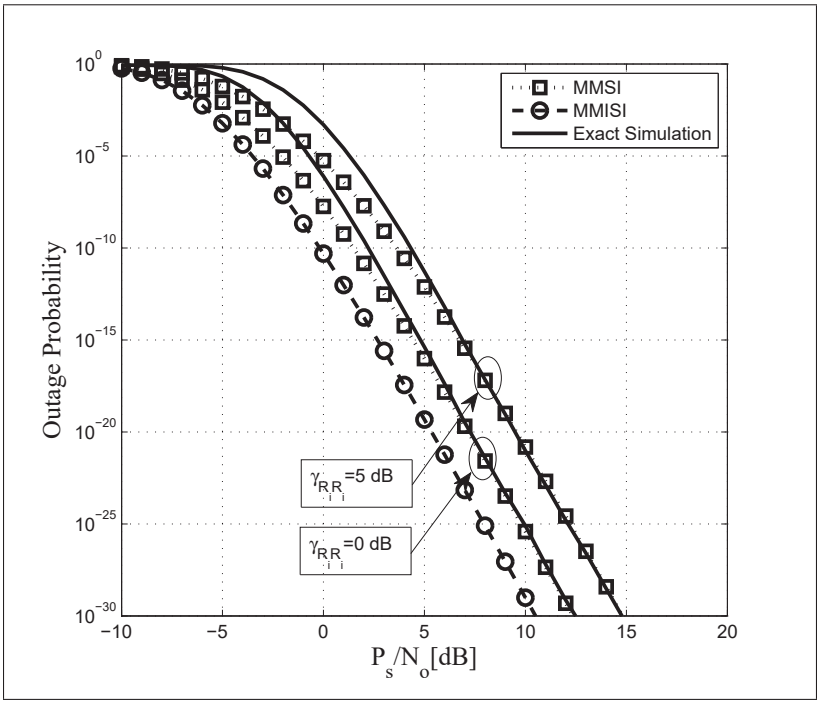


Figure 5.6 Analytical and simulation results for the outage probability vs. $P_S/N_o$ of V2V wireless communications in the presence of interference over Nakagami$-m$ fading channels for different values of $\overline{\gamma}_{R_iR_i}$, $m_{ij}=2$, where $i,j\in\{S,R,D\}$, $\delta=2$ vehicles/lane/unit length, $w=0.04$, $M_R=M_L=2$, $T_R=d_{SD}=1$, $d_{SR_i}=0.4$ and 0.7, $d_{R_iD}=0.6$ and 0.3, respectively, $d_{R_iR_i}=0.01$, $d_{R_iR_i}=0.01$, $R_T=1$ bit/sec/Hz and $\eta=3.18$.

increase. This result validates our theoretical analysis as narrated by Eq. (5.7), where the destructive influence of the self-interference on the outage probability as an important measure of the system performance is clearly indicated. the capacity of the proposed system is controlled by the ratio $(\gamma_{SR_i}/\gamma_{R_iR_i}+1)$ at high SNR regime and thus the lower bound agrees with the exact simulation for high $P_S/N_o$ values. Based on the aforementioned reason, using an interference cancellation scheme at relaying nodes in the full duplex mode reduces interference and enhances system performance. In this figure, the diversity gain between MMISI and MMSI is $\approx 2$ dB and $\approx 4$ dB for $\overline{\gamma}_{R_iR_i}=0$ dB and 5 dB respectively. Moreover, the MMISI performance shows no change with respect to self-interference because the latter is treated separately.

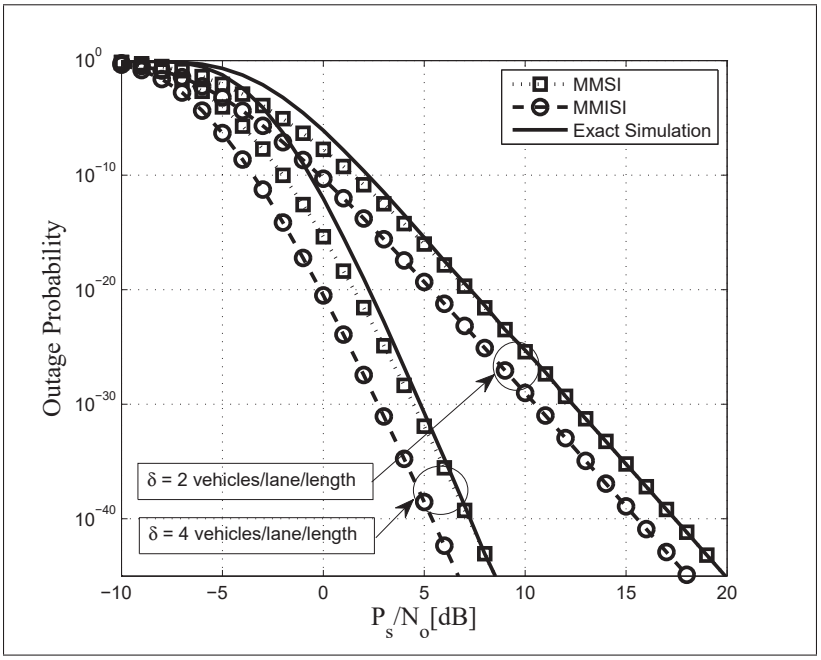


Figure 5.7 Analytical and simulation results for the outage probability vs. $P_S/N_o$ of V2V wireless communications in the presence of interference over Nakagami$-m$ fading channels for different values of $\delta$, $M_R = M_L = 2$, $m_{ij} = 2$, where $i, j \in \{S, R, D\}$, $w = 0.04$, $T_R = d_{SD} = 1$, $d_{SR_i} = 0.4$ and 0.7, $d_{R_iD} = 0.6$ and 0.3, respectively, $d_{R_iR_i} = 0.01$, $\overline{\gamma}_{R_iR_i} = 0$ dB, $R_T = 1$ bit/sec/Hz and $\eta = 3.18$.

Fig. 5.7 depicts a comparison of the outage probabilities for the approximated theoretical expressions versus simulation results under the different intensity of vehicles in each traffic lane. As the situation intensifies from dense to ultra dense, i.e. as the number of vehicles $\delta$ increase from 2 to 4 vehicles/lane/unit length, the performance of the proposed system improves. Note that the impact of $\delta$ and $T_R$ on the blockage probability is significant. This can be explained as follows, increasing the intensity of vehicles per lane including the central lane from $\delta = 2$ to 4 augments the blockage probability as shown in Table 5.1 and further obstructs the LOS. However, more selections of the *best relaying vehicle* become available within $T_R$ to process relaying. In addition, we observe that the blockage probability does not swiftly change over the time. This is because it depends on $\delta$, which changes very slowly in dense environments.

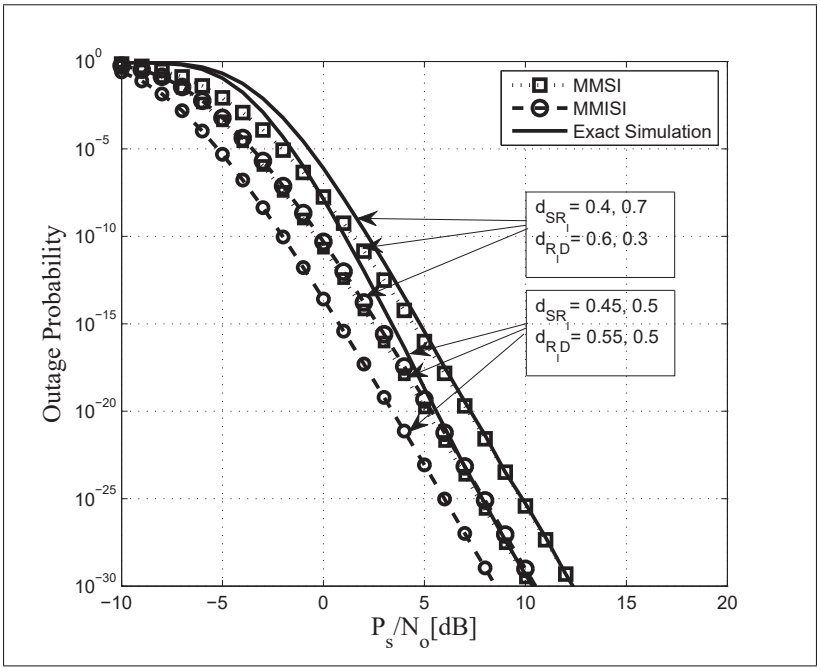


Figure 5.8 Analytical and simulation results for the outage probability vs. $P_S/N_o$ of V2V wireless communications in the presence of interference over Nakagami$-m$ fading channels for different distances between $S-R_i$ and $R_i-D$ links, $M_R = M_L = 2$, $m_{ij} = 2$, where $i, j \in \{S, R, D\}$, $\delta = 2$ vehicles/lane/unit length, $w = 0.04$, $T_R = d_{SD} = 1$, $d_{SR_i} = 0.4$ and 0.7, $d_{R_iD} = 0.6$ and 0.3, respectively, $d_{R_iR_i} = 0.01$, $\overline{\gamma}_{R_iR_i} = 0$ dB, $R_T = 1$ bit/sec/Hz and $\eta = 3.18$.

Fig. 5.8 exhibits the performance of the proposed system in terms of the outage probability with different distances between $S-R_i$ and $R_i-D$ links. It is clear form the figure that relaying vehicles enhance the system performance more effectively if located in the middle zone between the source and the destination, as this situation indicates a balanced average channel gain between $S-R_i$ and $R_i-D$ links. As we can see, if the relaying vehicles are placed in the middle zone between source and destination such that they observe balanced distances such as $d_{SR_i}$= 0.45, 0.5 and $d_{R_iD}$= 0.55 and 0.45, the system performance slightly improves and the outage probability decreases compared to cases where $d_{SR_i}$= 0.4, 0.7 and $d_{R_iD}$= 0.6 and 0.3.

Table 5.1 Blockage Probability

| | $T_R = 1$ | $T_R = 0.5$ |
|---|---|---|
| $\delta = 2$ vehicles/lane/unit length | $P_c = 0.8647$ | $P_c = 0.6321$ |
| $\delta = 4$ vehicles/lane/unit length | $P_c = 0.9817$ | $P_c = 0.8647$ |

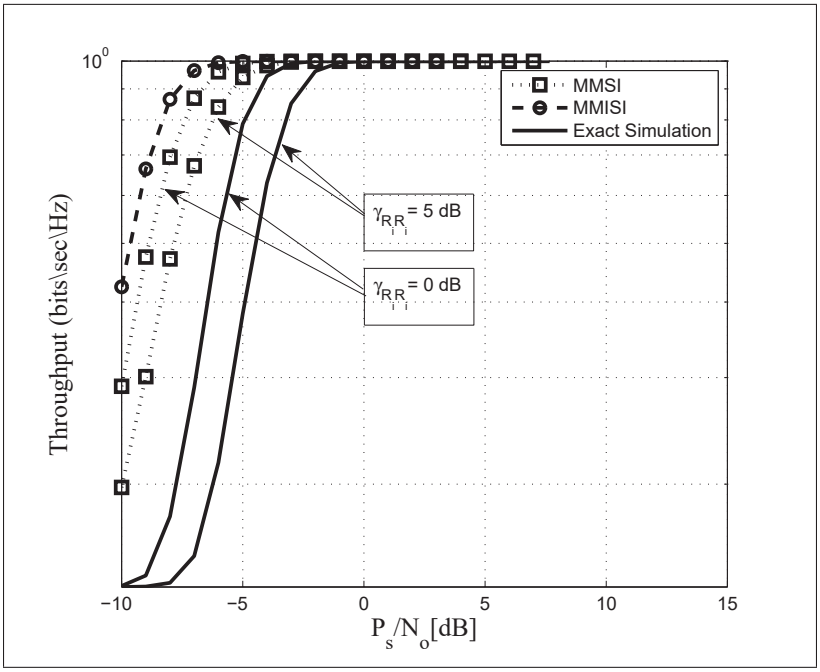


Figure 5.9 Throughput of V2V wireless communications in the presence of interference over Nakagami$-m$ fading channels for different values of $\overline{\gamma}_{R_iR_i}$, $m_{ij} = 2$, where $i, j \in \{S, R, D\}$, $R_S = R_T = 1$ bit/sec/Hz, $\delta = 2$ vehicles/lane/unit length, $w = 0.04$, $M_R = M_L = 2$, $T_R = d_{SD} = 1$, $d_{SR_i} = 0.4$ and 0.7, $d_{R_iD} = 0.6$ and 0.3, respectively, $d_{R_iR_i} = 0.01$ and $\eta = 3.18$.

Figs. 5.9-5.10 illustrate the throughput for V2V AF dual-hop wireless cooperative communications for the best vehicular relay selection versus $P_S/N_o$. Fig. 5.9 exhibits the destructive influence of self-interference at vehicular relays on the throughput. As seen, the throughput of the proposed system is higher for less self-interference.

Fig. 5.10 shows the improvement of the throughput when the number of lanes around the central lane is increased. This is because more adjacent lanes provide potentially more vehicular

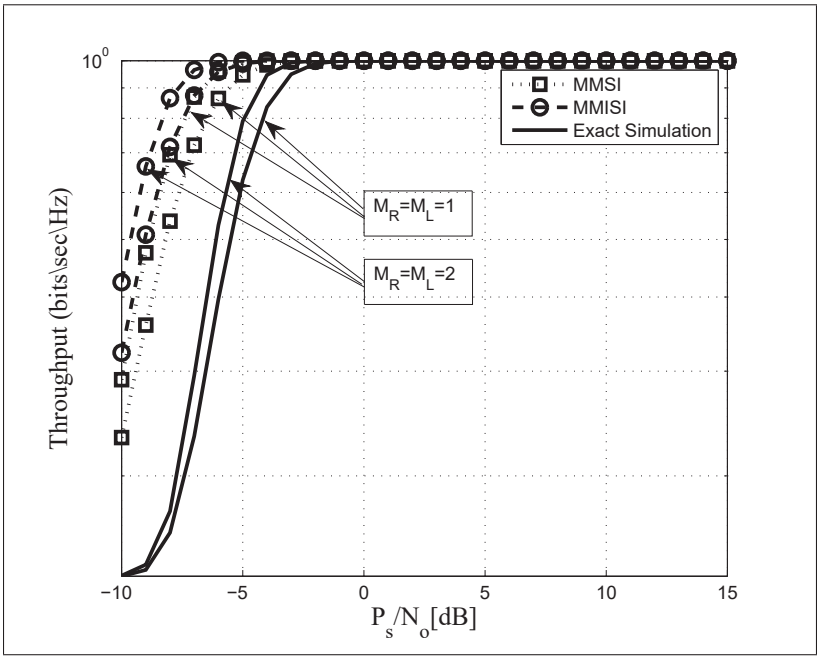


Figure 5.10 Throughput of V2V wireless communications in the presence of interference over Nakagami$-m$ fading channels for different values of $M_R$ and $M_L$, $m_{ij} = 2$, where $i, j \in \{S, R, D\}$, $R_S = R_T = 1$ bit/sec/Hz, $\delta = 2$ vehicles/lane/unit length, $w = 0.04$, $T_R = d_{SD} = 1$, $d_{SR_i} = 0.4$ and 0.7, $d_{R_iD} = 0.6$ and 0.3, respectively, $d_{R_iR_i} = 0.01$, $\overline{\gamma}_{R_iR_i} = 0$ dB and $\eta = 3.18$.

relays inside the transmission range, which enhances throughput. For example, when the number of lanes $M_R = M_L = 2$, the system accomplishes a high throughput at $\approx -5$ dB while reducing the number of lanes to $M_R = M_L = 1$, then $\approx -4$ dB is required to achieve the same throughput in the MMISI scheme. In the MMIS scheme, however, the throughput reaches its peak at $\approx -4$ dB for $M_R = M_L = 2$ and at $\approx -3$ dB for $M_R = M_L = 1$ lanes. As wider highways with more lanes around the central lane provide space for more potential vehicular relays, the overall system throughput is expected to grow on such infrastructure.

## 5.6 Conclusions

A V2V full duplex AF cooperative wireless network model was presented. Two dissimilar vehicular relay selection schemes in a dense multi-lane highway over Nakagami$-m$ fading channels were proposed in the absence/presence of LOS. In addition, vehicle displacement from one lane to an adjacent lane has taken place according to independent Poisson distribution. One of the selection schemes introduced in this work took into account the source-relay and the relay-relay links by one CSI coefficient, while the other one considered the effect of the self-interference individually and did not mingle it into the relay input. The vehicular relay selection schemes were evaluated in terms of the outage probability and the throughput. Our results indicate that , the MMSI provides a lower bound that is very close to the exact simulation results, especially at medium and high SNR, and the MMISI is simple to derive mathematically. Our analytical derivations revealed the trade-off between these two selection schemes based on the purpose of the application. We derived closed-form expressions for the CDF of the SINR and used it to develop the end-to-end outage probability. The end-to-end outage probability was derived based on the blockage probability in the central lane. The system performance was analysed and studied in various scenarios from several aspects, including fading severity, threshold, self-interference, number of lanes, the intensity of vehicles in each traffic lane, and inter-vehicle spacing. Indeed, this paper provided a comprehensive benchmark for measuring the performance of evolving V2V full duplex relaying in cooperative wireless networks.

# CHAPTER 6

# CONCLUSION AND RECOMMENDATIONS

## 6.1 Conclusion

In this thesis, we presented a comprehensive framework for the analysis and evaluation of FD variable AF relying-based vehicular cooperative wireless communications, where all the channels are assumed to be either i.n.i.d Nakagami-*m* or cascade Nakagami-*m* fading channels. Many FD vehicular cooperative wireless communications systems are considered and analyzed with regards to several aspects, including the fading severity, threshold, average SI at the relay node, number of lanes, intensity of vehicles in each traffic lane, inter-vehicle spacing, target rate, mean height of the obstacles, source's height, distances between the source and the obstacles, and average CCI at the destination node. Moreover, different performance metrics were analyzed and derived such as, the blockage probability, lower and exact end-to-end outage probability, throughput, lower end-to-end symbol error rate, PDF and CDF of the SINR at the relay and the destination, exact,lower and upper bounds of ergodic capacity.

The results we have presented in our research with respect to FD V2V wireless cooperative communications drawbacks indicate that increasing cascading degree significantly increase the outage probability and degrade the system performance. Interestingly, it is observed that the effect of cascading on the end-to-end outage probability is more pronounced for the source-relay link than the relay-destination link. Furthermore, the results demonstrate the significant impact of the considered SI, CCI and blockage on the system performance including outage probability, symbol error rate, and the throughput. Precisely, it is shown that the system performance is degraded when the average height of the obstacles is increased. This highlights the importance of taking into account these phenomena in the performance evaluation in order to assess the practical limit of V2V cooperative wireless communications. It is also noticed that when the obstacles are close to the source, the effective height of the straight line between the source and the destination decreases, and consequently the probability of obstruction increases which de-

teriorates the system performance. In addition, the results showed that the ergodic capacity of the system improves if the relay is placed in the middle between the source and the destination. Also, it is observed that FDR with SI offer a higher ergodic capacity than the interference-free HDR, especially at medium and high SNR. Interestingly, expanding the highway to contain more lanes increases the average number of vehicular relays inside the transmission range and improves performance. Meanwhile, increasing the intensity of vehicles per lane including the central lane augments the blockage probability and obstructs the LOS between the source and the destination which leads to diminish the system performance.

## 6.2 Future Work

The contributions presented in this dissertation could be extended to the following future work:

### 6.2.1 High Speed Mobility

VANETs are considered as highly dynamic networks due to the mobility of the vehicles which causes instability and reduces network efficiency. Therefore, all the nodes in vehicular cooperative wireless networks are assumed to be mobile Khattabi, Y. M. & Matalgah, M. M. (2015) and experience time-selective fading channels Eshteiwi, K., Kaddoum, G. & Gagnon, F. (2015). In this context, Jake's model could be used to model the channel gains which are considered uncorrelated with correlation coefficient $\rho_{ij}$. In such cases, the mobility effect could be analyzed in case of FDR vehicular wireless communications using AF relaying including SI at the relay node. Moreover, due to the movement of vehicles, It could be beneficial to design optimal cooperative networking protocols which assist to select the best vehicle relay in high dynamic vehicles environment Ahmed, E. & Gharavi, H. (2018).

### 6.2.2 The Network Topology

A typical VANET consists of a large number of vehicular cooperative wireless nodes, especially in highway road. In our previous works, it is assumed that the vehicles nodes' locations

are known Eshteiwi *et al.* (2019). However, in practical systems, it can be difficult to know the locations of the vehicles due to the vehicles' mobility which causes rapid topology changes and that leads to frequent link failure and fragmentation. Therefore, it would be interesting to extend our work and investigate FDR in vehicular cooperative communications that are distributed randomly inside the transmission range of the transmitter and examine their impacts on FDR vehicular communications Farooq, M. J., ElSawy, H. & Alouini, M. S. (2015); Haenggi, M. (2005).

### 6.2.3 Multiple Sources for V2V Cooperation

In this thesis, our focus was directed toward V2V cooperative wireless communications, where one vehicle acts as the central source of transmission at all times and other vehicles act as relays. Multi-vehicle sources share the same group of relays which can be used simultaneously to forward information between the source and the destination whilst utilizing the same channel. It is important to apply radio resources allocation algorithm at the relay nodes. It is possible to use the Round-Robin scheduler strategy to access available resources. Additionally, it could be possible to use opportunistic selection strategy to select the vehicle source based on the highest end-to-end SNR between source and destination in each time slot.

### 6.2.4 Seamless Connectivity between Vehicles and Infrastructures

In the next generation of vehicular communication, inclusive of smart cities, a typical VANET would consists of a large number of connected vehicular and infrastructure nodes in order to provide ITS services. Vehicles and infrastructures should have seamless connectivity with high throughput and low latency to avoid any abnormal occurrences. Vehicular networks face many challenges, some being rapid topology changes, variable node densities as well as random speeds which may interrupt seamless connectivity and might also be subject to high latency and low throughput. A possible solution for these situations is to enable vehicular networks to access any network, such as an heterogeneous network, by applying various connection techniques, including a combination of cellular networks and Wi-Fi, to allow for continual connec-

tivity at all times using link layer aggregation Sharma, V., You, I., Leu, F.-Y. & Atiquzzaman, M. (2018); Singh *et al.* (2019).

### 6.2.5 Mobile-Edge and Fog Computing

Considering the fact that a very large number of vehicles would be using the network simultaneously, thus inevitably leading to increased amounts of shared data being transmitted, we have determined that cloud computing could be used with vehicular communication networks to enhance resource utilization. However, if there is a large distance between vehicular cloud server's location and vehicles with which it is in communication, that could potentially cause a performance deterioration in terms of the off-loading content. Mobile-edge computing (MEC) could be used as an appropriate technology to enable the connection including vehicle-to-everything (V2X) and automated driving. This technology will enable the vehicle cloud services to be brought into closer proximity to the vehicles being operated which would lead to reductions in latency and would allow for faster access to the network Shahzadi, S., Iqbal, M., Dagiuklas, T. & Qayyum, Z. U. (2017). In addition, fog computing (FC) node could be used to reduce the latency by decreasing the amount of routing data to the cloud which leads to improve the quality of service and enhance the vehicles response time Hao, Z., Novak, E., Yi, S. & Li, Q. (2017); Mouradian, C., Naboulsi, D., Yangui, S., Glitho, R. H., Morrow, M. J. & Polakos, P. A. (2017). To this end, effective MEC deployment, load balancing and efficient data management could be explored in vehicular wireless communications.

## APPENDIX I

## PROOF FOR CHAPTER 3

### 1. Proof of equations for chapter 3

#### 1.1 Proof of Equation (3.7)

It was shown in Wang *et al.* (2016), that the CDF of $\gamma_2$ can be written as

$$F_{\gamma_2}(\gamma_{th}) = 1 - \frac{C_{ID}^{m_{ID}}}{\Gamma(m_{ID})}\exp(-\gamma_{th}C_{RD})\sum_{j=0}^{m_{RD}-1}\frac{(\gamma_{th}C_{RD})^j}{j!}\sum_{k=0}^{j}\binom{j}{k}\frac{(k+m_{ID}-1)!}{(\gamma_{th}C_{RD}+C_{ID})^{k+m_{ID}}} \quad \text{(A I-1)}$$

Moreover, the PDF of $\gamma_1$ can be expressed as Eshteiwi *et al.* (Sep. 2017)

$$f_{\gamma_1}(y) = \frac{C_{SR}^{m_{SR}}C_{RR}^{m_{RR}}y^{m_{SR}-1}\exp(-yC_{SR})}{\Gamma(m_{SR})\Gamma(m_{RR})}\sum_{l=0}^{m_{SR}}\binom{m_{SR}}{l}\frac{\Gamma(m_{RR}+l)}{(yC_{SR}+C_{RR})^{m_{RR}+l}}, \quad \text{(A I-2)}$$

Substituting (A I-1) and (A I-2) into (3.6), after some algebraic manipulations, we get

$$F_{\gamma_{eq}}(\gamma_{th}) = 1 - \varphi_1\int_0^{\infty} y^{r+k+m_{ID}+f-j}\exp\left[-\left(\frac{\gamma_{th}^2C_{RD}+\gamma_{th}C_{RD}}{y}\right)\right]\frac{\exp[-C_{SR}y]}{\left[y+\frac{\gamma_{th}^2C_{RD}+\gamma_{th}C_{RD}}{\gamma_{th}C_{RD}+C_{ID}}\right]^{k+m_{ID}}} \times \frac{1}{\left[y+\frac{\gamma_{th}C_{SR}+C_{RR}}{C_{SR}}\right]^{l+m_{RR}}}dy \quad \text{(A I-3)}$$

and

$$\varphi_1 = \frac{C_{RR}^{m_{RR}}C_{SR}^{m_{SR}}C_{ID}^{m_{ID}}}{\Gamma(m_{RR})\Gamma(m_{SR})\Gamma(m_{ID})}\exp[-\gamma_{th}(C_{SR}+C_{RD})]\sum_{j=0}^{m_{RD}-1}\frac{(C_{RD})^j}{j!}\sum_{k=0}^{j}\binom{j}{k}(k+m_{ID}-1)! \times\sum_{l=0}^{m_{SR}}\binom{m_{SR}}{l}\Gamma(m_{RR}+l)\sum_{r=0}^{j}\binom{j}{r}\frac{(\gamma_{th}+1)^{j-r}}{(\gamma_{th}C_{RD}+C_{ID})^{k+m_{ID}}}\sum_{f=0}^{m_{SR}-1}\binom{m_{SR}-1}{f}\frac{\gamma_{th}^{j+m_{SR}-f-1}}{(C_{SR})^{m_{RR}+l}} \quad \text{(A I-4)}$$

With the aid of the identity in (Mathai, A. M., Saxena, R. K. & Haubold, H. J., 2009, Eq. (1.38)), the second term in the integral can be expressed as

$$\begin{aligned}\exp\left[-(\frac{\gamma_{th}^2 C_{RD}+\gamma_{th}C_{RD}}{y})\right] &= G_{0,1}^{1,0}\left(\begin{matrix}-\\0\end{matrix}\middle|\frac{\gamma_{th}^2 C_{RD}+\gamma_{th}C_{RD}}{y}\right)\\ &= G_{1,0}^{0,1}\left(\begin{matrix}1\\-\end{matrix}\middle|\frac{y}{\gamma_{th}^2 C_{RD}+\gamma_{th}C_{RD}}\right)\end{aligned} \tag{A I-5}$$

While the denominator of third term and forth term in the integral in Eq. (A I-3) can be written as (Mathai *et al.*, 2009, Eq. (1.43))

$$\begin{aligned}\frac{1}{\left[y+\frac{\gamma_{th}^2 C_{RD}+\gamma_{th}C_{RD}}{\gamma_{th}C_{RD}+C_{ID}}\right]^{k+m_{ID}}} =& \frac{1}{\Gamma(k+m_{ID})}\left(\frac{\gamma_{th}C_{RD}+C_{ID}}{\gamma_{th}^2 C_{RD}+\gamma_{th}C_{RD}}\right)^{k+m_{ID}}\\ &\times G_{1,1}^{1,1}\left(\begin{matrix}1-(k+m_{ID})\\0\end{matrix}\middle|\frac{\gamma_{th}C_{RD}+C_{ID}}{\gamma_{th}^2 C_{RD}+\gamma_{th}C_{RD}}y\right)\end{aligned} \tag{A I-6}$$

$$\begin{aligned}\frac{1}{\left[y+\frac{\gamma_{th}C_{SR}+C_{RR}}{C_{SR}}\right]^{l+m_{RR}}} =& \frac{1}{\Gamma(l+m_{RR})}\left(\frac{C_{SR}}{\gamma_{th}C_{SR}+C_{RR}}\right)^{l+m_{RR}}\\ &\times G_{1,1}^{1,1}\left(\begin{matrix}1-(l+m_{RR})\\0\end{matrix}\middle|\frac{C_{SR}}{\gamma_{th}C_{SR}+C_{RR}}y\right)\end{aligned} \tag{A I-7}$$

Substituting (A I-4), (A I-5), (A I-6) and (A I-7) into (A I-3), we get Eq. (A I-8) on the top of next page.

The second and third Meijer G-functions in the R.H.S of Eq. (A I-8) are transformed into an extended generalized bivariate Meijer's G-function according to the functional relation in Trigui *et al.* (2013a) and then using (Verma, 1966, 4.1), yields (3.7) which concludes the proof.

It should be also noted that the extended generalized bivariate Meijer's G-function $G_{\Delta,[\Theta,\Omega],\Upsilon,[\Phi,\Psi]}^{\beta,\varepsilon,\varepsilon,\zeta,\nu}\left(\begin{matrix}a_1,\ldots,a_\Delta;b_1,\ldots,b_\Theta;c_1,\ldots,c_\Omega\\e_1,\ldots,e_\Upsilon;f_1,\ldots,f_\Phi;g_1,\ldots,g_\Psi\end{matrix}\middle|z_1,z_2\right)$ converges based on two conditions as mentioned in Agrawal, R. (1970): $\Delta+\Phi+\Upsilon+\Theta<2(\zeta+\beta+\varepsilon)$ and $\Delta+\Psi+\Upsilon+\Omega<2(\nu+\beta+\varepsilon)$. It

$$F_{\gamma_{eq}}(\gamma_{th}) = 1 - \varphi_1 \sum_{q=0}^{\infty} \frac{(-C_{SR})^q}{q!} \frac{1}{\Gamma(k+m_{ID})} \frac{1}{\Gamma(l+m_{RR})} \left( \frac{\gamma_{th}C_{RD}+C_{ID}}{\gamma_{th}^2 C_{RD}+\gamma_{th}C_{RD}} \right)^{k+m_{ID}} \times \left( \frac{C_{SR}}{\gamma_{th}C_{SR}+C_{RR}} \right)^{l+m_{RR}} \int_0^{\infty} y^{r+k+m_{ID}+f+q-j} G_{1,0}^{0,1} \left( \begin{matrix} 1 \\ - \end{matrix} \middle| \frac{y}{\gamma_{th}^2 C_{RD}+\gamma_{th}C_{RD}} \right) \times G_{1,1}^{1,1} \left( \begin{matrix} 1-(k+m_{ID}) \\ 0 \end{matrix} \middle| \frac{\gamma_{th}C_{RD}+C_{ID}}{\gamma_{th}^2 C_{RD}+\gamma_{th}C_{RD}} y \right) G_{1,1}^{1,1} \left( \begin{matrix} 1-(l+m_{RR}) \\ 0 \end{matrix} \middle| \frac{C_{SR}}{\gamma_{th}C_{SR}+C_{RR}} y \right) dy \tag{A I-8}$$

is easily to show that the parameters of the extended generalized bivariate Meijer's G-function in Eq. (3.7) satisfy these two conditions, and therefore the Meijer's G-functions converge.

### 1.2 Proof of Equation (3.9)

For $X$ and $Y$ are two i.n.i.d Nakagami-$m$ distributed random variables, the PDF of $X/Y$ can be obtained as Eshteiwi *et al.* (Sep. 2017)

$$f_{\gamma_{1_{asy}}}(x) = \int_0^{\infty} y f_{\gamma_{SR}}(xy) f_{\gamma_{RR}}(y) dy \tag{A I-9}$$

Substituting (5.8) into (A I-9) and following (Jeffrey & Zwillinger, 2007, Eq. (3.326.2)) and after some algebraic manipulations we get (3.9) which completes the proof.

### 1.3 Proof of Equation (3.10)

For $X$ and $Y$ two i.n.i.d Nakagami-$m$ distributed random variables, the CDF of $X/Y$ can be written as

$$F_{\gamma_{2_{asy}}}(\gamma_{th}) = \int_0^{\infty} F_{\gamma_{RD}}(\gamma_{th} y) f_{\gamma_{ID}}(y) dy \tag{A I-10}$$

where

$$F_{\gamma_{RD}}(\gamma_{th} y) = \frac{\gamma(m_{RD}, \gamma_{th} y)}{\Gamma(m_{RD})}, \tag{A I-11}$$

From (Jeffrey & Zwillinger, 2007, Eq. (8.352.6)), we have

$$\frac{\gamma(m_{RD},\gamma_{th}y)}{\Gamma(m_{RD})} = 1-\exp(-\gamma_{th}y)\sum_{k=0}^{m_{RD}-1}\frac{(\gamma_{th}y)^k}{k!} \tag{A I-12}$$

and

$$f_{\gamma_{ID}}(y) = \frac{C_{ID}^{m_{ID}}}{\Gamma(m_{ID})}y^{m_{ID}-1}\exp(-yC_{ID}), \tag{A I-13}$$

Substituting (A I-12) and (A I-13) into (A I-10), using (Jeffrey & Zwillinger, 2007, Eq. (3.351.3)) and after some algebraic manipulations, we get (3.10) which completes the proof.

### 1.4 Proof of Equation (3.12)

Plugging (3.9) and (3.10) into (3.11), we get

$$\begin{aligned} F_{\gamma_{asy}}(\gamma_{th}) \approx & 1-\varphi_2\int_0^{\infty}(\gamma_{th}+y)^{m_{SR}-1}\left[\frac{(\gamma_{th}+y)\gamma_{th}}{y}\right]^k\frac{1}{[(\gamma_{th}+y)C_{SR}+C_{RR}]^{m_{SR}+m_{RR}}} \\ & \times\frac{1}{\left[C_{ID}+\frac{(\gamma_{th}+y)\gamma_{th}C_{RD}}{y}\right]^{m_{ID}+k}}dy \end{aligned} \tag{A I-14}$$

and

$$\varphi_2 = \frac{C_{RR}^{m_{RR}}C_{SR}^{m_{SR}}C_{ID}^{m_{ID}}}{\Gamma(m_{RR})\Gamma(m_{SR})\Gamma(m_{ID})}\Gamma(m_{SR}+m_{RR})\sum_{k=0}^{m_{RD}-1}\frac{(C_{RD})^k}{k!}(k+m_{ID}-1)! \tag{A I-15}$$

with the aid of the identity in (Jeffrey & Zwillinger, 2007, Eq. (1.111)), the first term in the integral can be expressed as

$$(\gamma_{th}+y)^{m_{SR}-1} = \sum_{l=0}^{m_{SR}-1}\binom{m_{SR}-1}{l}\gamma_{th}^{m_{SR}-1-l}y^l \tag{A I-16}$$

meanwhile, the second term in the integral in Eq. (A I-14) can be expressed as

$$\left[\frac{(\gamma_{th}+y)\gamma_{th}}{y}\right]^{k} = \sum_{p=0}^{k}\binom{k}{p}\gamma_{th}^{2k-p}y^{p-k} \tag{A I-17}$$

whereas, the third and forth terms in the integral in Eq. (A I-14) can be expressed as

$$\begin{aligned}\frac{1}{[(\gamma_{th}+y)C_{SR}+C_{RR}]^{m_{SR}+m_{RR}}} &= \frac{1}{\Gamma(m_{SR}+m_{RR})}\left(\frac{1}{\gamma_{th}C_{SR}+C_{RR}}\right)^{m_{SR}+m_{RR}} \\ &\quad\times G_{1,1}^{1,1}\left(\begin{matrix}1-(m_{SR}+m_{RR})\\0\end{matrix}\middle|\frac{C_{SR}}{\gamma_{th}C_{SR}+C_{RR}}\right)\end{aligned} \tag{A I-18}$$

and

$$\frac{1}{\left[C_{ID}+\frac{(\gamma_{th}+y)\gamma_{th}C_{RD}}{y}\right]^{m_{ID}+k}} = \frac{1}{\Gamma(k+m_{ID})}\left(\frac{y}{\gamma_{th}^{2}C_{RD}}\right)^{k+m_{ID}}G_{1,1}^{1,1}\left(\begin{matrix}1-(k+m_{ID})\\0\end{matrix}\middle|\frac{C_{ID}+\gamma_{th}C_{RD}}{\gamma_{th}^{2}C_{RD}}y\right) \tag{A I-19}$$

respectively. Substituting (A I-15), (A I-16), (A I-17), (A I-18) and (A I-19) into (A I-14) and using (Prudnikov *et al.*, 1990, Eq. (2.24.1.1)), we get (3.12) which completes the proof.

### 1.5 Proof of Equation (3.19)

Since $F_{\gamma_{\text{eq}}}(x)$ in Eq. (3.18) can be written as

$$\begin{aligned}F_{\gamma_{\text{eq}}}(x) &= \Pr[\min(\gamma_1,\gamma_2)\le x] \\ &= 1-(1-F_{\gamma_1}(x))(1-F_{\gamma_2}(x))\end{aligned} \tag{A I-20}$$

The CDFs of $\gamma_1$ and $\gamma_2$ can be written respectively as

$$F_{\gamma_1}(x) = 1-\frac{C_{\text{RR}}^{m_{\text{RR}}}}{\Gamma(m_{\text{RR}})}\exp(-xC_{\text{SR}})\sum_{l=0}^{m_{\text{SR}}-1}\frac{(xC_{\text{SR}})^{l}}{l!}\sum_{t=0}^{l}\binom{l}{t}\frac{(t+m_{\text{RR}}-1)!}{(xC_{\text{SR}}+C_{\text{RR}})^{t+m_{\text{RR}}}} \tag{A I-21}$$

and

$$F_{\gamma_2}(x) = 1 - \frac{C_{\mathrm{ID}}^{m_{\mathrm{ID}}}}{\Gamma(m_{\mathrm{ID}})} \exp(-xC_{\mathrm{RD}}) \sum_{j=0}^{m_{\mathrm{RD}}-1} \frac{(xC_{\mathrm{RD}})^j}{j!} \sum_{k=0}^{j} \binom{j}{k} \frac{(k+m_{\mathrm{ID}}-1)!}{(xC_{\mathrm{RD}}+C_{\mathrm{ID}})^{k+m_{\mathrm{ID}}}} \tag{A I-22}$$

Substituting (A I-21) and (A I-22) into (A I-20), we get

$$\begin{aligned} F_{\gamma_{\mathrm{eq}}}(x) = 1 - \frac{C_{\mathrm{RR}}^{m_{\mathrm{RR}}}}{\Gamma(m_{\mathrm{RR}})} \exp(-xC_{\mathrm{SR}}) \sum_{l=0}^{m_{\mathrm{SR}}-1} \frac{(xC_{\mathrm{SR}})^l}{l!} \sum_{t=0}^{l} \binom{l}{t} \frac{(t+m_{\mathrm{RR}}-1)!}{(xC_{\mathrm{SR}}+C_{\mathrm{RR}})^{t+m_{\mathrm{RR}}}} \frac{C_{\mathrm{ID}}^{m_{\mathrm{ID}}}}{\Gamma(m_{\mathrm{ID}})} \\ \times \exp(-xC_{\mathrm{RD}}) \sum_{j=0}^{m_{\mathrm{RD}}-1} \frac{(xC_{\mathrm{RD}})^j}{j!} \sum_{k=0}^{j} \binom{j}{k} \frac{(k+m_{\mathrm{ID}}-1)!}{(xC_{\mathrm{RD}}+C_{\mathrm{ID}})^{k+m_{\mathrm{ID}}}}. \end{aligned} \tag{A I-23}$$

Moreover, inserting (A II-21) into (3.18), we get

$$\overline{\mathrm{SER}} = \frac{\alpha\sqrt{\beta}}{2\sqrt{2\pi}} [I_1 + I_2] \tag{A I-24}$$

where $I_1$ can be solved using (Jeffrey & Zwillinger, 2007, Eq. (3.361.2))

$$I_1 = \int_0^{\infty} \frac{\exp(-\beta x/2)}{\sqrt{x}} dx = \sqrt{\frac{2\pi}{\beta}} \tag{A I-25}$$

and

$$I_2 = A \int_0^{\infty} x^{l+j-1/2} \exp[-x(C_{SR} + C_{RD} + \frac{\beta}{2})] \frac{1}{(xC_{SR}+C_{RR})^{t+m_{RR}}} \frac{1}{(xC_{RD}+C_{ID})^{k+m_{ID}}} dx \tag{A I-26}$$

where

$$A = \frac{C_{RR}^{m_{RR}}}{\Gamma(m_{RR})} \sum_{l=0}^{m_{SR}-1} \frac{(C_{SR})^l}{l!} \sum_{t=0}^{l} \binom{l}{t} (t+m_{RR}-1)! \frac{C_{ID}^{m_{ID}}}{\Gamma(m_{ID})} \sum_{j=0}^{m_{RD}-1} \frac{(C_{RD})^j}{j!} \sum_{k=0}^{j} \binom{j}{k} (k+m_{ID}-1)!. \tag{A I-27}$$

Given the following identity

$$\left(\frac{1}{1+\upsilon x}\right)^{\tau} = \frac{1}{\Gamma(\tau)} G_{1,1}^{1,1}\left(\begin{smallmatrix} 1-\tau \\ 0 \end{smallmatrix} \middle| \upsilon x\right), \tag{A I-28}$$

The integral $I_2$ in Eq. (A I-26) can be simplified to

$$\begin{aligned} I_2 = & \frac{A}{C_{RR}^{t+m_{RR}} C_{ID}^{k+m_{ID}} \Gamma(t+m_{RR}) \Gamma(k+m_{ID})} \int_0^{\infty} x^{l+j-1/2} \exp[-x(C_{SR}+C_{RD}+\frac{\beta}{2})] \\ & \times G_{1,1}^{1,1}\left(\begin{smallmatrix} 1-(t+m_{RR}) \\ 0 \end{smallmatrix} \middle| \frac{C_{RD}}{C_{ID}} x\right) G_{1,1}^{1,1}\left(\begin{smallmatrix} 1-(k+m_{ID}) \\ 0 \end{smallmatrix} \middle| \frac{C_{RD}}{C_{ID}} x\right) dx \end{aligned} \tag{A I-29}$$

From (A I-29) and using (Mathai, A. M. & Saxena, R. K., 1978, Eq. (2.6.2)) to solve $I_2$, we get (A I-30), at the top of next page.

$$\begin{aligned} I_2 = & \frac{1}{\Gamma(m_{RR})\Gamma(m_{ID})} \sum_{l=0}^{m_{SR}-1} \frac{(C_{SR})^l}{l!} \sum_{t=0}^{l} \binom{l}{t} \sum_{j=0}^{m_{RD}-1} \frac{(C_{RD})^j}{j!} \sum_{k=0}^{j} \binom{j}{k} \frac{(C_{SR}+C_{RD}+\frac{\beta}{2})^{-(l+j+1/2)}}{C_{RR}^t C_{ID}^k} \\ & G_{1,[1,1],0,[1,1]}^{1,1,1,1,1}\left(\begin{smallmatrix} (j+l+1/2);1-(t+m_{RR});1-(k+m_{ID}) \\ -;0;0 \end{smallmatrix} \middle| \frac{C_{SR}}{C_{RR}(C_{SR}+C_{RD}+\frac{\beta}{2})}, \frac{C_{RD}}{C_{ID}(C_{SR}+C_{RD}+\frac{\beta}{2})}\right) \end{aligned} \tag{A I-30}$$

Finally, substituting (A I-25) and (A I-30) into (A I-24) completes this proof.

## APPENDIX II

## PROOF FOR CHAPTER 4

### 1. Proof of equations for chapter 4

#### 1.1 Proof of Equation (4.7)

Eq. (4.6) can be written as Almradi *et al.* (2018)

$$\frac{1}{\ln(2)}\mathbb{E}\left[\ln(1+\frac{\gamma_1\gamma_2}{\gamma_1+\gamma_2+1})\right]=\frac{1}{\ln(2)}\int_0^\infty\frac{1}{z}(1-M_{\gamma_1}(z))(1-M_{\gamma_2}(z))\exp(-z)dz, \quad \text{(A II-1)}$$

where $M_{\gamma_i}(z)=\mathbb{E}[\exp(-z\gamma_i)]$, $i\in\{1,2\}$. To solve Eq. (A II-1), we need to derive both $M_{\gamma_1}(z)$ and $M_{\gamma_2}(z)$. Now, $M_{\gamma_1}(z)$ can be written as Amarasuriya *et al.* (2012)

$$M_{\gamma_1}(z)=1-\int_0^\infty z\exp(-zx)\left[1-F_{\gamma_1}(x)\right]dx, \quad \text{(A II-2)}$$

where $F_{\gamma_1}(x)$ is the cumulative density function (CDF) of $\gamma_1$ which can be evaluated as Wang *et al.* (2016)

$$F_{\gamma_1}(x)=1-\frac{C_{RR}^{m_{RR}}}{\Gamma(m_{RR})}\exp(-xC_{SR})\sum_{j=0}^{m_{SR}-1}\frac{(xC_{SR})^j}{j!}\sum_{k=0}^{j}\binom{j}{k}\frac{(k+m_{RR}-1)!}{(xC_{SR}+C_{RR})^{k+m_{RR}}}. \quad \text{(A II-3)}$$

Substituting Eq. (A II-3) into Eq. (A II-2) and using (Jeffrey & Zwillinger, 2007, Eq. (1.211.1)) , we have

$$M_{\gamma_1}(z)=1-z\vartheta\int_0^\infty\frac{x^{j+q}}{(x+\frac{C_{RR}}{C_{SR}})^{k+m_{RR}}}dx, \quad \text{(A II-4)}$$

where

$$\vartheta=\frac{C_{RR}^{m_{RR}}}{\Gamma(m_{RR})}\sum_{j=0}^{m_{SR}-1}\sum_{k=0}^{j}\sum_{q=0}^{\infty}\binom{j}{k}\frac{(C_{SR})^{j-k-m_{RR}}}{j!}(k+m_{RR}-1)!\frac{(-1)^q}{q!}(z+C_{SR})^q. \quad \text{(A II-5)}$$

Taking $g = x + u$ in Eq. (A II-4), where $u = \frac{C_{RR}}{C_{SR}}$ and then using (Jeffrey & Zwillinger, 2007, Eq. (1.111)), $M_{\gamma_1}(z)$ can be expressed as

$$M_{\gamma_1}(z) = 1 - z\vartheta \sum_{f=0}^{j+q} \binom{j+q}{f} (-1)^{j+q-f} (\frac{C_{RR}}{C_{SR}})^{j+q-f} \left[ \frac{(f-k-m_{RR}+1) - (\frac{C_{RR}}{C_{SR}})^{f-k-m_{RR}+1}}{f-k-m_{RR}+1} \right]. \tag{A II-6}$$

Substituting $\vartheta$ from Eq. (A II-5) into Eq. (A II-6), yields

$$\begin{aligned} M_{\gamma_1}(z) =& 1 - z \frac{C_{RR}^{m_{RR}}}{\Gamma(m_{RR})} \sum_{j=0}^{m_{SR}-1} \sum_{k=0}^{j} \sum_{q=0}^{\infty} \binom{j}{k} \frac{(C_{SR})^{j-k-m_{RR}}}{j!} (k+m_{RR}-1)! \frac{(-1)^q}{q!} r \\ & \times (z+C_{SR})^q \sum_{f=0}^{j+q} \binom{j+q}{f} (-1)^{j+q-f} (\frac{C_{RR}}{C_{SR}})^{j+q-f} \\ & \times \left[ \frac{(f-k-m_{RR}+1) - (\frac{C_{RR}}{C_{SR}})^{f-k-m_{RR}+1}}{f-k-m_{RR}+1} \right]. \end{aligned} \tag{A II-7}$$

On the other hand, the CDF of $\gamma_2$ can be obtained from Wang *et al.* (2016)

$$F_{\gamma_2}(x) = 1 - \frac{C_{ID}^{m_{ID}}}{\Gamma(m_{ID})} \exp(-xC_{RD}) \sum_{l=0}^{m_{RD}-1} \frac{(xC_{RD})^l}{l!} \sum_{t=0}^{l} \binom{l}{t} \frac{(t+m_{ID}-1)!}{(xC_{RD}+C_{ID})^{t+m_{ID}}}. \tag{A II-8}$$

Following the same steps as for $M_{\gamma_1}(z)$, $M_{\gamma_2}(z)$ is obtained as

$$\begin{aligned} M_{\gamma_2}(z) =& 1 - z \frac{C_{ID}^{m_{ID}}}{\Gamma(m_{ID})} \sum_{l=0}^{m_{RD}-1} \sum_{t=0}^{l} \sum_{r=0}^{\infty} \binom{l}{t} \frac{(C_{RD})^{l-t-m_{ID}}}{l!} (t+m_{ID}-1)! \frac{(-1)^r}{r!} \\ & \times (z+C_{RD})^r \sum_{e=0}^{l+r} \binom{l+r}{e} (-1)^{l+r-e} (\frac{C_{ID}}{C_{RD}})^{l+r-e} \left[ \frac{(e-t-m_{ID}+1) - (\frac{C_{ID}}{C_{RD}})^{e-t-m_{ID}+1}}{e-t-m_{ID}+1} \right]. \end{aligned} \tag{A II-9}$$

Hence, substituting Eq. (A II-7) and Eq. (A II-9) into Eq. (A II-1) and after some mathematical manipulations, the proof is completed.

### 1.2 Proof of Equation (4.10)

From Eq. (4.8), $\mathrm{EC}_{\gamma_i} = \mathbb{E}[\log_2(1+\gamma_i)] = \frac{1}{\ln 2}\mathbb{E}[\ln(1+\gamma_i)]$ can be evaluated as Almradi *et al.* (2018)

$$\mathbb{E}[\ln(1+\gamma_i)] = \int_0^\infty \frac{1}{z}\left(1 - M_{\gamma_i}(z)\right)\exp(-z)dz, \tag{A II-10}$$

where $M_{\gamma_i}(z)$, $i \in \{1,2\}$, is given in Eq. (A II-7) and Eq. (A II-9). Here, Eq. (A II-10) is valid for any $\gamma_i \geq 0$ Almradi *et al.* (2018).

Now, substituting the value of $M_{\gamma_1}(z)$ from Eq. (A II-7) into Eq. (A II-10), and utilizing (Jeffrey & Zwillinger, 2007, Eq. (1.111)) and (Jeffrey & Zwillinger, 2007, Eq. (3.351.3)), we have

$$\begin{aligned}\mathrm{EC}_{\gamma_1} =& \frac{1}{\ln 2}\frac{C_{RR}^{m_{RR}}}{\Gamma(m_{RR})}\sum_{j=0}^{m_{SR}-1}\sum_{k=0}^{j}\sum_{q=0}^{\infty}\binom{j}{k}\frac{(C_{SR})^{j-k-m_{RR}}}{j!}(k+m_{RR}-1)!\frac{(-1)^q}{q!}\\ &\times\sum_{f=0}^{j+q}\binom{j+q}{f}(-1)^{j+q-f}\left(\frac{C_{RR}}{C_{SR}}\right)^{j+q-f}\sum_{s=0}^{q}\binom{q}{s}(C_{SR})^{q-s}\Gamma(s+1)\\ &\times\left[\frac{(f-k-m_{RR}+1)-\left(\frac{C_{RR}}{C_{SR}}\right)^{f-k-m_{RR}+1}}{f-k-m_{RR}+1}\right].\end{aligned} \tag{A II-11}$$

Similarly,

$$\begin{aligned}\mathrm{EC}_{\gamma_2} =& \frac{1}{\ln 2}\frac{C_{ID}^{m_{ID}}}{\Gamma(m_{ID})}\sum_{l=0}^{m_{RD}-1}\sum_{t=0}^{l}\sum_{r=0}^{\infty}\binom{l}{t}\frac{(C_{RD})^{l-t-m_{ID}}}{l!}(t+m_{ID}-1)!\frac{(-1)^r}{r!}\\ &\times\sum_{e=0}^{l+r}\binom{l+r}{e}(-1)^{l+r-e}\left(\frac{C_{ID}}{C_{RD}}\right)^{l+r-e}\sum_{u=0}^{r}\binom{r}{u}(C_{RD})^{r-u}\Gamma(u+1)\\ &\times\left[\frac{(e-t-m_{ID}+1)-\left(\frac{C_{ID}}{C_{RD}}\right)^{e-t-m_{ID}+1}}{e-t-m_{ID}+1}\right]\end{aligned} \tag{A II-12}$$

Since, the probability density function (PDF) of $\gamma_1$ is given by Eshteiwi *et al.* (Sep. 2017)

$$f_{\gamma_1}(y) = \frac{C_{SR}^{m_{SR}} C_{RR}^{m_{RR}} y^{m_{SR}-1}}{\Gamma(m_{SR})\Gamma(m_{RR})} \exp(-yC_{SR}) \sum_{l_1=0}^{m_{SR}} \binom{m_{SR}}{l_1} \frac{\Gamma(m_{RR}+l_1)}{(yC_{SR}+C_{RR})^{m_{RR}+l_1}} \tag{A II-13}$$

We can evaluate $\mathbb{E}[(\gamma_1)]$ and $\mathbb{E}[(\gamma_2)]$ in Eq. (4.9) using Eq. (A II-13), as follows

$$\mathbb{E}[(\gamma_1)] = \frac{C_{SR}^{m_{SR}} C_{RR}^{m_{RR}}}{\Gamma(m_{SR})\Gamma(m_{RR})} \sum_{l_1=0}^{m_{SR}} \binom{m_{SR}}{l_1} \frac{\Gamma(m_{RR}+l_1)}{C_{SR}^{m_{RR}+l_1}} \underbrace{\int_0^\infty \frac{y^{m_{SR}} \exp(-yC_{SR})}{(y+\frac{C_{RR}}{C_{SR}})^{m_{RR}+l_1}} dy}_{I_1}. \tag{A II-14}$$

For the integral $I_1$, taking $w = y + u$ with $u = \frac{C_{RR}}{C_{SR}}$ and using the binomial expansion (Jeffrey & Zwillinger, 2007, Eq. (1.111)), we get

$$I_1 = \exp(C_{RR}) \sum_{l_2=0}^{m_{SR}} (-1)^{m_{SR}-l_2} (\frac{C_{RR}}{C_{SR}})^{m_{SR}-l_2} \int_u^\infty w^{l_2-m_{RR}-l_1} \exp(-wC_{SR}) dw. \tag{A II-15}$$

Utilizing (Jeffrey & Zwillinger, 2007, Eq. (3.381.3)), $I_1$ is obtained as

$$I_1 = \exp(C_{RR}) \sum_{l_2=0}^{m_{SR}} (-1)^{m_{SR}-l_2} (\frac{C_{RR}}{C_{SR}})^{m_{SR}-l_2} (C_{SR})^{-(l_2-m_{RR}-l_1+1)} \Gamma(l_2-m_{RR}-l_1+1, C_{RR}) \tag{A II-16}$$

Inserting Eq. (A II-16) into Eq. (A II-15) and substituting $I_1$ into Eq. (A II-14), we get

$$\begin{aligned} \mathbb{E}[(\gamma_1)] =& \frac{C_{SR}^{m_{SR}} C_{RR}^{m_{RR}}}{\Gamma(m_{SR})\Gamma(m_{RR})} \sum_{l_1=0}^{m_{SR}} \binom{m_{SR}}{l_1} \frac{\Gamma(m_{RR}+l_1)}{C_{SR}^{m_{RR}+l_1}} \exp(C_{RR}) \sum_{l_2=0}^{m_{SR}} (-1)^{m_{SR}-l_2} \\ & \times (\frac{C_{RR}}{C_{SR}})^{m_{SR}-l_2} (C_{SR})^{-(l_2-m_{RR}-l_1+1)} \Gamma(l_2-m_{RR}-l_1+1, C_{RR}). \end{aligned} \tag{A II-17}$$

Furthermore, the PDF of $\gamma_2$ can be written as Eshteiwi *et al.* (Sep. 2017)

$$f_{\gamma_2}(y) = \frac{C_{RD}^{m_{RD}} C_{ID}^{m_{ID}} y^{m_{RD}-1} \exp(-yC_{RD})}{\Gamma(m_{RD})\Gamma(m_{ID})} \sum_{j_1=0}^{m_{RD}} \binom{m_{RD}}{j_1} \frac{\Gamma(m_{ID}+j_1)}{(yC_{RD}+C_{ID})^{m_{ID}+j_1}}. \tag{A II-18}$$

Following the same steps, $\mathbb{E}[(\gamma_2)]$ is obtained as

$$\begin{aligned}\mathbb{E}[(\gamma_2)] =& \frac{C_{RD}^{m_{RD}} C_{ID}^{m_{ID}}}{\Gamma(m_{RD})\Gamma(m_{ID})} \sum_{j_1=0}^{m_{RD}} \binom{m_{RD}}{j_1} \frac{\Gamma(m_{ID}+j_1)}{C_{RD}^{m_{ID}+j_1}} \exp(C_{ID}) \sum_{j_2=0}^{m_{RD}} (-1)^{m_{RD}-j_2} \\ & \times (\frac{C_{ID}}{C_{RD}})^{m_{RD}-j_2} (C_{RD})^{-(j_2-m_{ID}-j_1+1)} \Gamma(j_2-m_{ID}-j_1+1, C_{ID}).\end{aligned}$$

Finally, substituting Eq. (A II-11), Eq. (A II-12), Eq. (A II-17), and Eq. (A II-19) into Eq. (4.8) yields Eq. (4.10).

### 1.3 Proof of Equation (4.11)

The upper bound of the ergodic capacity can be evaluated as Shi *et al.* (2015)

$$\mathrm{EC}_{upper} = \frac{1}{\ln 2} \int_0^{\infty} \frac{1 - F_{\gamma_{eq}}(x)}{1+x} dx, \tag{A II-19}$$

where

$$\begin{aligned} F_{\gamma_{eq}}(x) &= \Pr[\min(\gamma_1, \gamma_2) \leq x] \\ &= 1 - (1 - F_{\gamma_1}(x))(1 - F_{\gamma_2}(x)). \end{aligned} \tag{A II-20}$$

Substituting Eq. (A II-3) and Eq. (A II-8) into Eq. (A II-20), we get

$$\begin{aligned} F_{\gamma_{eq}}(x) =& 1 - \frac{C_{RR}^{m_{RR}}}{\Gamma(m_{RR})} \exp(-xC_{SR}) \sum_{j=0}^{m_{SR}-1} \frac{(xC_{SR})^j}{j!} \sum_{k=0}^{j} \binom{j}{k} \frac{(k+m_{RR}-1)!}{(xC_{SR}+C_{RR})^{k+m_{RR}}} \\ & \times \frac{C_{ID}^{m_{ID}}}{\Gamma(m_{ID})} \exp(-xC_{RD}) \sum_{l=0}^{m_{RD}-1} \frac{(xC_{RD})^l}{l!} \sum_{t=0}^{l} \binom{l}{t} \frac{(t+m_{ID}-1)!}{(xC_{RD}+C_{ID})^{t+m_{ID}}}. \end{aligned} \tag{A II-21}$$

Substituting Eq. (A II-21) into Eq. (A II-19), we get

$$\mathrm{EC}_{upper} = \frac{A}{\ln 2}\int_0^{\infty} x^{j+l}\exp[-x(C_{SR}+C_{RD})]\frac{1}{1+x}\frac{1}{(xC_{SR}+C_{RR})^{k+m_{RR}}}\frac{1}{(xC_{RD}+C_{ID})^{t+m_{ID}}}dx, \tag{A II-22}$$

where

$$A = \frac{C_{RR}^{m_{RR}}}{\Gamma(m_{RR})}\sum_{j=0}^{m_{SR}-1}\frac{(C_{SR})^j}{j!}\sum_{k=0}^{j}\binom{j}{k}(k+m_{RR}-1)!\frac{C_{ID}^{m_{ID}}}{\Gamma(m_{ID})}\sum_{l=0}^{m_{RD}-1}\frac{(C_{RD})^l}{l!}\sum_{t=0}^{l}\binom{l}{t}(t+m_{ID}-1)! \tag{A II-23}$$

Now, our task is to solve the integral in Eq. (A II-22). Given the following identity

$$\left(\frac{1}{1+\upsilon x}\right)^{\beta} = \frac{1}{\Gamma(\beta)}G_{1,1}^{1,1}\left(\begin{matrix}1-\beta\\0\end{matrix}\middle|\,\upsilon x\right), \tag{A II-24}$$

Equation (A II-22) can be rewritten as

$$\begin{aligned}\mathrm{EC}_{upper} =& \frac{A}{\ln 2}\sum_{q=0}^{\infty}\frac{(-1)^q(C_{SR}+C_{RD})^q}{q!}\frac{1}{\Gamma(k+m_{RR})C_{RR}^{k+m_{RR}}\Gamma(t+m_{ID})C_{ID}^{t+m_{ID}}}\\ &\times\int_0^{\infty}x^{j+l+q}G_{1,1}^{1,1}\left(\begin{matrix}0\\0\end{matrix}\middle|x\right)G_{1,1}^{1,1}\left(\begin{matrix}1-(k+m_{RR})\\0\end{matrix}\middle|\frac{C_{SR}}{C_{RR}}x\right)G_{1,1}^{1,1}\left(\begin{matrix}1-(t+m_{ID})\\0\end{matrix}\middle|\frac{C_{RD}}{C_{ID}}x\right)dx.\end{aligned} \tag{A II-25}$$

The second and third Meijer's G-functions in the right hand side (R.H.S) of Eq. (A II-25) are transformed into an extended generalized bivariate Meijer's G-function according to the functional relation in Trigui *et al.* (2013a). Using (Verma, 1966, 4.1) and then inserting Eq. (A II-23) into Eq. (A II-25), yields (4.11) which concludes the proof.

It should also be noted that the extended generalized bivariate Meijer's G-function $G_{\Delta,[\Theta,\Omega],\Upsilon,[\Phi,\Psi]}^{\beta,\varepsilon,\varepsilon,\zeta,\nu}\left(\begin{matrix}a_1,\ldots,a_\Delta;b_1,\ldots,b_\Theta;c_1,\ldots,c_\Omega\\e_1,\ldots,e_\Upsilon;f_1,\ldots,f_\Phi;g_1,\ldots,g_\Psi\end{matrix}\middle|z_1,z_2\right)$ converges based on two conditions as mentioned in Agrawal (1970): $\Delta+\Phi+\Upsilon+\Theta<2(\zeta+\beta+\varepsilon)$ and $\Delta+\Psi+\Upsilon+\Omega<2(\nu+\beta+\varepsilon)$. It is straightforward to show that the parameters of the extended generalized bivariate Meijer's G-

function in Eq. (4.11) satisfy these two conditions, and therefore the Meijer's G-functions converge.

## APPENDIX III

## PROOF FOR CHAPTER 5

### 1. Proof of equations for chapter 5

#### 1.1 Proof of Equation (5.11)

The CDF of $\gamma_{SR_iR_i}$ can be attained as

$$F_{\gamma_{SR_iR_i}}(\gamma_{th}) = \int_0^{\gamma_{th}} f_{\gamma_{SR_iR_i}}(x)dx = 1 - \int_{\gamma_{th}}^{\infty} f_{\gamma_{SR_iR_i}}(x)dx. \tag{A III-1}$$

Substituting Eq. (5.10) into Eq. (A III-1), we get

$$F_{\gamma_{SR_iR_i}}(x) = 1 - \frac{C_{SR_i}^{m_{SR_i}} C_{R_iR_i}^{m_{R_iR_i}}}{\Gamma(m_{SR_i})\Gamma(m_{R_iR_i})} \times \sum_{j=0}^{m_{SR_i}} \binom{m_{SR_i}}{j} \frac{\Gamma(m_{R_iR_i}+j)}{(C_{SR_i})^{m_{R_iR_i}+j}} \underbrace{\int_{\gamma_{th}}^{\infty} \frac{x^{m_{SR_i}-1}\exp(-xC_{SR_i})}{(x+\frac{C_{R_iR_i}}{C_{SR_i}})^{m_{R_iR_i}+j}} dx}_{I_1}. \tag{A III-2}$$

Solving the integral ($I_1$) to obtain the CDF by letting $g = x+z$ and $z = \frac{C_{R_iR_i}}{C_{SR_i}}$

$$\int_{\gamma_{th}+z}^{\infty} \frac{(g-z)^{m_{SR_i}-1}\exp(-(g-z)C_{SR_i})}{g^{m_{R_iR_i}+j}} dg. \tag{A III-3}$$

Adopting the binomial theorem, expands $(g-z)^{m_{SR_i}-1}$ as

$$(g-z)^{m_{SR_i}-1} = \sum_{q=0}^{m_{SR_i}-1} \binom{m_{SR_i}-1}{q} (-1)^{m_{SR_i}-1-q} z^{m_{SR_i}-1-q} g^q. \tag{A III-4}$$

Substituting Eq. (A III-4) into Eq. (A III-3) results in

$$I_1 = \exp(C_{R_iR_i}) \sum_{q=0}^{m_{SR_i}-1} \binom{m_{SR_i}-1}{q} (-1)^{m_{SR_i}-1-q} z^{m_{SR_i}-1-q} \underbrace{\int_{\gamma_{th}+z}^{\infty} g^{q-m_{R_iR_i}-j-1} \exp(-C_{SR_i} g) dg}_{I_2}. \tag{A III-5}$$

Using (Jeffrey & Zwillinger, 2007, Eq. (3.381.3)) produces

$$I_2 = C_{SR_i}^{-q+m_{R_iR_i}+j-1} \Gamma\left(q - m_{R_iR_i} - j + 1, (C_{SR_i} x + C_{R_iR_i})\right). \tag{A III-6}$$

Finally, making $z = \frac{C_{R_iR_i}}{C_{SR_i}}$, $x = \gamma_{th}$, substituting Eq. (A III-6) into Eq. (A III-5), and then in Eq. (A III-2) will complete the proof of Eq. (5.11)

### 1.2 Proof of Equation (5.15)

The outage probability of the proposed system including indirect *S-D* links can be written as

$$P_{\text{ind}_{\text{MMSI}}}(\gamma_{th}) = P(\gamma^{\text{sc}}_{\text{ind}_{\text{total}}} \leq \gamma_{th}). \tag{A III-7}$$

Substituting Eq. (5.14) into Eq. (A III-7)

$$P_{\text{ind}_{\text{MMSI}}}(\gamma_{th}) = P[\max_{i \in \{1,\ldots,\mathbb{E}[|N|]\}} [\min(\gamma_{SR_iR_i}, \gamma_{R_iD})]]. \tag{A III-8}$$

In addition, $P_{\gamma_{SR_iR_iD}}(\gamma_{th})$ can be expressed as

$$\begin{aligned} P_{\gamma_{SR_iR_iD}}(\gamma_{th}) &= P_{\min(\gamma_{SR_iR_i}, \gamma_{R_iD})}(\gamma_{th}) \\ &= 1 - [1 - P_{\gamma_{SR_iR_i}}(\gamma_{th})][1 - P_{\gamma_{R_iD}}(\gamma_{th})]. \end{aligned} \tag{A III-9}$$

where $P_{\gamma_{SR_iR_i}}(\gamma_{th})$ is defined in Eq. (5.11) and

$$P_{\gamma_{R_iD}}(\gamma_{th}) = \frac{\gamma(m_{R_iD}, \gamma_{th}C_{R_iD})}{\Gamma(m_{R_iD})}. \tag{A III-10}$$

Substituting Eq. (5.11) and Eq. (A III-10) into Eq. (A III-9) results in Eq. (A III-11) that represents the outage probability of one *S*-$R_i$-$R_i$-*D* link including self-interference at the relay node.

$$P_{\gamma_{SR_iR_iD}}(\gamma_{th}) = 1 - \left[T_1 \frac{\Gamma(m_{R_iD}, \gamma_{th}C_{R_iD})}{\Gamma(m_{R_iD})}\right], \tag{A III-11}$$

where $T_1$ is defined in Eq. (5.15) To generalize the analytical expression obtained in Eq. (A III-11), multi-vehicular relays are included. Doing so yields

$$P_{\text{ind}_{\text{MMSI}}}(\gamma_{th}) = \prod_{i=1}^{\lfloor N \rfloor} P_{\gamma_{SR_iR_iD}}(\gamma_{th}). \tag{A III-12}$$

Substituting Eq. (A III-11) into Eq. (A III-12) yields the outage probability for the proposed system with indirect *S*-*D* as

$$P_{\text{ind}_{\text{MMSI}}}(\gamma_{th}) = \prod_{i=1}^{\lfloor N \rfloor} 1 - \left[T_1 \frac{\Gamma(m_{R_iD}, \gamma_{th}C_{R_iD})}{\Gamma(m_{R_iD})}\right]. \tag{A III-13}$$

It is then possible to derive the outage probability for the proposed system with indirect links as follows:

From (Jeffrey & Zwillinger, 2007, Eq. (8.352.4)) and (Jeffrey & Zwillinger, 2007, Eq. (8.339.1)), we have

$$\frac{\Gamma(m_{R_iD}, \gamma_{th}C_{R_iD})}{\Gamma(m_{R_iD})} = \exp(-\gamma_{th}C_{R_iD}) \sum_{h=0}^{m_{R_iD}-1} \frac{(\gamma_{th}C_{R_iD})^h}{h!}. \tag{A III-14}$$

Utilizing (Jeffrey & Zwillinger, 2007, Eq. (1.111)) and substituting Eq. (A III-14) into Eq. (A III-13), reduces to Eq. (5.15), that concludes the proof.

### 1.3 Proof of Equation (5.20)

The outage probability in this case is derived using $\max(\gamma_{SD}, \gamma_{SR_iR_iD})$ and is expressed as

$$P_{\text{dir}_{\text{MMSI}}}(\gamma_{th}) = P[\max_{i\in\{1,\ldots,\mathbb{E}[|N|]\}}(\gamma_{SD}, \gamma_{SR_iR_iD}) \leq \gamma_{th}]. \tag{A III-15}$$

which can rewritten as

$$P_{\text{dir}_{\text{MMSI}}}(\gamma_{th}) = P_{\gamma_{SD}}(\gamma_{th}) \times P_{\text{ind}_{\text{MMSI}}}(\gamma_{th}), \tag{A III-16}$$

where $P_{\text{ind}_{\text{MMSI}}}(\gamma_{th})$ is obtained previously in Eq. (5.15), and

$$P_{SD}(\gamma_{th}) = \frac{\gamma(m_{SD}, \gamma_{th}C_{SD})}{\Gamma(m_{SD})}. \tag{A III-17}$$

with $\gamma(x,y) = \int_0^y t^{x-1}e^{-t}dt$ being the lower incomplete Gamma function (Jeffrey & Zwillinger, 2007, Eq. (8.350.1)). From (Jeffrey & Zwillinger, 2007, Eq. (8.352.6)), we have

$$\frac{\gamma(m_{SD}, \gamma_{th}C_{SD})}{\Gamma(m_{SD})} = \left[1 - \exp(-\gamma_{th}C_{SD}) \sum_{l=0}^{m_{SD}-1} \frac{(\gamma_{th}C_{SD})^l}{l!}\right]. \tag{A III-18}$$

Eq. (5.20) is obtained by substituting Eq. (5.15) and Eq. (A III-18) into Eq. (A III-16).

## REFERENCES


*The Wolfram Functions Site. Accessed: 2016. [Online]. Available: http://functions.wolfram.com*.

Aalo, V. A., Peppas, K. P., Efthymoglou, G. P., Alwakeel, M. M. & Alwakeel, S. S. (2013). Serial amplify-and-forward relay transmission systems in Nakagami-m fading channels with a Poisson interference field. *IEEE Trans. Vehicul. Technol.*, 63(5), 2183–2196.

Abuashour, A. & Kadoch, M. (2017). Performance improvement of cluster-based routing protocol in VANET. *IEEE Access*, 5, 15354–15371.

Acosta, G. & Ingram, M. A. (2006). Model development for the wide band expressway vehicle-to-vehicle 2.4 GHz channel. *IEEE Wireless Commun. and Net. Conf., 2006. WCNC 2006.*, 3, 1283–1288.

Agrawal, R. (1970). On certain transformation formulae and Meijer's G-function of two variables. *Indian J. Pure Appl. Math.*, 1(4), 537–551.

Ahmed, E. & Gharavi, H. (2018). Cooperative vehicular networking: A survey. *IEEE Trans. Intelligent Trans. Sys.*, 19(3), 996–1014.

Ahmed, E., Eltawil, A. M. & Sabharwal, A. (2013). Self-interference cancellation with non-linear distortion suppression for full-duplex systems. *2013 Asilomar Conf. on Signals, Sys. and Comp.*, pp. 1199–1203.

Ahmed, M. A., Tsimenidis, C. C. & Al Rawi, A. F. (2016). Performance analysis of full-duplex-MRC-MIMO with self-interference cancellation using null-space-projection. *IEEE Trans. Signal Process.*, 64(12), 3093–3105.

Ahrems, J. (2015). Implementation of collision warning algorithm based on V2V communications. *2015 25th Int. Conf. Radioelektronika (RADIOELEKTRONIKA)*, pp. 395–398.

Ai, Y. & Cheffena, M. Performance Analysis of Hybrid-ARQ over Full-Duplex Relaying Network Subject to Loop Interference under Nakagami-*m* Fading Channels. *IEEE Veh. Technol. Conf. (VTC Spring)*, pp. 1–5, 2017.

Airod, F. E., Chafnaji, H. & Tamtaoui, A. (2017). Performance analysis for amplify and forward full-duplex relaying with direct link over Nakagami-*m* fading channel. *Int. Conf. on Wireless Netw. and Mobile Commun. (WINCOM)*, pp. 1–6.

Akhtar, N., Ergen, S. C. & Ozkasap, O. (2014). Vehicle mobility and communication channel models for realistic and efficient highway VANET simulation. *IEEE Trans. Veh. Technol.*, 64(1), 248–262.

Akhtar, N., Ergen, S. C. & Ozkasap, O. (2015). Vehicle mobility and communication channel models for realistic and efficient highway VANET simulation. *IEEE Trans. Veh. Technol.*, 64(1), 248–262.

Akin, A. I., Ilhan, H. & Özdemir, Ö. (2015). Relay selection for DF-based cooperative vehicular systems. *EURASIP J. Wireless Commun. Netw.*, 2015(1), 1–9.

Alghorani, Y. & Seyfi, M. (2017). On the Performance of Reduced-Complexity Transmit/Receive-Diversity Systems Over MIMO-V2V Channel Model. *IEEE Wireless Commun. Lett.*, 6(2), 214–217.

Alghorani, Y., Kaddoum, G., Muhaidat, S. & Pierre, S. (2015a). On the Approximate Analysis of Energy Detection Over $N^*$ Rayleigh Fading Channels Through Cooperative Spectrum Sensing. *IEEE Wireless Commun. Lett.*, 4(4), 413–416.

Alghorani, Y., Kaddoum, G., Muhaidat, S., Pierre, S. & Al-Dhahir, N. (2015b). On the Performance of Multihop-Intervehicular Communications Systems Over n* Rayleigh Fading Channels. *IEEE Wireless Commun. Lett.*, 5(2), 116–119.

Alghorani, Y., Kaddoum, G., Muhaidat, S., Pierre, S. & Al-Dhahir, N. (2016). On the performance of multihop-intervehicular communications systems over n* Rayleigh fading channels. *IEEE Wireless Commun. Lett.*, 5(2), 116–119.

Almradi, A. & Hamdi, K. A. (2017a). MIMO full-duplex relaying in the presence of co-channel interference. *IEEE Trans. on Veh. Techno.*, 66(6), 4874–4885.

Almradi, A. & Hamdi, K. A. (2017b). On the Outage Probability of MIMO Full-Duplex Relaying: Impact of Antenna Correlation and Imperfect CSI. *IEEE Trans. Veh. Technol.*, 66(5), 3957–3965.

Almradi, A., Xiao, P. & Hamdi, K. A. (2018). Hop-by-Hop ZF Beamforming for MIMO Full-Duplex Relaying with Co-Channel Interference. *IEEE Trans. on Commun.*, 66(12), 6135–6149.

Altshuler, E. E., Marr, R. et al. A comparison of experimental and theoretical values of atmospheric absorption at the longer millimeter wavelengths. *IEEE Trans. Antennas and Propag.*, 36(10), 1471–1480, 1988.

Alves, H., Fraidenraich, G., Souza, R. D., Bennis, M. & Latva-aho, M. (2012). Performance analysis of full duplex and selective and incremental half duplex relaying schemes. *Proc. IEEE Wireless Commun. Netw. Conf*, pp. 771–775.

Alves, H., Souza, R. D., da Costa, D. B. & Latva-aho, M. (2015). Full-duplex relaying systems subject to co-channel interference and noise in nakagami-m fading. *Vehicular Technology Conference (VTC Spring), 2015 IEEE 81st*, pp. 1–5.

Alves, H., da Costa, D. B., Souza, R. D. & Latva-aho, M. (June 2013). Performance of block-Markov full duplex relaying with self interference in Nakagami-*m* fading. *IEEE Wireless Commun. Lett.*, 2(3), 311–314.

Amarasuriya, G., Tellambura, C. & Ardakani, M. (2012). Performance analysis of hop-by-hop beamforming for dual-hop MIMO AF relay networks. *IEEE Trans. Commun.*, 60(7), 1823–1837.

Andersen, J. B. (2002). Statistical distributions in mobile communications using multiple scattering. *Proc. 27th URSI General Assembly*, pp. 1–4.

Ansari, I. S., Al-Ahmadi, S., Yilmaz, F., Alouini, M.-S. & Yanikomeroglu, H. (2011). A new formula for the BER of binary modulations with dual-branch selection over generalized-K composite fading channels. *IEEE Trans. Commun.*, 59(10), 2654–2658.

Antonio-Rodríguez, E., López-Valcarce, R., Riihonen, T., Werner, S. & Wichman, R. (2014). SINR optimization in wideband full-duplex MIMO relays under limited dynamic range. *2014 IEEE 8th Sensor Array and Multichannel Signal Proce,. Workshop (SAM)*, pp. 177–180.

Arifin, A. S. & Ohtsuki, T. (2015). Ergodic capacity analysis of full-duplex amplify-forward MIMO relay channel using Tracy-Widom distribution. *2015 IEEE 26th Annual Int. Symposium Personal, Indoor, and Mobile Radio Commun. (PIMRC)*, pp. 266–270.

Asghari, V., Maaref, A. & Aissa, S. (2010). Symbol error probability analysis for multihop relaying over Nakagami fading channels. *Wireless Commun. Conf., 2010 IEEE*, pp. 1–6.

Ata, S. Ö. & Altunbaş, İ. (2016). Fixed-gain AF PLNC over cascaded Nakagami-m fading channels for vehicular communications. *AEU-Int. J. Electron. Commun.*, 70(4), 510–516.

Bazzi, A., Masini, B. M. & Zanella, A. (2015). Performance analysis of V2V beaconing using LTE in direct mode with full duplex radios. *IEEE Wireless Commun. Lett.*, 4(6), 685–688.

Bithas, P. S., Kanatas, A. G., da Costa, D. B., Upadhyay, P. K. & Dias, U. S. (2017). On the double-generalized gamma statistics and their application to the performance analysis of V2V communications. *IEEE Trans. Commun.*, 66(1), 448–460.

Bithas, P. S., Efthymoglou, G. P. & Kanatas, A. G. (Kuala Lumpur, Malaysia 2016). Inter-vehicular communication systems under co-channel interference and outdated channel estimates. *Proc. IEEE Int. Conf. Commun. (ICC)*, pp. 1–6.

Björnson, E., Larsson, E. G. & Marzetta, T. L. (2016). Massive MIMO: Ten myths and one critical question. *IEEE Commu. Mag.*, 54(2), 114–123.

Bletsas, A., Khisti, A., Reed, D. P. & Lippman, A. (2006). A simple cooperative diversity method based on network path selection. *IEEE J. Selected Areas in Commun.*, 24(3), 659–672.

Boban, M., Vinhoza, T. T., Ferreira, M., Barros, J. & Tonguz, O. K. (2010). Impact of vehicles as obstacles in vehicular ad hoc networks. *IEEE journal on selected areas in communications*, 29(1), 15–28.

Boban, M., Vinhoza, T. T., Ferreira, M., Barros, J. & Tonguz, O. K. (2011). Impact of vehicles as obstacles in vehicular ad hoc networks. *IEEE journal on selected areas in communications*, 29(1), 15–28.

Boban, M., Dupleich, D., Iqbal, N., Luo, J., Schneider, C., Müller, R., Yu, Z., Steer, D., Jamsa, T., Li, J. et al. (2019). Multi-band Vehicle-to-Vehicle Channel Characterization in the Presence of Vehicle Blockage. *IEEE Access*.

Caire, G., Jindal, N., Kobayashi, M. & Ravindran, N. (2010). Multiuser MIMO achievable rates with downlink training and channel state feedback. *IEEE Trans. Info. Theory*, 56(6), 2845–2866.

Campolo, C., Molinaro, A., Berthet, A. O. & Vinel, A. (2017). Full-Duplex Radios for Vehicular Communications. *IEEE Commun. Mag.*, 55(6), 182–189.

Cheng, L. & Qiao, T. (2016). Localization in the parking lot by parked-vehicle assistance. *IEEE Trans. Intell. Transp. Syst.*, 17(12), 3629–3634.

Cheng, L., Henty, B. E., Stancil, D. D., Bai, F. & Mudalige, P. (2007). Mobile vehicle-to-vehicle narrow-band channel measurement and characterization of the 5.9 GHz dedicated short range communication DSRC frequency band. *IEEE J. Sel. Areas Commu.*, 25(8), 1501–1516.

Choi, J. I., Jain, M., Srinivasan, K., Levis, P. & Katti, S. (2010). Achieving single channel, full duplex wireless communication. *Proceedings of the sixteenth annual int. conference on Mobile comp. and networking*, pp. 1–12.

Chu, T. M. C. & Zepernick, H.-J. (2018). Performance of a non-orthogonal multiple access system with full-duplex relaying. *IEEE Commun. Lett.*, 22(10), 2084–2087.

Commission, F. C. et al. (2001). Code of Federal Regulation, title 47 Telecommunication.

Cover, T. M. & Gamal, A. E. (1979). Capacity theorems for the relay channel. *IEEE Trans. Inform. Theory*, 25(5), 572–584.

Cui, H., Ma, M. & Song, L. (2014). Relay selection for two-way full duplex relay networks with amplify-and-forward protocol. *IEEE Trans. Wireless Commun.*, 13(7), 3768–3777.

da Costa, D. B. & Aissa, S. (2009). Performance analysis of relay selection techniques with clustered fixed-gain relays. *IEEE Signal Process. lett.*, 17(2), 201–204.

Database, T. C. N. C. (2017). Association for safe international road travel.

Day, B. P., Margetts, A. R., Bliss, D. W. & Schniter, P. (2012). Full-duplex MIMO relaying: Achievable rates under limited dynamic range. *IEEE J. Sel. Areas Commun.*, pp. 1541–1553.

Duarte, M. & Sabharwal, A. (Nov. 2010). Full-duplex wireless communications using off-the-shelf radios: Feasibility and first results. *in Proc. Asilomar Conf. Signals Syst., Pacific Grove, CA, USA*, pp. 1558–1562.

Duarte, M., Dick, C. & Sabharwal, A. (2012). Experiment-driven characterization of full-duplex wireless systems. *IEEE Trans. Wireless Commun.*, 11(12), 4296–4307.

Eshteiwi, K., Kaddoum, G. & Gagnon, F. (2015). Impact of imperfect channel estimation error and jamming on the performance of decode-and-forward relaying. *Ubiquitous Wireless Broadband (ICUWB), 2015 IEEE International Conference on*, pp. 1–5.

Eshteiwi, K., Kaddoum, G., Fredj, K. B., Soujeri, E. & Gagnon, F. (2019). Performance analysis of full-duplex vehicle relay-based selection in dense multi-lane highways. *IEEE Access*, 7, 61581–61595.

Eshteiwi, K., Kaddoum, G. & Alam, M. (2020). Ergodic Capacity Analysis of Full Duplex Relaying in the Presence of Co-Channel Interference in V2V Communications. *Sensors*, 20(1), 1–16.

Eshteiwi, K., Ben Fredj, K., Kaddoum, G. & Gagnon, F. (Sep. 2017). Performance Analysis of Peer-to-Peer V2V Wireless Communications in the Presence of Interference. *Proc. IEEE 26th Annu. Int. Symp. Pers., Indoor, Mobile Radio Commun. (PIMRC)*, pp. 1–6.

Everett, E., Duarte, M., Dick, C. & Sabharwal, A. (2011). Empowering full-duplex wireless communication by exploiting directional diversity. *2011 Conference Record of the Forty Fifth Asilomar Conference on Signals, Systems and Computers (ASILOMAR)*, pp. 2002–2006.

Farhadi, G. & Beaulieu, N. C. (2008). On the performance of amplify-and-forward cooperative systems with fixed gain relays. *IEEE Trans. wireless commun.*, 7(5), 1851–1856.

Farooq, M. J., ElSawy, H. & Alouini, M. S. (2015). A stochastic geometry model for multi-hop highway vehicular communication. *IEEE Trans. Wireless Communic.*, 15(3), 2276–2291.

Farooq, M. J., ElSawy, H. & Alouini, M.-S. (2016). A Stochastic Geometry Model for Multi-hop Highway Vehicular Communication. *IEEE Trans. Wireless Commun.*, 15(3), 2276–2291.

Feng, J., Ma, S., Yang, G. & Poor, H. V. (2018). Impact of Antenna Correlation on Full-Duplex Two-Way Massive MIMO Relaying Systems. *IEEE Trans. Wireless Commun.*, 17(6), 3572–3587.

Forghani, A. H. & Aissa, S. (2012). Performance evaluation of multi-hop multi-branch relaying networks with multiple co-channel interferers. *2012 IEEE Int. Conf. Commun. (ICC)*, pp. 4011–4015.

Forghani, A. H., Ikki, S. S. & Aïssa, S. (2013). On the performance and power optimization of multihop multibranch relaying networks with cochannel interferers. *IEEE Trans. Veh. Technol.*, 62(7), 3437–3443.

Fu, H., Roy, S. & Cheng, J. (2018). Applying Hankel's Expansion for Performance Analysis in Double-Nakagami (Generalized-*K*) Fading Channels. *IEEE Trans. Commun.*, 66(10), 4893–4906.

Gaafar, M., Khafagy, M. G., Amin, O., Schaefer, R. F. & Alouini, M.-S. (2017). Full-Duplex Relaying With Improper Gaussian Signaling Over Nakagami-*m* Fading Channels. *IEEE Trans. on Commun.*, 66(1), 64–78.

Gaafar, M., Khafagy, M. G., Amin, O., Schaefer, R. F. & Alouini, M.-S. (2018). Full-Duplex Relaying With Improper Gaussian Signaling Over Nakagami-*m* Fading Channels. *IEEE Trans. Commun.*, 66(1), 64–78.

Garg, S., Kaur, K., Ahmed, S. H., Bradai, A., Kaddoum, G. & Atiquzzaman, M. (2019a). MobQoS: Mobility-Aware and QoS-Driven SDN Framework for Autonomous Vehicles. *IEEE Wireless Commun.*, 26(4), 12–20.

Garg, S., Kaur, K., Kaddoum, G., Ahmed, S. H. & Jayakody, D. N. K. (2019b). SDN-based secure and privacy-preserving scheme for vehicular networks: a 5G perspective. *IEEE Trans. Vehicul. Technol.*, 68(9), 8421–8434.

Gesbert, D., Bolcskei, H., Gore, D. A. & Paulraj, A. J. (2002). Outdoor MIMO wireless channels: Models and performance prediction. *IEEE Trans. Commun.*, 50(12), 1926–1934.

Ghosh, A., Thomas, T. A., Cudak, M. C., Ratasuk, R., Moorut, P., Vook, F. W., Rappaport, T. S., MacCartney, G. R., Sun, S. & Nie, S. (2014). Millimeter-wave enhanced local area systems: A high-data-rate approach for future wireless networks. *IEEE J. Se.l Areas Commun.*, 32(6), 1152–1163.

Gohary, R. H. & Yanikomeroglu, H. (2014). Grassmannian signalling achieves tight bounds on the ergodic high-SNR capacity of the noncoherent MIMO full-duplex relay channel. *IEEE Trans. Info. Theory*, 60(5), 2480–2494.

Goldsmith, A. (2005). *Wireless communications*. Cambridge university press.

Guo, J., Pei, C. & Yang, H. (2014). Performance analysis of TAS/MRC in MIMO relay systems with outdated CSI and co-channel interference. *IEEE Trans. on Wireless Commun.*, 13(9), 4848–4856.

Haenggi, M. (2005). On distances in uniformly random networks. *IEEE Trans. Inf. Theory*, 51(10), 3584–3586.

Han, S., Chen, L., Meng, W. & Li, C. (2015). Outage probability of multi-hop full-duplex DF relay system over Nakagami-*m* fading channels. *Communications in China (ICCC), 2015 IEEE/CIC International Conference on*, pp. 1–6.

Hao, Z., Novak, E., Yi, S. & Li, Q. (2017). Challenges and software architecture for fog computing. *IEEE Internet Computing*, 21(2), 44–53.

Hasna, M. O. & Alouini, M.-S. (2003). Outage probability of multihop transmission over Nakagami fading channels. *IEEE Commun. Lett.*, 7(5), 216–218.

He, R., Molisch, A. F., Tufvesson, F., Zhong, Z., Ai, B. & Zhang, T. (2014). Vehicle-to-vehicle propagation models with large vehicle obstructions. *IEEE Trans. Intell. Transp. Syst.*, 15(5), 2237–2248.

He, R., Molisch, A. F., Tufvesson, F., Wang, R., Zhang, T., Li, Z., Zhong, Z. & Ai, B. (2016). Measurement-based analysis of relaying performance for Vehicle-to-Vehicle communications with large vehicle obstructions. *IEEE 84th Veh. Technol. Conf.*, pp. 1–6.

Hu, R., Hu, C., Jiang, J., Xie, X. & Song, L. (2014a). Full-duplex mode in amplify-and-forward relay channels: Outage probability and ergodic capacity. *Int. J. of Antennas and Propagation*, 2014.

Hu, Y., Li, H., Zhang, C. & Li, J. (2014b). Partial relay selection for a roadside-based two-way amplify-and-forward relaying system in mixed Nakagami-*m* and double Nakagami-*m* fading. *IET Commun.*, 8(5), 571–577.

Ikki, S. & Ahmed, M. H. (2007). Performance analysis of cooperative diversity wireless networks over Nakagami-m fading channel. *IEEE Commun. lett.*, 11(4), 334–336.

Ikki, S. S. & Ahmed, M. H. (2008). Performance of multiple-relay cooperative diversity systems with best relay selection over Rayleigh fading channels. *EURASIP J. Advances Signal Process.*, 2008(1), 1–7.

Ikki, S. S. & Ahmed, M. H. (Spring 2009). Performance analysis of decode-and-forward incremental relaying cooperative-diversity networks over Rayleigh fading channels. *Proc. IEEE 26th Annu. Int. Symp. Pers., Indoor, Mobile Radio Commun. (PIMRC)*, pp. 1–6.

Ikki, S. S. & Aissa, S. (2012a). Performance analysis of two-way amplify-and-forward relaying in the presence of co-channel interferences. *IEEE Trans. on Commun.*, 60(4), 933–939.

Ikki, S. S. & Aissa, S. (2012b). Multihop wireless relaying systems in the presence of cochannel interferences: Performance analysis and design optimization. *IEEE Trans. Veh. Technol.*, 61(2), 566–573.

Ilhan, H. (2015). Performance analysis of cooperative vehicular systems with co-channel interference over cascaded Nakagami-*m* fading channels. *Wireless Pers. Commun.*, 83(1), 203–214.

Ilhan, H., Altunbas, I. & Uysal, M. (2008). Cooperative diversity for relay-assisted intervehicular communication. *Process. IEEE VTC Spring*, pp. 605–609.

Ilhan, H., Uysal, M. & Altunbas, I. (2009). Cooperative diversity for intervehicular communication: Performance analysis and optimization. *IEEE Trans. Veh. Technol.*, 58(7), 3301–3310.

Jain, M., Choi, J. I., Kim, T., Bharadia, D., Seth, S., Srinivasan, K., Levis, P., Katti, S. & Sinha, P. (2011). Practical, real-time, full duplex wireless. *Proc. int. conf. Mobile Comput. Netw.*, pp. 301–312.

Jaiswal, V. (2010). *Performance of Switched Relay Diversity Systems in Wireless Fading Channels*. (Ph.D. thesis, Department of Electronics and Communications Engineering, National, Institute of Technology, Durgapur).

Jalil, A. M., Meghdadi, V. & Cances, J.-P. (2010). Relay assignment in decode-and-forward cooperative networks based on order-statistics. *21st Ann. IEEE Int. Symp. Pers., Indoor Mobile Radio Commun.*, pp. 2404–2409.

Jebur, B. A., Tsimenidis, C. C. & Chambers, J. A. (2016). Tight upper bound ergodic capacity of an AF full-duplex physical-layer network coding system. *2016 IEEE 27th Annual Int. Symposium on Personal, Indoor, and Mobile Radio Communications (PIMRC)*, pp. 1–6.

Jeffrey, A. & Zwillinger, D. (2007). *Table of integrals, series, and products*. Academic press.

Ju, H., Oh, E. & Hong, D. (2009). Improving efficiency of resource usage in two-hop full duplex relay systems based on resource sharing and interference cancellation. *IEEE Transactions on Wireless Communications*, 8(8).

Jurgen, R. (2012). *V2V/V2I communications for improved road safety and efficiency*. SAE: Warrendale, PA, USA, pp. 1-6.

Kader, M. F., Shin, S. Y. & Leung, V. C. (2018). Full-duplex non-orthogonal multiple access in cooperative relay sharing for 5G systems. *IEEE Trans. Veh. Technol.*, 67(7), 5831–5840.

Karagiannidis, G. K., Sagias, N. C. & Mathiopoulos, P. T. (2007). $N^*$ Nakagami: A Novel Stochastic Model for Cascaded Fading Channels. *IEEE Trans. Commu.s*, 55(8), 1453–1458.

Katla, R. & Babu, A. (2016). Outage performance of multihop full duplex relaying system over Nakagami-*m* fading channels. *India Conference (INDICON), 2016 IEEE Annual*, pp. 1–6.

Kaur, K., Garg, S., Kaddoum, G., Kumar, N. & Gagnon, F. (2019). SDN-Based Internet of Autonomous Vehicles: An Energy-Efficient Approach for Controller Placement. *IEEE Wireless Commun.*, 26(6), 72–79.

Kenney, J. B. (2011). Dedicated short-range communications (DSRC) standards in the United States. *in Proc. IEEE*, 99(7), 1162–1182.

Khafagy, M., Ismail, A., Alouini, M. S. & Aissa, S. (2013). On the outage performance of full-duplex selective decode-and-forward relaying. *IEEE Commun. Lett.*, 17(6), 1180–1183.

Khafagy, M. G., Alouini, M.-S. & Aïssa, S. (2015a). On the performance of future full-duplex relay selection networks. *2015 IEEE 20th Int. Workshop on Computer Aided Modelling and Design of Commu. Links and Networks (CAMAD)*, pp. 11–16.

Khafagy, M. G., Ismail, A., Alouini, M.-S. & Aïssa, S. (2015b). Efficient Cooperative Protocols for Full-Duplex Relaying Over Nakagami-*m* Fading Channels. *IEEE Trans. Wireless Commun.*, 14(6), 3456–3470.

Khafagyx, M. G., Alouini, M. S. & Aïssa, S. (Sep. 2015). On the performance of future full-duplex relay selection networks. *Proc. IEEE CAMAD*, pp. 11–16.

Khattabi, Y. M. & Matalgah, M. M. (2015). Performance analysis of multiple-relay AF cooperative systems over Rayleigh time-selective fading channels with imperfect channel estimation. *IEEE Trans. . vehicul. technol.*, 65(1), 427–434.

Kim, D., Lee, H. & Hong, D. (2015). A survey of in-band full-duplex transmission: From the perspective of PHY and MAC layers. *IEEE Commun. Surveys*, 17(4), Dec. 2017–2046.

Kim, Y. & Liu, H. (2008). Infrastructure relay transmission with cooperative MIMO. *IEEE Trans. Veh. Technol.*, 57(4), 2180–2188.

Koç, A., Altunbas, I. & Yongaçoglu, A. (2016). Outage probability of two-way full-duplex AF relay systems over Nakagami-m fading channels. *2016 IEEE 84th Veh. Technol. Conf. (VTC-Fall)*, pp. 1–5.

Kong, C., Zhong, C., Papazafeiropoulos, A. K., Matthaiou, M. & Zhang, Z. (2015). Effect of channel aging on the sum rate of uplink massive MIMO systems. *2015 IEEE Int. Symposium on Inf. Theory (ISIT)*, pp. 1222–1226.

Kothapalli, N., Sharma, P. & Kumar, V. (2016). Performance of a bi-directional relaying system with one full duplex relay. *AEU-Int. J. Electron. Commun.*, 70(10), 1426–1432.

Krikidis, I., Thompson, J., McLaughlin, S. & Goertz, N. (2008). Amplify-and-forward with partial relay selection. *IEEE Commun. lett.*, 12(4), 235–237.

Krikidis, I., Suraweera, H. A., Smith, P. J. & Yuen, C. (2012). Full-duplex relay selection for amplify-and-forward cooperative networks. *IEEE Trans. on Wireless Commun.*, 11(12), 4381–4393.

Kumar, N., Singya, P. K. & Bhatia, V. (2017). Performance analysis of orthogonal frequency division multiplexing-based cooperative amplify-and-forward networks with non-linear power amplifier over independently but not necessarily identically distributed Nakagami-*m* fading channels. *IET Commun.*, 11(7), 1008–1020.

Kwon, T., Lim, S., Choi, S. & Hong, D. (Sep. 2010). Optimal duplex mode for DF relay in terms of the outage probability. *IEEE Trans. Veh. Technol.*, 59(7), 3628–3634.

Laneman, J. N., Tse, D. N. & Wornell, G. W. (Dec. 2004). Cooperative diversity in wireless networks: Efficient protocols and outage behavior. *IEEE Trans. Inf. theory*, 50(12), 3062–3080.

Laneman, J. (2006). Cooperative diversity in wireless networks: Efficient protocols and outage behavior. *IEEE Trans. Inf. Theory*, 50(12), 283–289.

Lateef, H., McLernon, D. C. & Ghogho, M. (June 2010). Performance analysis of cooperative communications with opportunistic relaying. *Proc. IEEE Int. Workshop Signal Process. Advances Wireless Commun. (SPAWC)*, pp. 1–5.

Le, T.-D. & Kaddoum, G. (2020). A Distributed Channel Access Scheme for Vehicles in Multi-agent V2I Systems. *IEEE Trans. Cognitive Commun. and Net.*, 1–12.

Lee, K.-C., Li, C.-P., Wang, T.-Y. & Li, H.-J. (2014). Performance analysis of dual-hop amplify-and-forward systems with multiple antennas and co-channel interference. *IEEE Trans. on Wireless Commun.*, 13(6), 3070–3087.

Li, M., Lin, M., Zhu, W.-P., Huang, Y., Wong, K.-K. & Yu, Q. (2017a). Performance analysis of dual-hop MIMO AF relaying network with multiple interferences. *IEEE Trans on Veh. Technol.*, 66(2), 1891–1897.

Li, Q., Feng, S., Ge, X., Mao, G. & Hanzo, L. (2017b). On the performance of full-duplex multi-relay channels with DF relays. *IEEE Transactions on Vehicular Technology*.

Li, S., Yang, K., Zhou, M., Wu, J., Song, L., Li, Y. & Li, H. (2017c). Full-duplex amplify-and-forward relaying: Power and location optimization. *IEEE Trans. Veh. Technol.*, 66(9), 8458–8468.

Li, Z., Zhao, Y., Chen, H. & Hu, H. (2010). Outage probability bound analysis in vehicle-assisted inter-vehicular communications. *Proc. IEEE 14th Int. Conf. on Comput. Supported Cooperative Work in Design (CSCWD)*, pp. 783–787.

Liu, K. R., Sadek, A. K., Su, W. & Kwasinski, A. (2009). *Cooperative communications and networking*. Cambridge university press.

Liu, Y., Roblin, P., Quan, X., Pan, W., Shao, S. & Tang, Y. (2017). A full-duplex transceiver with two-stage analog cancellations for multipath self-interference. *IEEE Trans. Microwave Theory and Tech.*, 65(12), 5263–5273.

Mafra, S. B., Fernandez, E. M. & Souza, R. D. (2016). Performance Analysis of Full-Duplex Cooperative Communication in Vehicular Ad-Hoc Networks. *IFAC-Papers OnLine*, 49(30), 227–232.

Maham, B., Saad, W., Debbah, M. & Han, Z. (2014). Interference analysis and management for spatially reused cooperative multihop wireless networks. *IEEE Trans. Commun.*, 62(11), 3778–3790.

Mahmood, A. (2010). Cooperative diversity in wireless networks. *J. of Computer Science and Eng.*, 184–187.

Mathai, A. M. & Saxena, R. K. (1978). The H function with applications in statistics and other disciplines.

Mathai, A. M., Saxena, R. K. & Haubold, H. J. (2009). *The H-function: theory and applications*. Springer Science & Business Media.

Matolak, D. W. & Frolik, J. (2011). Worse-than-Rayleigh fading: Experimental results and theoretical models. *Commun. Mag., IEEE*, 49(4), 140–146.

Meireles, R., Boban, M., Steenkiste, P., Tonguz, O. & Barros, J. (2010). Experimental study on the impact of vehicular obstructions in VANETs. *IEEE Veh. Net. Conf.*, pp. 338–345.

Mishra, A. K., Gowda, S. C. & Singh, P. (2017). Impact of hardware impairments on TWRN and OWRN AF relaying systems with imperfect channel estimates. *2017 IEEE Wireless Commun. and Networking Conf. (WCNC)*, pp. 1–6.

Molisch, A. F. (2012). *Wireless communications*. John Wiley & Sons.

Molisch, A. F., Tufvesson, F., Karedal, J. & Mecklenbrauker, C. F. (2009). A survey on vehicle-to-vehicle propagation channels. *IEEE Wireless Commun.*, 16(6), 12–22.

Mouradian, C., Naboulsi, D., Yangui, S., Glitho, R. H., Morrow, M. J. & Polakos, P. A. (2017). A comprehensive survey on fog computing: State-of-the-art and research challenges. *IEEE Commun. Surveys and Tutorials*, 20(1), 416–464.

Ng, D. W. K., Lo, E. S. & Schober, R. (2012). Dynamic resource allocation in MIMO-OFDMA systems with full-duplex and hybrid relaying. *IEEE Trans. Commun.*, 60(5), 1291–1304.

Nguyen, B. C. & Tran, X. N. Performance analysis of full duplex amplify and forward relay system with hardware impairments and imperfect self interference cancellation. *Wireless Commun. and Mobile Comp.*

Nguyen, B. C. & Tran, X. N. (2019). Performance analysis of full-duplex amplify-and-forward relay system with hardware impairments and imperfect self-interference cancellation. *Wireless Commun. and Mobile Comp.*, 2019, 1–11.

Nguyen, B. C., Hoang, T. M. et al. (2019). Performance analysis of vehicle-to-vehicle communication with full duplex amplify and forward relay over double-Rayleigh fading channels. *Veh. Commun.*, 19, 1–9.

Nguyen, S. Q. & Kong, H. Y. (2016). Outage Probability Analysis in Dual-Hop Vehicular Networks with the Assistance of Multiple Access Points and Vehicle Nodes. *Wireless Pers. Commun.*, 87(4), 1175–1190.

Nguyen, X.-X. & Do, D.-T. (2019). System Performance of Cooperative NOMA with Full-Duplex Relay over Nakagami-m Fading Channels. *Mobile Inf. Sys.*, 2019.

Nosratinia, A., Hunter, T. E. & Hedayat, A. (2004). Cooperative communication in wireless networks. *IEEE commun. Mag.*, 42(10), 74–80.

Osorio, D. M., Olivo, E. B., Alves, H., Santos Filho, J. C. S. & Latva-aho, M. (2015). Exploiting the direct link in full-duplex amplify-and-forward relaying networks. *IEEE Signal Processing Lett.*, 22(10), 1766–1770.

Paier, A., Karedal, J., Czink, N., Hofstetter, H., Dumard, C., Zemen, T., Tufvesson, F., Molisch, A. F. & Mecklenbrauker, C. F. (2007). Car-to-car radio channel measurements at 5 GHz: Path loss, power-delay profile, and delay-Doppler spectrum. *2007 4th Int. Symposium*

*on Wireless Commun. Syst.*, pp. 224–228.

Papazafeiropoulos, A. & Ratnarajah, T. (2017). Toward a realistic assessment of multiple antenna HCNs: Residual additive transceiver hardware impairments and channel aging. *IEEE Trans. Veh. Technol.*, 66(10), 9061–9073.

Papazafeiropoulos, A., Sharma, S. K., Ratnarajah, T. & Chatzinotas, S. (2017a). Impact of residual additive transceiver hardware impairments on Rayleigh-product MIMO channels with linear receivers: Exact and asymptotic analyses. *IEEE Trans. Commun.*, 66(1), 105–118.

Papazafeiropoulos, A. K. (2015). Impact of user mobility on optimal linear receivers in cellular networks. *2015 IEEE Int. Conf. Commun. (ICC)*, pp. 2239–2244.

Papazafeiropoulos, A. K. & Ratnarajah, T. (2015). Deterministic equivalent performance analysis of time-varying massive MIMO systems. *IEEE Trans. Wireless Commun.*, 14(10), 5795–5809.

Papazafeiropoulos, A. K., Sharma, S. K. & Chatzinotas, S. (2016). MMSE filtering performance of DH-AF massive MIMO relay systems with residual transceiver impairments. *2016 IEEE Int. Conf. Commun. Workshops (ICC)*, pp. 644–649.

Papazafeiropoulos, A. K., Sharma, S. K., Chatzinotas, S. & Ottersten, B. (2017b). Ergodic capacity analysis of AF DH MIMO relay systems with residual transceiver hardware impairments: Conventional and large system limits. *IEEE Trans. Veh. Technol.*, 66(8), 7010–7025.

Papoulis, A. & Pillai, S. U. (2002). *Probability, random variables, and stochastic processes*. Tata McGraw-Hill Education.

Peppas, K. P. (2012). A new formula for the average bit error probability of dual-hop amplify-and-forward relaying systems over generalized shadowed fading channels. *IEEE Wireless Commun. Lett.*, 1(2), 85–88.

Pitsiladis, G. T., Papanikolaou, D., Panagopoulos, A. D. & Antoniou, C. (2015). Vehicle-to-vehicle communication: End-to-end performance evaluation in dense propagation environments. *IEEE 9th European Antennas Propag. Conf.*, pp. 1–5.

Prudnikov, A., Brychkov, Y. & Marichev, O. (1990). Integrals Series: More Special Functions, Volume III of Integrals and Series. *New York: Gordon and Breach Science Publishers*.

Qian, S., Zhou, X., He, X., He, J., Juntti, M. & Matsumoto, T. (2017). Performance Analysis for Lossy-Forward Relaying Over Nakagami-*m* Fading Channels. *IEEE Trans. Veh. Technol.*, 66(11), 10035–10043.

Qin, D., Wang, Y. & Zhou, T. (2018). Average SEP of AF Relaying in Nakagami-Fading Environments. *Wireless Commun, and Mobile Compu.*, 2018.

Quan, X., Liu, Y., Chen, D., Shao, S., Tang, Y. & Kang, K. (2018). Blind nonlinear self-interference cancellation for wireless full-duplex transceivers. *IEEE Access*, 6, 37725–37737.

Qureshi, K. N. & Abdullah, A. H. (2013). A survey on intelligent transportation systems. *Middle-East J. Sci. Res.*, 15(5), 629–642.

Raiyn, J. (2019). Road Intersection Intelligent Traffic Management Based on V2V Wireless Communication. *2019 IEEE Int. Conf.on Electrical, Comp. and Commun.Technol.(ICECCT)*, pp. 1–6.

Rappaport, T. S. et al. (1996). *Wireless communications: principles and practice*. Prentice Hall PTR New Jersey.

Ribeiro, A., Cai, X. & Giannakis, G. B. (2005). Symbol error probabilities for general cooperative links. *IEEE Trans. wireless commun.*, 4(3), 1264–1273.

Riihonen, T., Werner, S. & Wichman, R. (2009a). Comparison of full-duplex and half-duplex modes with a fixed amplify-and-forward relay. *2009 IEEE Wireless Commun. and Networking Conf.*, pp. 1–5.

Riihonen, T., Werner, S. & Wichman, R. (2009b). Optimized gain control for single-frequency relaying with loop interference. *IEEE Transactions on Wireless Communications*, 8(6), 2801.

Riihonen, T., Werner, S., Wichman, R. & Zacarias, E. (2009c). On the feasibility of full-duplex relaying in the presence of loop interference. *2009 IEEE 10th Workshop on Signal Proc. Advances in Wireless Commun.*, pp. 275–279.

Riihonen, T., Werner, S. & Wichman, R. (2011a). Hybrid full-duplex/half-duplex relaying with transmit power adaptation. *IEEE Transactions on Wireless Communications*, 10(9), 3074–3085.

Riihonen, T., Werner, S. & Wichman, R. (2011b). Hybrid full-duplex/half-duplex relaying with transmit power adaptation. *IEEE Transactions on Wireless Communications*, 10(9), 3074–3085.

Riihonen, T., Werner, S. & Wichman, R. (2011c). Mitigation of loopback self-interference in full-duplex MIMO relays. *IEEE Transactions on Signal Processing*, 59(12), 5983–5993.

Rui, X., Hou, J. & Zhou, L. (2010). On the performance of full-duplex relaying with relay selection. *Electronics lett.*, 46(25), 1674–1676.

Rui, X., Hou, J. & Zhou, L. (2013). Performance analysis of full-duplex relaying with parial relay selection. *Wireless personal commun.*, 72(2), 1327–1332.

Sagias, N. C. & Tombras, G. S. (2007). On the cascaded Weibull fading channel model. *J. Franklin Institute*, 344(1), 1–11.

Salo, J., El-Sallabi, H. M. & Vainikainen, P. (2006). Impact of double-Rayleigh fading on system performance. *2006 1st Int. Symposium on Wireless Pervasive Computing*, pp. 1–5.

Schenk, T. (2008). *RF imperfections in high-rate wireless systems: impact and digital compensation*. Springer Science & Business Media.

Seyfi, M., Muhaidat, S., Liang, J. & Uysal, M. (2011). Relay selection in dual-hop vehicular networks. *IEEE Signal Processing Letters*, 18(2), 134–137.

Shahzadi, S., Iqbal, M., Dagiuklas, T. & Qayyum, Z. U. (2017). Multi-access edge computing: open issues, challenges and future perspectives. *J. Cloud Computing*, 6(1), 30.

Shakeri, R., Khakzad, H., Taherpour, A. & Gazor, S. (2014). Performance of two-way multi-relay inter-vehicular cooperative networks. *IEEE Wireless Commun. Netw. Conf. (WCNC)*, pp. 520–525.

Sharma, G., Sharma, P. K. & Garg, P. (2014). Performance analysis of full duplex relaying in multicell environment. *2014 Int. Conf. on Advances in Computing, Commun. and Informatics (ICACCI)*, pp. 2501–2505.

Sharma, P. K. & Garg, P. (Feb. 2013). Outage analysis of full duplex decode and forward relaying over Nakagami-*m* channels. *Proc. IEEE Nat. Conf. Commun.*, pp. 1–5.

Sharma, V., You, I., Leu, F.-Y. & Atiquzzaman, M. (2018). Secure and efficient protocol for fast handover in 5G mobile Xhaul networks. *J. Net. Comp. Applications*, 102, 38–57.

Shi, Z., Ma, S., Hou, F. & Tam, K.-W. (2015). Analysis on full duplex amplify-and-forward relay networks under Nakagami fading channels. *2015 IEEE Global Commun. Conf. (GLOBECOM)*, pp. 1–6.

Shojaeifard, A., Wong, K.-K., Di Renzo, M., Zheng, G., Hamdi, K. A. & Tang, J. (2017a). Massive MIMO-enabled full-duplex cellular networks. *IEEE Trans. on Commun.*, 65(11), 4734–4750.

Shojaeifard, A., Wong, K.-K., Di Renzo, M., Zheng, G., Hamdi, K. A. & Tang, J. (2017b). Self-interference in full-duplex multi-user MIMO channels. *IEEE Commun. Lett.*, 21(4), 841–844.

Shukla, M. K., Yadav, S. & Purohit, N. (2018). Performance evaluation and optimization of traffic-aware cellular multiuser two-way relay networks over Nakagami-*m* fading. *IEEE Syst. J.*, 12(2), 1933–1944.

Silva, C. M., Masini, B. M., Ferrari, G. & Thibault, I. (2017). A survey on infrastructure-based vehicular networks. *Mobile Info. Syst.*, 2017.

Simon, M. K. & Alouini, M.-S. (2005). *Digital communication over fading channels*. John Wiley & Sons.

Singh, P. K., Nandi, S. K. & Nandi, S. (2019). A tutorial survey on vehicular communication state of the art, and future research directions. *Vehicul. Commun.*, 18, 100164.

Sivaraman, S. & Trivedi, M. M. (2013). Towards cooperative, predictive driver assistance. *16th IEEE Int, Conf. on Intelligent Tran. Sys. (ITSC 2013)*, pp. 1719–1724.

Soliman, S. S. & Beaulieu, N. C. (2012). Exact analysis of dual-hop AF maximum end-to-end SNR relay selection. *IEEE Trans. Commun.*, 60(8), 2135–2145.

Soliman, S. S. & Beaulieu, N. C. (2013). The bottleneck effect of Rician fading in dissimilar dual-hop AF relaying systems. *IEEE Trans. on Vehicul. Technol.*, 63(4), 1957–1965.

Souid, I., Chikha, H. B. & Attia, R. (2014). Blind spectrum sensing in cognitive vehicular ad hoc networks over Nakagami-m fading channels. *Int. Conf. on Electrical Sciences and Technol. in Maghreb (CISTEM)*, pp. 1–5.

Studer, C., Wenk, M. & Burg, A. (2010). MIMO transmission with residual transmit-RF impairments. *arXiv preprint arXiv:1002.0406*.

Surobhi, N. A. (2009). *Outage performance of cooperative cognitive relay networks*. (Ph.D. thesis, Victoria University).

Tadayon, N. & Kaddoum, G. (2018). Packet-level modeling of cooperative diversity: A queueing network approach. *IEEE Access*, 6, 35223–35242.

Taghizadeh, O., Rothe, M., Cirik, A. C. & Mathar, R. (2015). Distortion-Loop analysis for Full-Duplex Amplify-and-Forward relaying in cooperative multicast scenarios. *2015 9th Int. Conf. Signal Proce. Commun. Sys. (ICSPCS)*, pp. 1–9.

Taghizadeh, O., Zhang, J. & Haardt, M. (2016). Transmit beamforming aided amplify-and-forward MIMO full-duplex relaying with limited dynamic range. *Signal Proce.*, 127, 266–281.

Taghizadeh, O., Cirik, A. C. & Mathar, R. (2017). Hardware impairments aware transceiver design for full-duplex amplify-and-forward MIMO relaying. *IEEE Trans. Wireless Commun.*, 17(3), 1644–1659.

Tassi, A., Egan, M., Piechocki, R. J. & Nix, A. (2017). Modeling and Design of Millimeter-Wave Networks for Highway Vehicular Communication. *IEEE Trans. Veh. Technol.*, 66(12), 10676–10691.

Tirkan, Z., Shirkhani, M., Taherpour, A. & Uysal, M. (2012). Performance of cooperative amplify-and-forward protocols in vehicular ad-hoc networks. *Wireless Communications & Signal Processing (WCSP), 2012 International Conference on*, pp. 1–6.

Toka, M. & Kucur, O. (2018). Performance of dual-hop full-duplex relay networks with orthogonal space-time block coding in Nakagami-m fading channels. *IET Commun.*, 13(5), 601–609.

Tran, X. N., Nguyen, B. C. & Tran, D. T. (2019). Outage probability of two-way full-duplex relay system with hardware impairments. *Int. Conf. on Recent Advances in Signal Proce., Telecommun. Computing (SigTelCom)*, pp. 135–139.

Trigui, I., Affes, S. & Stephenne, A. (2010). Closed-Form Error Analysis of Dual-Hop Relaying Systems over Nakagami-*m* Fading Channels. *Wireless Communications and Networking Conference (WCNC), 2010 IEEE*, pp. 1–5.

Trigui, I., Affes, S. & Stephenne, A. (2013a). On the ergodic capacity of amplify-and-forward relay channels with interference in Nakagami-m fading. *IEEE Trans. Commun.*, 61(8), 3136–3145.

Trigui, I., Affes, S. & Stéphenne, A. (2013b). Ergodic capacity analysis for interference-limited AF multi-hop relaying channels in Nakagami-m fading. *IEEE Trans. Commun.*, 61(7), 2726–2734.

Trigui, I., Affes, S. & Stéphenne, A. (2015). Ergodic capacity of two-hop multiple antenna AF systems with co-channel interference. *IEEE Wireless Commun. Lett.*, 4(1), 26–29.

Uddin, M. B., Kader, M. F. & Shin, S. Y. (2019). On the Capacity of Full-Duplex Diamond Relay Networks Using NOMA. *2019 7th Int. Conf. Info. Commun. Technol. (ICoICT)*, pp. 1–6.

Van Der Meulen, E. C. (1971). Three-terminal communication channels. *Advances in applied Probability*, 120–154.

Verma, R. (1966). On some integrals involving Meijer's G-fucntion of two variables. *Proc. Nat. Inst. Sci. India*, 39(5/6), 509–515.

Wang, Y., Xu, K., Li, Y., Xu, Y., Shen, X. & Wang, F. (2015). Outage performance of full-duplex selective decode-and-forward relaying over Nakagami-m fading channels. *2015 Int. Conf. Wireless Commun. Signal Proce. (WCSP)*, pp. 1–6.

Wang, Y., Xu, Y., Li, N., Xie, W., Xu, K. & Xia, X. (2016). Relay selection of full-duplex decode-and-forward relaying over Nakagami-*m* fading channels. *IET Commun.*, 10(2), 170–179.

Wu, Q., Matolak, D. W. & Sen, I. (2010). 5-GHz-band vehicle-to-vehicle channels: Models for multiple values of channel bandwidth. *IEEE Trans. Veh. Technol.*, 59(5), 2620–2625.

Xu, Y., Wang, Y., Wang, C. & Xu, K. (2014). On the performance of full-duplex decode-and-forward relaying over Nakagami-m fading channels. *2014 Sixth International Conf. on Wireless Commun. and Signal Proc. (WCSP)*, pp. 1–6.

Xu, Z. & Nguyen, N.-P. (2018). Securing full-duplex cognitive relay networks over Nakagami-m fading channels with partial relay selection. *2018 2nd Int. Conf. on Recent Advances in Signal Proce.Telecommun. and Computing (SigTelCom)*, pp. 182–186.

Yamao, Y. & Minato, K. (2009). Vehicle-roadside-vehicle relay communication network employing multiple frequencies and routing function. *IEEE Wireless Commun. Syst., 6th International Symposium on*, pp. 413–417.

Yang, K., Cui, H., Song, L. & Li, Y. (2015). Efficient full-duplex relaying with joint antenna-relay selection and self-interference suppression. *IEEE Trans. Wireless Commun.*, 14(7), 3991–4005.

Yang, M., Ai, B., He, R., Chen, L., Li, X., Huang, Z., Li, J. & Huang, C. (2018). Path Loss Analysis and Modeling for Vehicle-to-Vehicle Communications with Vehicle Obstructions. *2018 10th Int. Conf. Wireless Commun. and Signal Proce. (WCSP)*, pp. 1–6.

Yang, T., Zhang, R., Cheng, X. & Yang, L. (2016). A graph coloring resource sharing scheme for full-duplex cellular VANET heterogeneous networks. *IEEE int. conf. Compu. Netw. Commun. (ICNC)*, pp. 1–5.

Yang, X., Liu, L., Vaidya, N. H. & Zhao, F. (2004). A vehicle-to-vehicle communication protocol for cooperative collision warning. *Proc. MobiQuitous*, pp. 114–123.

Yılman, E. (2006). An Information Theoretic Study of Spatial Diversity Techniques for Wireless Relay Networks. (Master Thesis Koç University).

You, J., Zhong, Z., Dou, Z., Dang, J. & Wang, G. (2016). Wireless relay communication on high speed railway: Full duplex or half duplex? *China Commun.*, 13(11), 14–26.

Zhang, C., Ge, J., Li, J. & Hu, Y. (2013). Performance analysis for mobile-relay-based M2M two-way AF relaying in N* Nakagami-m fading. *Electron. Lett.*, 49(5), 344–346.

Zhang, X., Matthaiou, M., Björnson, E., Coldrey, M. & Debbah, M. (2014). On the MIMO capacity with residual transceiver hardware impairments. *2014 IEEE Int. Conf. Commun.*

*(ICC)*, pp. 5299–5305.

Zhong, B., Zhang, D., Zhang, Z., Pan, Z., Long, K. & Vasilakos, A. V. (2014). Opportunistic full-duplex relay selection for decode-and-forward cooperative networks over Rayleigh fading channels. *2014 IEEE Int. Conf. Commun. (ICC)*, pp. 5717–5722.

Zhong, C. & Zhang, Z. (2016). Non-orthogonal multiple access with cooperative full-duplex relaying. *IEEE Commun. Let.*, 20(12), 2478–2481.

Zhu, G., Zhong, C., Suraweera, H. A., Zhang, Z. & Yuen, C. (2014a). Outage probability of dual-hop multiple antenna AF systems with linear processing in the presence of co-channel interference. *IEEE Trans. on Wireless Commun.*, 13(4), 2308–2321.

Zhu, G., Zhong, C., Suraweera, H. A., Zhang, Z., Yuen, C. & Yin, R. (2014b). Ergodic capacity comparison of different relay precoding schemes in dual-hop AF systems with co-channel interference. *IEEE Trans. Commun.*, 62(7), 2314–2328.